SURFER v3.0 : an upgrade of the carbon cycle for longer time scales

Victor Couplet[1], Marina Martínez Montero[1], and Michel Crucifix[1]

[1]Earth and Life Institute, UCLouvain, Louvain-la-Neuve, Belgium

Correspondence: Victor Couplet (victor.couplet@uclouvain.be)

Abstract. TODO

Contents

1 Introduction

Human activities have significantly altered Earth's climate by releasing greenhouse gases, primarily carbon dioxide (CO_2) and methane (CH_4), into the atmosphere at unprecedented rates (cite IPCC). The consequences of these emissions are already palpable, with 2023 marking the warmest year on record. Moreover, the frequency and intensity of extreme weather events, such as heatwaves, wildfires, droughts, and hurricanes have increased and are projected to increase further under global warming (cite IPCC or other?). While these impacts are immediate and observable, others unfold over longer time frames. For instance, the melting polar ice caps will contribute to sea level rise for centuries, and even millennia, after emissions of greenhouse gases are reduced or stopped (Clark et al., 2016; Breedam et al., 2020). There is also growing concern over climate tipping points, where potentially abrupt and irreversible changes could occur and lead to cascades of unforeseen consequences in the long term trajectories of the Earth system (Lenton et al., 2008, 2019; Armstrong McKay et al., 2022; Steffen et al., 2018).

Making informed decisions about climate change thus necessitates a comprehensive examination across multiple temporal scales, to balance the immediate needs of current populations with the imperative of safeguarding the planet's habitability for future generations (cite ethical frameworks for intergenerational equity in climate policy).To this end climate models are indispensable for scientists and policymakers. They come in different sizes and complexities. On the one side of the complexity spectrum, state-of-the-art Earth system models include detailed representation of physical and biogeochemical processes are capable of relatively accurate, high-resolution, short-term predictions. However, due to their size and complexity, they are hard to analyse and computationally expensive to run, with most simulations ending in 2100. On the other side of the spectrum, conceptual box models trade complexity and spatial resolution for speed and understandability. They provide valuable insights into fundamental climate processes and feedbacks, facilitating transparent and intuitive assessments of long-term climate trends. Due to their low computational cost, they can be run many times, with different choices of parameters and for different forcing scenarios. This allows an extensive exploration of mitigation and adaptation strategies, such as to take into account possible errors caused by simplifications and other lacks of knowledge.

This is the spirit in which SURFER was designed (Martínez Montero et al., 2022). SURFER v2.0 is a model based on nine ordinary differential equations designed to estimate global mean temperature increase, sea level rise and ocean acidification in response to CO_2 emissions and aerosols injections. It is fast, easy to understand and modify, making it appropriate for use in policy assessments. In (Montero et al., 2023), it helped assess the long term sustainability of short term climate policies based on a novel commitment metric. Yet, SURFER v2.0 lacks some processes in its carbon cycle implementation. It can only simulate quantities reliably for up to two or three millennia, and only accounts for carbon dioxide emissions in the carbon cycle. Here, we introduce an extended version of the model with new processes, SURFER v3.0. Among other things, we have added : a representation of atmospheric methane, a distinction between land-use and fossil emissions, an additional oceanic layer, a dependence of the solubility and dissociation constants on temperature and pressure, a dynamic representation of alkalinity, a sediments box, and weathering processes.

This paper is structured as follow. We explain in detail the new additions of SURFER v3.0 in section 2. In section 3, we compare the results of SURFER v3.0 to other models on time scales ranging from centuries to a million year. We first show that

SURFER can reproduce the historical record. Then, we show that SURFER is in the range of IPCC class models for different quantities modelled up to 2100 and 2300 AD. We then compare the CO_2 drawdown computed by SURFER over 10000 years to models that participated in the LTMIP project. Lastly, we compare SURFER v3.0 outputs to 1 Myr runs performed with the cGENIE climate model of intermediate complexity. In section 4, we show that including new processes in the carbon cycle changes dramatically the SLR estimations on millennial time scales compared to SURFER v2.0. In section 5 we discuss the advantages and limitations of our model. Finally, in section 6, we conclude and provide some perspectives on future research.

2 Model specification

The nine ordinary differential equations of SURFER v2.0 describe the exchanges of for the masses of carbon in four different reservoirs (atmosphere, upper ocean layer, deeper ocean layer and land), the response of temperature anomalies of two different reservoirs (upper ocean layer and deeper ocean layer), and that of the volumes of Greenland and Antarctic ice sheets and sea level rise related to glaciers (Martínez Montero et al., 2022). In version v3.0, we have added :

- an ocean layer of intermediate depth,
- a sediment box with $CaCO_3$ accumulation and burial fluxes,
- dynamic alkalinity cycling between the 3 ocean layers,
- an explicit description of the soft-tissue and carbonate pumps in the ocean,
- volcanic outgassing and weathering fluxes,
- an equation for the methane evolution in the atmosphere,
- a temperature and depth (pressure) dependence of the solubility and dissociation constants,
- a second equation for the land reservoir that allows for a better distinction between land-use and fossil greenhouse gas emissions.

SURFER v3.0 now consists of 17 coupled ordinary differential equations, while keeping its original architecture. It contains three main components, for, respectively, the carbon cycle, climate and the sea-level. The model is forced by land-use and fossil emissions of CO_2 and CH_4, and by aerosols injections. All the model components, the carbon and energy fluxes between those components, and the forcings are schematically summarised in figure 1.

In the following section, we explain in detail the model implementation. Sub-sections 2.1, 2.2, and 2.3 focus respectively on the implementation of the the carbon, climate and sea-level rise submodels. In sub-section 2.4 we show how the model was calibrated and how the initial conditions are chosen. Sub-section 2.5 discusses the algorithmic implementation and speed.

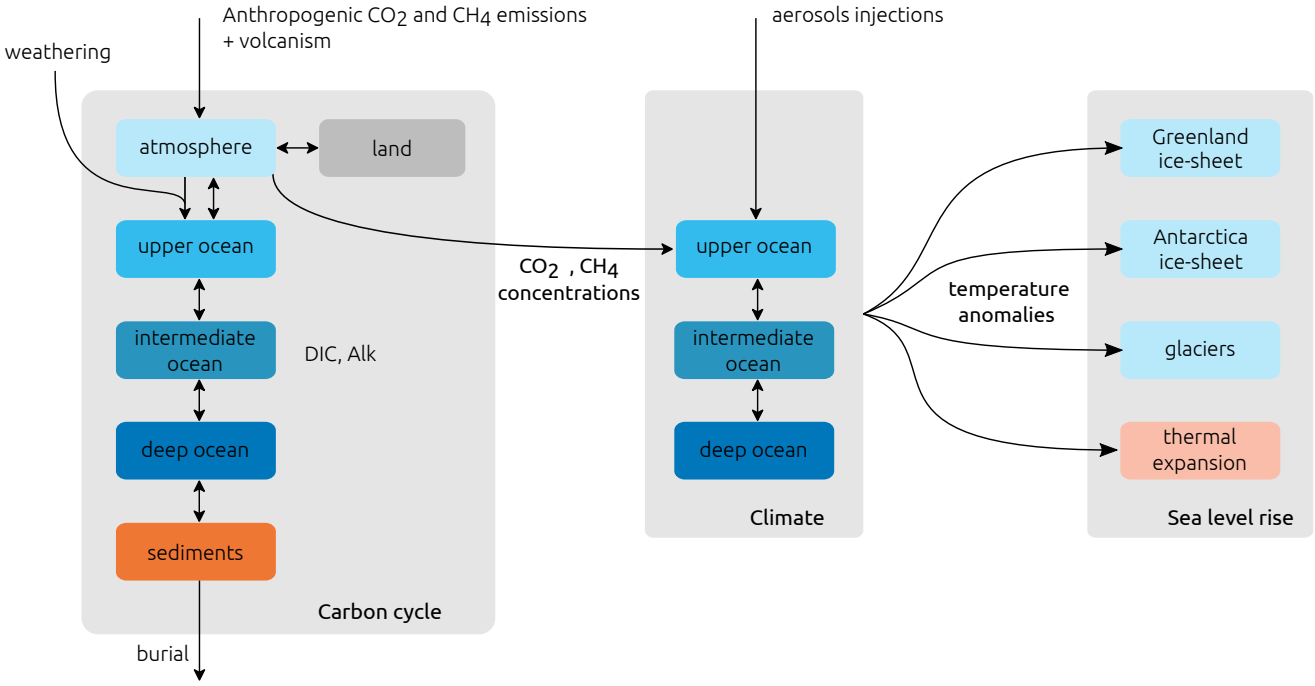

Figure 1. Conceptual diagram of SURFER v3.0.

2.1 Carbon cycle submodel

The equations for the carbon cycle submodel are given by

$$\frac{dM_A}{dt} = V + E^{\mathrm{CO_2}}_{\text{fossil}} + E^{\mathrm{CO_2}}_{\text{landuse}} - F_{A\to U} - F_{A\to L} + F_{\mathrm{CH_4}ox} - E^{\mathrm{CH_4}}_{\text{natural}} - F_{\text{weathering}} \tag{1}$$

$$\frac{dM_A^{\mathrm{CH_4}}}{dt} = E^{\mathrm{CH_4}}_{\text{fossil}} + E^{\mathrm{CH_4}}_{\text{landuse}} + E^{\mathrm{CH_4}}_{\text{natural}} - F_{\mathrm{CH_4}ox} \tag{2}$$

$$\frac{dM_L}{dt} = F_{A\to L} - E^{\mathrm{CO_2}}_{\text{landuse}} - E^{\mathrm{CH_4}}_{\text{landuse}} \tag{3}$$

$$\frac{dM_U}{dt} = F_{A\to U} - F_{U\to I} + F_{\text{river influx}} \tag{4}$$

$$\frac{dM_I}{dt} = F_{U\to I} - F_{I\to D} \tag{5}$$

$$\frac{dM_D}{dt} = F_{U\to D} - F_{\text{acc}} \tag{6}$$

$$\frac{d\tilde{Q}_U}{dt} = -\tilde{F}_{U\to I} + \tilde{F}_{\text{river influx}} \tag{7}$$

$$\frac{d\tilde{Q}_I}{dt} = \tilde{F}_{U\to I} - \tilde{F}_{I\to D} \tag{8}$$

$$\frac{d\tilde{Q}_D}{dt} = \tilde{F}_{I\to D} - \tilde{F}_{\text{acc}} \tag{9}$$

$$\frac{dM_S}{dt} = F_{\text{acc}} - F_{\text{burial}} \tag{10}$$

They describe the fluxes of carbon between six reservoirs, the atmosphere (A) , the land (L), the upper (U), intermediate (I), and deep (D) ocean layers, and the deep sea sediments (S). M_A and $M_A^{\mathrm{CH_4}}$ are the masses of carbon in the atmosphere in $\mathrm{CO_2}$ and CH_4 forms respectively. M_L is the mass of carbon on land (in vegetation and soils) and M_S is the mass of carbon in the erodible $\mathrm{CaCO_3}$ deep sea sediments. M_U, M_I and M_D are the masses of dissolved inorganic carbon in the ocean layers, while $\tilde{Q}_U$, $\tilde{Q}_I$, $\tilde{Q}_D$ are total alkalinities. All these quantities are expressed in PgC, and the fluxes in PgC yr $^{-1}$.

Variable names are chosen to be self-explanatory: Volcanism (V) and anthropogenic $\mathrm{CO_2}$ emissions ($E^{\mathrm{CO_2}}_{\text{fossil}}$, $E^{\mathrm{CO_2}}_{\text{landuse}}$) increase the $\mathrm{CO_2}$ content of the atmosphere. Methane anthropogenic emissions ($E^{\mathrm{CH_4}}_{\text{fossil}}$, $E^{\mathrm{CH_4}}_{\text{landuse}}$) as well as natural emissions ($E^{\mathrm{CH_4}}_{\text{natural}}$) increase the $\mathrm{CH_4}$ content in the atmosphere. Methane is rapidly oxidized into $\mathrm{CO_2}$ ($F_{\mathrm{CH_4}ox}$). Atmosphere and land reservoirs exchange $\mathrm{CO_2}$ through photosynthesis and respiration (combined in $F_{A\to L}$). Weathering fluxes ($F_{\text{weathering}}$) remove carbon dioxide from the atmosphere through chemical reactions with rocks and minerals. The products of these reactions are then transported to the ocean by the rivers ($F_{\text{river influx}}$, $\tilde{F}_{\text{river influx}}$). Carbon is exchanged between the different layers of the ocean by mixing and the different carbon pumps ($F_{U\to I}$, $F_{I\to D}$, $\tilde{F}_{U\to I}$, $\tilde{F}_{I\to D}$). Some carbon accumulates as sediments on the ocean floor (F_{acc}, $\tilde{F}_{\text{acc}}$) where it can be permanently buried (F_{burial}) and removed from the system. Ultimately, plate tectonics movements will transport this carbon in the mantle of the Earth (not explictely modelled in SURFER) where it will be transformed back to $\mathrm{CO_2}$ and eventually emitted in the atmosphere through volcanism, closing the cycle.

We detail the implementation of the above fluxes in sections 2.1.4 to 2.1.9. Before that, we motivate the addition of a new oceanic layer (section 2.1.1) and discuss the treatment of alkalinity (section 2.1.2) and of the solubility and dissociation constants (section 2.1.3).

2.1.1 Additional ocean layer

SURFER v2.0 used two ocean layers : an upper layer (U) of depth 150 m deep layer (D) of depth 3000 m. In SURFER v3.0, we split the original deep layer into an intermediate layer (I) of depth 500m and a deep layer (D) of depth 2500m. The depth of the bottom boundaries of these new layers are thus 150m , 650m and 3150m. The new layer allows for a smoother transition between the upper and deeper layers which have different properties (temperature, salinity, pH,...), see figure 5. It also allows for a faster carbon transport out of the upper layer, because the exchange with the new intermediate layer is faster than with the old deep layer. The modification partly fixes 2 problems we had in SURFER v2.0 : CO_2 uptake by the ocean was to slow and the surface pH decreased too fast (surface ocean acidified too quickly). Indeed, since the dissolved CO_2 now leaves the upper layer quicker, the surface ocean is able to absorb CO_2 from the atmosphere at faster rates. Moreover, with reduced "stagnation" of dissolved CO_2 in the upper layer, surface acidity increases slower (pH decreases slower). Differences in atmosphere to ocean carbon flux and surface ocean pH between SURFER v2.0 and SURFER v3.0 are plotted on figure 12.

2.1.2 Total alkalnity

Dissolved inorganic carbon (DIC) is defined as the sum of the carbonate species : carbonate ions CO_3^{2-}, bicarbonate ions HCO_3^- and $H_2CO_3^*$ which represents a mix of aqueous carbon dioxide , CO_2(aqueous) and carbonic acid H_2CO_3. In terms of concentrations, we have

$$\mathrm{DIC} = [H_2CO_3^*] + \left[HCO_3^-\right] + \left[CO_3^{2-}\right] \tag{11}$$

Alkalinity, on the other hand, is defined as the excess of bases over acids in water :

$$\mathrm{Alk} = \left[HCO_3^-\right] + 2\left[CO_3^{2-}\right] + \left[OH^-\right] - \left[H^+\right] + \left[B(OH)_4^-\right] + \text{ minor bases} \tag{12}$$

Intuitively, it measures the ability of a water mass to resist changes in pH when an acid is added. This happens for example when excess CO_2 in the atmosphere dissolves in seawater (see eqs 17-19). Alkalinity thus plays a crucial role in buffering ocean acidification, which is important for many marine organisms who depend on stable pH levels for their survival and growth. Being related to the concentrations of dissolved inorganic carbon species (CO_3^{2-} and HCO_3^-), alkalinity also has a role in regulating the oceanic uptake of atmospheric CO_2. In SURFER v2.0, alkalinity is considered constant and is furthermore approximated by carbonate alkalinity $\mathrm{Alk} \approx \mathrm{Alk}_c = \left[HCO_3^-\right] + 2\left[CO_3^{2-}\right]$. In SURFER v3.0, we include $CaCO_3$ sediment dissolution, and this required having variable alkalinity (equations 7-9). We estimate alkalinity based on the carbonate, borate and water self-ionisation alkalinity, which includes the contributions of the hydroxide ions $\left[OH^-\right]$, free protons $[H^+]$ and borate ions $\left[B(OH)_4^-\right]$:

$$\mathrm{Alk} \approx \mathrm{Alk}_{CBW} = \left[HCO_3^-\right] + 2\left[CO_3^{2-}\right] + \left[OH^-\right] - \left[H^+\right] + \left[B(OH)_4^-\right] \tag{13}$$

Compared to SURFERv2.0, this treatment produces more accurate computations of the concentration of chemical species, specifically $[H^+]$ and thus pH, but comes at a greater computational cost. See appendix B for more details.

We use units of PgC for the for the variables representing alkalinity $\tilde{Q}_U$, $\tilde{Q}_I$, and $\tilde{Q}_D$ even though our working approximation now include terms that do no contain carbon. We do this for purely practical reasons, as all other variables of the carbon cycle submodel are also in PgC. The alkalinity concentration Alk_i for the layer $i \in \{U, I, D\}$ in μmol kg^{-1}, a more common unit, is simply given by

$$\mathrm{Alk}_i = \frac{Q_i}{W_i \bar{m}_c} \times 10^{18} \tag{14}$$

where W_i is the weight in kg of ocean layer i, and $\bar{m}_c$ is the molar mass of carbon in mol kg^{-1}. This is the same equation as for the conversion from dissolved organic carbon mass in PgC to concentration in μmol kg^{-1}

$$\mathrm{DIC}_i = \frac{M_i}{W_i \bar{m}_c} \times 10^{18} \tag{15}$$

The weight of layer i is given by

$$W_i = \frac{h_i \bar{m}_w m_O}{h_U + h_I + h_D} \tag{16}$$

with $\bar{m}_w$ the molar mass of water and m_O the number of moles in the ocean.

2.1.3 Solubility and dissociation constants

When atmospheric CO_2 enters the ocean, it undergoes a series of chemical reactions

$$\mathrm{CO}_{2(\mathrm{gas})} + \mathrm{H}_2\mathrm{O} \rightleftharpoons \mathrm{H}_2\mathrm{CO}_3^* \tag{17}$$

$$\mathrm{H}_2\mathrm{CO}_3^* \rightleftharpoons \mathrm{HCO}_3^- + \mathrm{H}^+ \tag{18}$$

$$\mathrm{HCO}_3^- \rightleftharpoons \mathrm{CO}_3^{2-} + 2\mathrm{H}^+ \tag{19}$$

These reactions are fast and so we assume that they are in equilibrium. The relationships between the equilibrium concentrations of the different chemical species are determined by the dissociation constants :

$$K_1 = \frac{[\mathrm{H}^+][\mathrm{HCO}_3^-]}{[\mathrm{H}_2\mathrm{CO}_3^*]} \tag{20}$$

$$K_2 = \frac{[\mathrm{H}^+][\mathrm{CO}_3^{2-}]}{[\mathrm{HCO}_3^-]} \tag{21}$$

Similarly, we have for the equilibrium concentrations of OH^- and $\mathrm{B(OH)}_4^-$

$$K_w = \left[\mathrm{H}^+\right]\left[\mathrm{OH}^-\right] \tag{22}$$

$$K_b = \frac{[\mathrm{H}^+]\left[\mathrm{B(OH)}_4^-\right]}{[\mathrm{H}_3\mathrm{BO}_3]} \tag{23}$$

where we additionally assume that the total equilibrium boron concentration is proportional to salinity (Uppström, 1974) :

$$\mathrm{TB} = \left[\mathrm{B(OH)}_4^-\right] + [\mathrm{H}_3\mathrm{BO}_3] = c_b \cdot S \tag{24}$$

with $c_b = 11.88$ μmol kg^{-1} psu^{-1}. The solubility of CO_2 in seawater, K_0, relates the concentration of $H_2CO_3^*$ and the partial pressure of dissolved CO_2, pCO_2 :

$$K_0 = \frac{[H_2CO_3^*]}{pCO_2} \tag{25}$$

In SURFER v2.0, we kept K_0, K_1 and K_2 constant. In this new version, we introduce a dependence on temperature, salinity, and pressure (depth). Salinity is assumed to be constant, so we effectively only have a dependence on temperature and depth. For the temperature (and salinity) dependence, we use the equations from Sarmiento and Gruber (2006), and originally from Weiss (1974); Mehrbach et al. (1973); Dickson and Millero (1987); Millero (1995); Dickson (1990)

$$\begin{aligned}\ln K_0 =& -60.2409 + 93.4517\left(\frac{100}{T}\right) + 23.3585\ln\left(\frac{T}{100}\right)\\ &+ S\left(0.023517 - 0.023656\left(\frac{T}{100}\right) + 0.0047036\left(\frac{T}{100}\right)^2\right)\end{aligned} \tag{26}$$

$$\begin{aligned}-\log K_1^0 =& -62.008 + \frac{3670.7}{T} + 9.7944\ln(T)\\ &- 0.0118S + 0.000116S^2\end{aligned} \tag{27}$$

$$-\log K_2^0 = +4.777 + \frac{1394.7}{T} - 0.0184S + 0.000118S^2 \tag{28}$$

$$\begin{aligned}\ln K_b^0 =& \frac{1}{T}\left(-8966.9 - 2890.53S^{1/2} - 77.942S + 1.728S^{3/2} - 0.0996S^2\right)\\ &+ 148.0248 + 137.1942S^{1/2} + 1.62142S + 0.053105S^{1/2}T\\ &+ \ln T(-24.4344 - 25.085S^{1/2} - 0.2474S)\end{aligned} \tag{29}$$

$$\begin{aligned}\ln K_w^0 =& 148.96502 + \frac{-13847.26}{T} - 23.6521\ln T\\ &S^{1/2}\left(-5.977 + \frac{118.67}{T} + 1.0495\ln T\right) - 0.01615S\end{aligned} \tag{30}$$

Here, K_0, K_1^0, K_2^0, K_w^0 and K_b^0 are the values of the constants at atmospheric pressure, given in mol (kg atm)$^{-1}$ for K_0, in mol kg^{-1} for K_1^0, K_2^0, K_b^0, and in (mol kg^{-1})^2 for K_w^0 , T is the temperature in Kelvin and S is the salinity on the practical salinity scale. In SURFER, only temperature anomalies are computed, meaning that to compute the absolute temperature and then the dissociation constants, we need to provide an initial temperature for each layer. This is done in section 2.4.2.

The pressure (depth) dependence for K_1, K_2, K_w and K_b is from Millero (1995),

$$\ln\left(K_i^p / K_i^0\right) = -\frac{\Delta V_i}{RT}P + \frac{0.5\Delta K_i}{RT}P^2 \tag{31}$$

where K_i^p is the value of the dissociation constant at pressure P (in bar), K_i^0 is the value of the dissociation constant at atmospheric pressure (1.01325 bar or 101325 Pa), T is the temperature in Kelvin and R is the gas constant in bar cm^3 mol^{-1} K^{-1} (10 times the value in J mol^{-1} K^{-1}) . The quantities ΔV_i and ΔK_i are changes in molal volume and compressibility and are

	a_0	a_1	a_2	b_0	b_1
K_1	-25.50	0.1271	0	-3.08	0.0877
K_2	-15.82	-0.0219	0	1.13	-0.1475
K_b	-29.48	0.1622	-0.002608	-2.84	0
K_w	-25.60	0.2324	0.0036246	-5.13	0.0794

Table 1. Parametrisation for the effect of pressure on dissociation constants ; coefficients for equations 32 and 33. The values are taken from Millero (1995). We have flipped the signs of a_1 and a_2 for K_b to match the values given in Millero (1979). Also, note that there are some typos in Millero (1995): right hand side of equation 92 should be multiplied by 1000.

estimated following :

$$\Delta V_i = a_{0,i} + a_{1,i}(T - 273.15) + a_{2,i}(T - 273.15)^2 \tag{32}$$

$$1000\Delta K_i = b_{0,i} + b_{1,i}(T - 273.15) \tag{33}$$

Values for the coefficients can be found in table 1. Hydrostatic balance provides the pressure at a given depth, thus, pressure (in bar) is given by $P = \rho g z/100000$ where $\rho = 1026kg/m^3$ is sea water mean density, $g = 9.81kgm/s^2$ is the gravitational acceleratino and z is the depth (in m). For the different ocean levels U,I and D, we use the depths $z_U = 75$ m , $z_I = 400$ m and $z_D = 1900$ m which corresponds to the mid depth points of the layers.

2.1.4 $F_{A\to U}$

We derive an expression for the atmosphere to ocean flux $F_{A\to U}$ in a slightly different way than in SURFER v2.0. The sea-air CO_2 exchange is proportional to the difference in CO_2 partial pressure between the atmosphere and the surface ocean layer. We have

$$F_{A\to U} = \bar{m}_C A_O \rho k K_0 (p^A_{CO_2} - p^U_{CO_2}) \tag{34}$$

where A_O is the ocean surface area (in m^2), ρ is the density of sea-water (in kg m^3), $\bar{m}_C$ is the molar mass of carbon (in kg mol^{-1}), k is the gas transfer velocity (in m yr^{-1}) and K_0 is the solubility constant of CO_2 (in mol kg^{-1} atm^{-1}). This same expression is used by Lenton (2000) and Zeebe (2012), for carbon cycles models of similar complexity, with a multiplication by the molar mass of carbon $\bar{m}_C$ to obtain a flux in kg yr^{-1} instead of mol yr^{-1}. We can express $p^A_{CO_2}$ and $p^U_{CO_2}$ in terms of

model variables M_A and M_U

$$F_{A\to U} = \bar{m}_C A_O \rho k K_0 (p^A_{\mathrm{CO}_2} - p^U_{\mathrm{CO}_2}) \tag{35}$$

$$= \bar{m}_C A_O \rho k K_0 \left(\frac{M_A}{m_A \bar{m}_C} \cdot 1\,\mathrm{atm} - \frac{M'_U}{W_U \bar{m}_C K_0} \right) \tag{36}$$

$$= \frac{A_O \rho k}{m_A} K_0 \left(M_A \cdot 1\,\mathrm{atm} - \frac{m_A}{W_U K_0} \frac{M'_U}{M_U} M_U \right) \tag{37}$$

$$= \bar{k}_{A\to U} K_0 \left(M_A \cdot 1\,\mathrm{atm} - \frac{m_A}{W_U K_0} B(M_U, \tilde{Q}_U, T_U) M_U \right) \tag{38}$$

Here, M'_U represents the mass of $\mathrm{H_2CO_3^*}$ in the upper ocean layer. The factor $1\,\mathrm{atm}$ is introduced for unit consistency and if M_A and M_U are expressed in PgC, then the flux will be in $PgCyr^{-1}$. We have defined $\bar{k}_{A\to U} = \frac{A_O \rho k}{m_A}$. We would recover the equation of SURFERv2.0 with $k_{A\to U} = \bar{k}_{A\to U} K_0$, but we do not do that since K_0 now depends on temperature. There are two advantages of proceeding as we did here compared to SURFER v2.0. First the coefficient $\bar{k}_{A\to U}$ is a function of known physical quantities. Second, we have not used the equilibrium condition for $F_{A\to U}(t_{PI})$ for the derivation of our expression, meaning that we can use it to constrain other quantities. Indeed, once $\bar{k}_{A\to U}$ and M_A are set, the equilibrium condition $F_{A\to U}(t_{PI}) = -(F_{\mathrm{CaCO_3},0} + F_{\mathrm{CaSiO_3},0})$ will determine M'_U (see section 2.4.2).

The term B_U is a factor tracking the ocean's buffer capacity. In SURFER v2.0, it only was a function of M_U (an constant $\tilde{Q}_U$). Now, the buffer factor also depends on the variable alkalinity and on temperature through the dissociation constants:

$$B_U\left(M_U, \tilde{Q}_U, T_U\right) \equiv \frac{M'_U}{M_U} = \frac{[\mathrm{H_2CO_3}^*]_U}{\mathrm{DIC}_U} = \left(1 + \frac{K_1}{[\mathrm{H}^+]_U} + \frac{K_1 K_2}{[\mathrm{H}^+]_U^2}\right)^{-1} \tag{39}$$

To obtain this equation, we have used equations 20 and 21 to write DIC (eq 11) in terms of $[\mathrm{H_2CO_3^*}]_U$ and $[\mathrm{H}^+]$. In SURFER v2.0, we could simply simply $[\mathrm{H}^+]$ and B as a function of M_U and $\tilde{Q}_U$. We cannot do that anymore because we use a more complete approximation for alkalinity. We can still compute $[\mathrm{H}^+]$ as a function of M_U and $\tilde{Q}_U$ (and the dissociation constants), but we have to numerically solve a degree 5 equation in $[\mathrm{H}^+]$. Appendix B provides more details on how we proceed.

2.1.5 $F_{U\to I}$, $F_{I\to D}$, $\tilde{F}_{U\to I}$, and $\tilde{F}_{I\to D}$

We now focus on carbon transport within the ocean. The processes and fluxes included in SURFER v3.0 are schematised in figure 2. Carbon enters the upper ocean layer (U) through $\mathrm{CO_2}$ exchanges with the atmosphere and through riverine influx of weathering products. $\mathrm{CO_2}$ intake from the atmosphere increases DIC but doesn't change alkalinity (see equations 17-19). This is why we have a $F_{A\to U}$ DIC flux but no $\tilde{F}_{A\to U}$ alkalinity flux. The riverine influx of weathering products increases DIC and alkalinity in the same amount (1:1 ratio); see section 2.1.7. We divide the exchange of carbon between the ocean layers in three parts which we explain below : the carbonate pump, the soft-tissue pump and residual processes.

In the surface layer, calcifying organisms take up bicarbonate ions to form their calcium carbonate ($\mathrm{CaCO_3}$) shells (forward reaction 40).

$$\mathrm{Ca^{2+} + 2HCO_3^- \rightleftharpoons CO_2 + H_2O + CaCO_3} \tag{40}$$

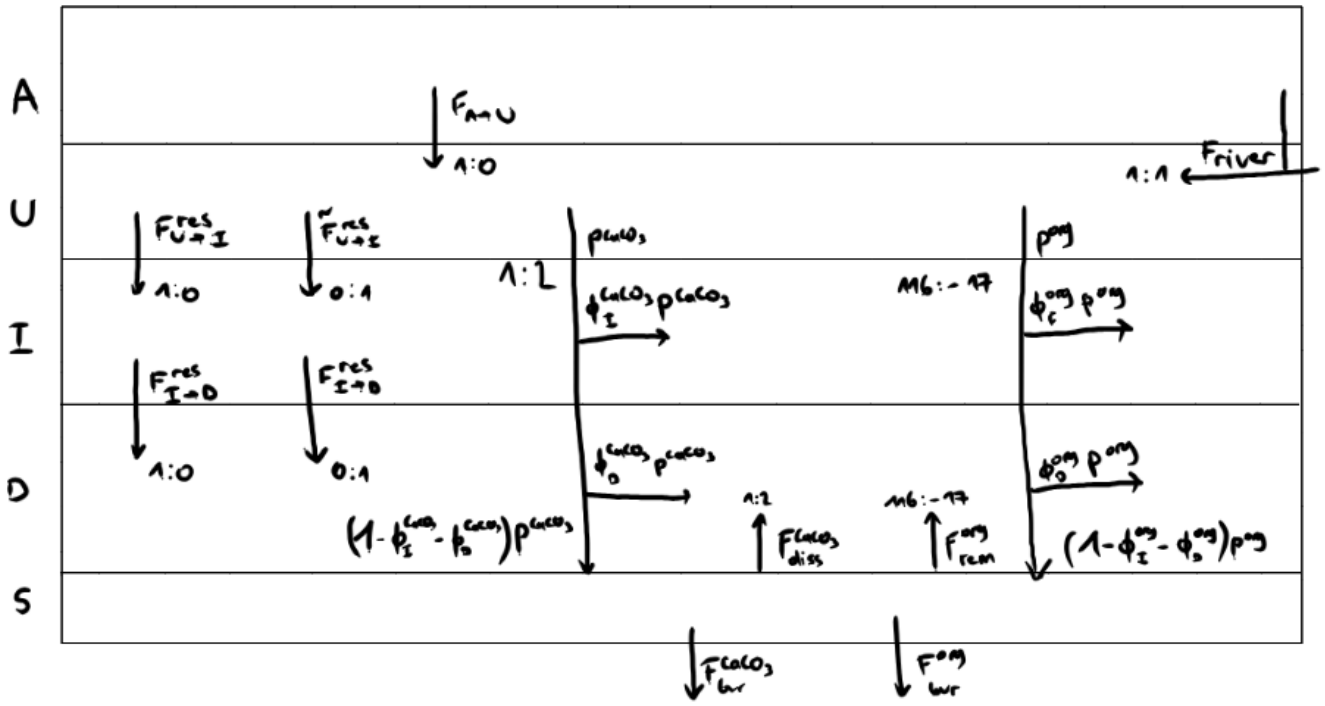

Figure 2. Schematic diagram of the DIC and Alk fluxes. For the moment, only quick draft of the figure. If it is useful, I will make a cleaner version. The ratios are ratios of DIC to alkalinity changes, i.e a $a : b$ ratio indicates that for a change in DIC of a moles, there is an associated alkalinity change of b moles.

These organisms eventually die and sink to the bottom ocean. On the way down some of the $CaCO_3$ is dissolved (reverse reaction 40), resulting in a downward transport of DIC and alkalinity at a 1:2 ratio. This is the carbonate pump. We represent the export of $CaCO_3$ at a depth of 150m (so from layer U to I) by P^{CaCO_3}. We consider that a fraction $\phi_I^{CaCO_3}$ of this export simultaneously dissolves in the intermediate layer (I) and that a fraction $\phi_D^{CaCO_3}$ simultaneously dissolves in the deep layer (D). That leaves a fraction $1 - \phi_I^{CaCO_3} - \phi_D^{CaCO_3}$ that reaches the bottom ocean sediments, in what we call the $CaCO_3$ rain. Of the $CaCO_3$ that reaches the bottom of the ocean, some will dissolve and some will be permanently buried (more detail on sediments dissolution and burial in section 2.1.6).

In the surface layer, organisms also take up carbon through photosynthesis (primary production, forward reaction 41).

$$106CO_2 + 16NO_3^- + HPO_4^{2-} + 122H_2O + 18H^+ \rightleftharpoons (CH_2O)_{106}(NH_3)_{16}(H_3PO_4) + 138O_2 \quad (41)$$

The CO_2 is transformed into organic carbon that will eventually sink to the bottom ocean. On the way down some of the organic carbon is remineralised (reverse reaction 41), resulting in a downward transport of DIC. This is the soft-tissue pump. It also acts on alkalinity, mainly through the uptake and release of H^+ needed for the transformation of inorganic nitrate (NO_3^-) into organic nitrogen. Primary production of organic matter increases alkalnity, while remineralisaton decreases alkalinity. We

represent the ratio of alkalinity to DIC change for primary production and remineralisation with the parameter $\sigma_{\mathrm{Alk:DIC}}$. We represent the export of organic carbon at a depth of 150m (so from layer U to I) by P^{org}. We consider that a fraction ϕ_I^{org} of this export is simultaneously remineralised in the intermediate layer (I) and that a fraction ϕ_D^{org} is simultaneously remineralised in the deep layer (D). That leaves a fraction $1-\phi_I^{org}-\phi_D^{org}$ that reaches the bottom ocean sediments, in what we call the organic carbon rain. Of the organic carbon that reaches the bottom of the ocean, most will be remineralised in the surface sediments and some will be permanently buried (more detail on sediments remineralisation and burial in section 2.1.6).

Apart from the carbonate and soft tissue pumps (called together the biological pumps), other processes are responsible for the transport of carbon between the ocean layers. Ocean circulation and mixing will propagate variations in DIC caused by spatial and temporal variations of air-sea gas exchanges. This is termed the gas exchange pump by Sarmiento and Gruber (2006). For example, a component of the gas exchange pump is the solubility pump (Volk and Hoffert, 1985) : cold waters have a higher solubility and are thus enriched in CO_2, they are also denser and will sink in the high latitudes, resulting in a downward transport of DIC. Besides, at equilibrium, upwelling waters are responsible for an upward transport of DIC and alkalinity, that is necessary to counteract the carbonate and soft-tissue pumps and and to avoid having ever increasing DIC and alkalinity vertical gradients. We gather all the processes related to ocean circulation and mixing in the residual terms $F^{\mathrm{res}}_{U\to I}$ and $F^{\mathrm{res}}_{I\to D}$, $\tilde{F}^{\mathrm{res}}_{U\to I}$ and $\tilde{F}^{\mathrm{res}}_{I\to D}$. We consider the residual fluxes of DIC and alkalinity to be independent because some processes such as the solubility pump only act on DIC.

In equations, this gives for the masses of dissolved organic carbon and the mass of carbon in the sediments

$$\frac{dM_U}{dt} = F_{A\to U} - P^{CaCO_3} - P^{\mathrm{org}} - F^{\mathrm{res}}_{U\to I} + F_{\text{river influx}} \tag{42}$$

$$\frac{dM_I}{dt} = \phi_I^{CaCO_3} P^{CaCO_3} + \phi_I^{\mathrm{org}} P^{\mathrm{org}} + F^{\mathrm{res}}_{U\to I} - F^{\mathrm{res}}_{I\to D} \tag{43}$$

$$\frac{dM_D}{dt} = \phi_D^{CaCO_3} + \phi_D^{\mathrm{org}} P^{\mathrm{org}} + F^{\mathrm{res}}_{I\to D} + F^{CaCO_3}_{\text{dissolution}} + F^{\mathrm{org}}_{\text{remineralisation}} \tag{44}$$

$$\frac{dM_S}{dt} = (1-\phi_I^{CaCO_3}-\phi_D^{CaCO_3})P^{CaCO_3} - F^{CaCO_3}_{\text{dissolution}} - F^{CaCO_3}_{\text{burial}} \tag{45}$$

$$\frac{dM_S^{\mathrm{org}}}{dt} = (1-\phi_I^{\mathrm{org}}-\phi_D^{\mathrm{org}})P^{\mathrm{org}} - F^{\mathrm{org}}_{\text{remineralisation}} - F^{\mathrm{org}}_{\text{burial}} \tag{46}$$

where M_S^{org} is the mass of organic carbon in the sediments that are "remineralisable". In fact, the majority of organic carbon that rains on the sea-floor sediments is remineralised and only a very small amount is permanently buried (need ref). Here, we neglect this burial by setting $F^{\mathrm{org}}_{\text{burial}} = 0$ and $F^{\mathrm{org}}_{\text{remineralisation}} = (1-\phi_I^{\mathrm{org}}-\phi_D^{\mathrm{org}})P^{\mathrm{org}}$, such that all organic carbon that falls on sediments is remineralised. We are thus left with $\frac{dM_S^{\mathrm{org}}}{dt} = 0$ for the evolution of organic carbon mass in the sediments and this is the reason it is not included the model equations. We can recover equations 1-10 by setting

$$F_{U\to I} = F^{CaCO_3}_{U\to I} + F^{\mathrm{org}}_{U\to I} + F^{\mathrm{res}}_{U\to I} \tag{47}$$

$$F_{I\to D} = F^{CaCO_3}_{I\to D} + F^{\mathrm{org}}_{I\to D} + F^{\mathrm{res}}_{I\to D} \tag{48}$$

$$F_{\text{acc}} = (1-\phi_I^{CaCO_3}-\phi_D^{CaCO_3})P^{CaCO_3} - F^{CaCO_3}_{\text{dissolution}} \tag{49}$$

$$F_{\text{burial}} = F^{CaCO_3}_{\text{burial}} \tag{50}$$

with fluxes associated to the carbonate pump defined as

$$F_{U\to I}^{CaCO_3} = P^{CaCO_3} \tag{51}$$

$$F_{I\to D}^{CaCO_3} = (1-\phi_I^{CaCO_3})P^{CaCO_3} \tag{52}$$

and the fluxes associated to the soft-tissue pump defined as

$$F_{U\to I}^{\text{org}} = P^{\text{org}} \tag{53}$$

$$F_{I\to D}^{\text{org}} = (1-\phi_I^{\text{org}})P^{\text{org}} \tag{54}$$

Consequently, for the carbonate alkalinity fluxes, we have

$$\tilde{F}_{U\to I} = 2\times F_{U\to I}^{CaCO_3} + \sigma_{Alk:\mathrm{DIC}} \times F_{U\to I}^{\text{org}} + \tilde{F}_{U\to I}^{\text{res}} \tag{55}$$

$$\tilde{F}_{I\to D} = 2\times F_{I\to D}^{CaCO_3} + \sigma_{Alk:\mathrm{DIC}} \times F_{I\to D}^{\text{org}} + \tilde{F}_{I\to D}^{\text{res}} \tag{56}$$

$$\tilde{F}_{\text{acc}} = 2\times F_{\text{acc}}^{CaCO_3} \tag{57}$$

In the experiments presented here (IN SECTION XX), we will keep P^{CaCO_3}, $\phi_I^{CaCO_3}$, $\phi_D^{CaCO_3}$, P^{org}, ϕ_I^{org}, and ϕ_D^{org} constant. In reality, they can change. Production and export of $\mathrm{CaCO_3}$ and organic matter are biological processes and thus depend on the temperature, pH, salinity, nutrient concentration and other properties of the ocean. For example, changes in primary production (and thus export of organic matter) is one of the processes suspected to have contributed to the $\mathrm{CO_2}$ changes during the glacial-intergalcial cycles (Kohfeld and Ridgwell (2009)). In the future, changes in the biological pumps are also possible and might lead to additional feedbacks in the carbon cycle (Henson et al., 2022; Planchat et al., 2023).

As the residual exchange terms represent processes linked with ocean circulation, they should depend on DIC and alkalinity in each layer. Similarly as in SURFER v2.0, we set

$$F_{U\to I}^{\text{res}} = k_{U\to I}M_U - k_{I\to U}M_I \tag{58}$$

$$F_{I\to D}^{\text{res}} = k_{I\to D}M_I - k_{D\to I}M_D \tag{59}$$

$$\tilde{F}_{U\to I}^{\text{res}} = \tilde{k}_{U\to I}\tilde{Q}_U - \tilde{k}_{I\to U}\tilde{Q}_I \tag{60}$$

$$\tilde{F}_{I\to D}^{\text{res}} = \tilde{k}_{I\to D}\tilde{Q}_I - \tilde{k}_{D\to I}\tilde{Q}_D \tag{61}$$

2.1.6 $\boldsymbol{F}_{\text{acc}}$, $\boldsymbol{F}_{\text{acc}}^{\text{alk}}$, and $\boldsymbol{F}_{\text{burial}}$

The process of $\mathrm{CaCO_3}$ accumulation on the ocean floor begins with the precipitation of calcium carbonate ($\mathrm{CaCO_3}$) in the form of shells or skeletons by marine organisms, through equation 40. These shells and skeletons eventually sink to the ocean floor, in what is called the $\mathrm{CaCO_3}$ rain ($(1-\phi_I^{\mathrm{CaCO_3}}-\phi_D^{\mathrm{CaCO_3}})P^{\mathrm{CaCO_3}}$ in our model). There, they either accumulate and are eventually buried in sediments or they dissolve, depending on the saturation state of the ocean waters with respect to $\mathrm{CO_3^{2-}}$. Typically, the upper ocean is supersaturated in $\mathrm{CO_3^{2-}}$ while the deeper ocean is under-saturated, mainly due to the pressure dependence of $\mathrm{CaCO_3}$ solubility. This means that most of the accumulation in sediments will happen in a region above where

most of the dissolution happens. A transition zone separates the accumulation and dissolution regions. The top boundary of the transition zone is the lysocline, which is defined as the depth where the calcium carbonate content of sediments starts to decrease sharply, or in other words, the depth below which the rate of dissolution of $\mathrm{CaCO_3}$ starts to increase significantly. The bottom boundary of the transition zone is called the carbonate (or calcite) compensation depth (CCD), and is the depth at which the rate of $\mathrm{CaCO_3}$ dissolution is equal to the rate of supply through the $\mathrm{CaCO_3}$ rain. Below this depth, no $\mathrm{CaCO_3}$ is preserved in the sediments. The depth of the transition zone varies between places and ocean basins but is generally between 3000 and 5000 m deep. This means that we can consider that both dissolution and accumulation mainly happen in the deep ocean layer (D) of our model and that is why we group both processes in a single term, F_{acc} which can be positive or negative (with negative values indicating net dissolution). We neglect accumulation processes on continental shelves.

Let us focus on a sediment column at a particular location on the ocean floor. Say that we are below the carbonate compensation depth, a situation where the rate of dissolution of $\mathrm{CaCO_3}$ already present on the sea floor exceeds the rate of deposition from $\mathrm{CaCO_3}$ rain. The situation is depicted in figure 3. Dissolution only happens in the first few centimeters of the sediments, near the ocean-sediments interface. However, mixing from biological activity (bioturbation) exposes deeper sediments to dissolution. The bioturbation activity decreases with depth and takes place only in what is called the bioturbation layer. The depth of this layer varies but is typically of the order of 10 cm. If dissolution exceeds the total rain rate of $\mathrm{CaCO_3}$ and non-$\mathrm{CaCO_3}$ (non-erodible/detrital) material, the sediments will loose mass. Bioturbation will then bring back to the surface old $\mathrm{CaCO_3}$ that was previously out of reach for dissolution; this is called chemical erosion. As long as the amount of dissolved $\mathrm{CaCO_3}$ exceeds the rain rate of $\mathrm{CaCO_3}$, its concentration in the bioturbated layer of the sediments will decrease while the concentration of non-erodible material will increase. The bioturbated layer will eventually become saturated in non-erodible material and once this happens, dissolution will stop. There is still some $\mathrm{CaCO_3}$ in the sediments, but it is too deep beneath the sediment-ocean interface to be exposed to dissolution, even with the help of bioturbation. This is why there only is a limited amount of erodible $\mathrm{CaCO_3}$ in the ocean sediments. This amount is evaluated to be around 1750 PgC as of today (int, 2023).

The local dissolution rate of $\mathrm{CaCO_3}$ can be described with the following equation

$$\frac{d[CaCO_3]}{dt} = -k_{CaCO_3}[CaCO_3](1-\Omega)^n \quad \text{, for } \Omega > 1 \tag{62}$$

where $[\mathrm{CaCO_3}]$ is the concentration of $\mathrm{CaCO_3}$ in the sediments, $k_{\mathrm{CaCO_3}}$ is a dissolution rate constant, n is an exponent representing the order of the reaction and Ω is the saturation state of pore water around the sediments with respect to carbonate (Sarmiento and Gruber, 2006). The saturation state of the sediment pore water can be approximated as $\Omega \approx [\mathrm{CO_3^{2-}}]/[\mathrm{CO_3^{2-}}]_{\text{sat}}$ where $[\mathrm{CO_3^{2-}}]_{\text{sat}}$ is different for calcite and aragonite. It depends, on the saturation state of the water just above the sediment-ocean interface, but also on the remineralisation rate of organic mater in the sediments (Berger, 1970; Archer, 1991) . This is because remineralisation of organic mater (reverse reaction 41) releases $\mathrm{CO_2}$ into pore water and thus changes the equilibrium of the carbonate species (see equations 17-19).

To obtain the global dissolution flux, we need to integrate equation 62 over the sediment column and over the ocean floor

$$F_{diss} = \int\limits_{\text{ocean floor}} \left(\int\limits_{z_{max}}^{0} k_{\mathrm{CaCO_3}}[\mathrm{CaCO_3}](1-\Omega)^n \, dz \right) dA \tag{63}$$

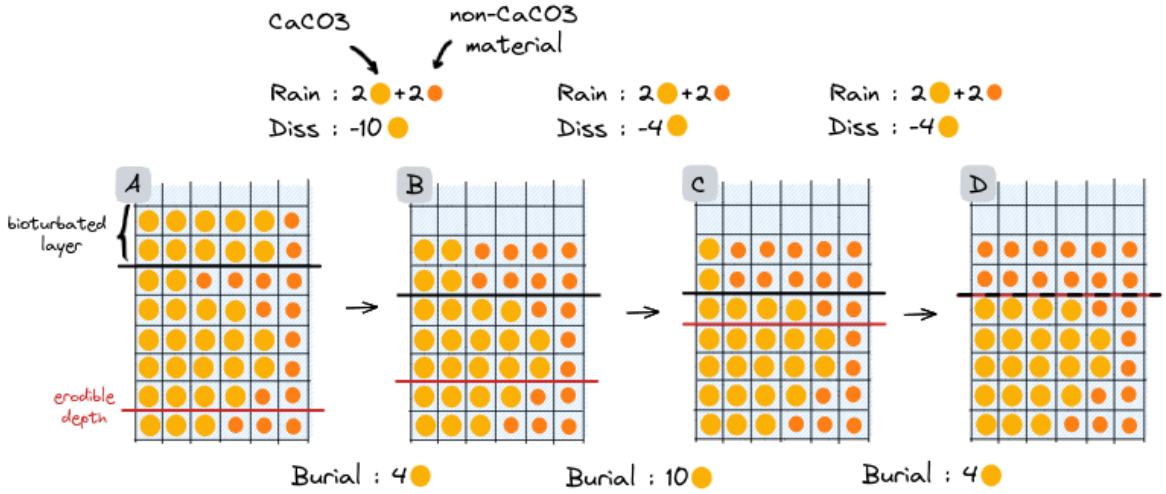

Figure 3. Schematic diagram of dissolution and accumulation processes in a sediment column. Here, we are below the carbonate compensation depth and the loss of $CaCO_3$ from dissolution is greater than input from rain. The sediment column is divided in little squares which represent units of sediment volume. Sediments are composed of pore water (blue), $CaCO_3$ (yellow) and non-$CaCO_3$ material that is not dissolvable (orange). The thick black line delimits the bioturbated layer, which we take here as the two top layers of the sediment column. The magenta line is the erodible depth. It delineates a region that contains the volume of non-$CaCO_3$ material necessary to fill the bioturbated layer. In the schematic example depicted here, the bioturbated layer has a volume of 12 units, and so the erodible depth will dilineate a region in which there are 12 units of non-$CaCO_3$ material (orange dots). We consider the evolution of the sediment column for 3 (arbitrary) time steps. The rain rates of $CaCO_3$ and non-$CaCO_3$ material are considered constant (2 units of each per time step) whereas dissolution rate can change. From **A** to **B**, 10 units of $CaCO_3$ are dissolved. The net accumulation of $CaCO_3$ is -8 units and so we should be left with two units of $CaCO_3$ in the bioturbated layer. However, because the net accumulation of material in the sediments is negative (-6 volume units), the sediments loose mass and bioturbation, which always happen in the top two layers of our column, effectively brings back 2 additional units of old $CaCO_3$ in the bioturbated layer. This is the process of chemical erosion. Also, since rain has added two units of non-$CaCO_3$ material on the top of the sediment column, the erodible depth has to move up to keep enclosing a region containing 12 units of non-$CaCO_3$ material. If we place ourselves in the referential of the erodible depth, we can say that 4 units of $CaCO_3$ "passed through" the erodible depth. By definition, those 4 units will never be dissolved and we say that they are buried. From **B** to **C**, 4 units of $CaCO_3$ are dissolved. The net accumulation of material in the sediments is zero and there is no chemical erosion. However, since the net accumulation of $CaCO_3$ is negative (-2 units), the amount of $CaCO_3$ in the bioturbated layer is still decreasing. The erodible depth has to move up by two layers. This leads to the burial of 10 units of $CaCO_3$. In general, the volume of sediments passing through the erodible depth per time step can be computed as the rain rate of non-$CaCO_3$ material (2 units per time step), divided by the concentration of non-$CaCO_3$ at the erodible depth (here 1 unit per 6 volume units of sediments). Further multiplying by the concentration of $CaCO_3$ at the erodible depth (here 5 units per 6 volume units of sediments), we obtain the amount of $CaCO_3$ buried per time step. From **C** to **D**, 4 units of $CaCO_3$ are dissolved. The net accumulation of material in the sediments is zero and there is no chemical erosion. Since the net accumulation of $CaCO_3$ is negative (-2 units), the amount of $CaCO_3$ in the bioturbated layer is still decreasing and reaches zero. The bioturbated layer is entirely filled with non-erodible material and dissolution stops, even though there is still some $CaCO_3$ deeper in the sediment column.

Here, z is the depth below the ocean-sediment interface, and z_{max} is a cut-off depth below which there is no dissolution. Now, we make a simplifying hypothesis : we suppose that the right hand side of equation 66 is a function of only two variables, the deep ocean mean concentration of CO_3^{2-} and the total mass of erodible $CaCO_3$ in the sediments. We do not explicitly include a dependence on the rate of organic mater remineralisation (F_{rem}^{org}) since we consider it constant. Furthermore, since we do not know the functional dependence of dissolution rate on these two quantities, we assume a Taylor expansion around the preindustrial state. We get the following parametrisation

$$F_{diss} = F_{diss}([CO_3^{2-}]_D, M_S) \tag{64}$$

$$\begin{aligned} &= F_{diss,0} + \alpha_{diss}\left([CO_3^{2-}]_D - [CO_3^{2-}]_D(t_{PI})\right) + \beta_{diss}\left(M_S - M_S(t_{PI})\right) \\ &\quad + \gamma_{diss}\left([CO_3^{2-}]_D - [CO_3^{2-}]_D(t_{PI})\right)\left(M_S - M_S(t_{PI})\right) \end{aligned} \tag{65}$$

A similar parametrisation is proposed and tested in Archer et al. (1998), but they use the CO_3^{2-} concentration at a particular point in the deep pacific and the mass of $CaCO_3$ in the bioturbated layer of the sediments as their two variables, instead of the mean deep ocean CO_3^{2-} and the mass of erodible $CaCO_3$. They show that the parametrised version of their model is comparable to the non-parametrised one, except for a dissolution spike in the first 1000-2000 years following the fossil fuel emissions and invasion in the ocean. We choose the coefficient of our parametrisation based on theirs. Details can be found in section 2.4.1.

To describe burial fluxes, a useful concept is the one of "erodible depth". It is defined as the potential reach of dissolution when there is no rain of non-$CaCO_3$ material. In other words, it is the depth that delineates a region (from the sediment-ocean interface to this depth) which contains exactly the amount of non-$CaCO_3$ material necessary to fill the bioturbated layer (for an example, see figure 3). By definition, the amount of non-$CaCO_3$ material in the sediment column above the erodible depth is constant. Consequently, when an amount x of non-$CaCO_3$ material reaches the top, the same amount must leave (the????) the erodible depth. The volume of sediments passing through the erodible depth is$x/[\text{non-}CaCO_3]_{z_{\text{erodible}}}$, where $[\text{non-}CaCO_3]_{z_{\text{erodible}}}$ is the concentration of non-$CaCO_3$ material in the sediments at the erodible depth. This volume contains a $CaCO_3$ amount equal to $x \times [CaCO_3]_{z_{\text{erodible}}}/[\text{non-}CaCO_3]_{z_{\text{erodible}}}$, where $[CaCO_3]_{z_{\text{erodible}}}$ is the concentration of $CaCO_3$ material in the sediments at the erodible depth. The $CaCO_3$ that is now below the erodible depth will never be dissolved and we say that it has been buried. The global burial flux can thus be described as erodible

$$F_{bur} = \int_{\text{ocean floor}} r_{det} \frac{[CaCO_3]_{z_{\text{erodible}}}}{[\text{non-}CaCO_3]_{z_{\text{erodible}}}}\, dA \tag{66}$$

$$= \int_{\text{ocean floor}} r_{det} \frac{[CaCO_3]_{z_{\text{erodible}}}}{[sed]_{z_{\text{erodible}}} - [CaCO_3]_{z_{\text{erodible}}}}\, dA \tag{67}$$

where r_{det} is the rain rate of detrital/non-$CaCO_3$ material and $[sed]_{z_{\text{erodible}}}$ is the total concentration of sediments at the erodible depth ($[sed]_{z_{\text{erodible}}} = [CaCO_3]_{z_{\text{erodible}}} + [\text{non-}CaCO_3]_{z_{\text{erodible}}}$). Similarly as for the dissolution flux, we make a simplifying hypothesis and suppose the total burial flux depends only on the total mass of $CaCO_3$ erodible sediments assuming, again, a Taylor

expansion around the preindustrial reference:

$$\begin{aligned} F_{bur} &= F_{bur}(M_S) \\ &= F_{bur,0} + \alpha_{bur}(M_S - M_S(t_{PI})) \end{aligned} \tag{68}$$

To avoid introducing too many tunable parameters, we keep only the linear term of the Taylor expansion. We further impose the condition that burial should be zero when $M_S = 0$. This means that the parameters must obey $\alpha_{bur} = F_{bur,0}/M_S(t_{PI})$ and that we can reduce our parametrisation of burial to

$$F_{bur} = \alpha_{bur} M_S \tag{69}$$

MICHEL A RELU JUSQU'ICI.

2.1.7 V, $F_{\text{weathering}}$, $F_{\text{river influx}}$, $\tilde{F}_{\text{river influx}}$

Weathering of carbonate and silicate rocks can suck CO_2 out of the atmosphere through the following chemical reactions :

$$CO_2 + H_2O + CaCO_3 \rightleftharpoons Ca^{2+} + 2HCO_3^- \tag{70}$$

$$2CO_2 + H_2O + CaSiO_3 \rightleftharpoons Ca^{2+} + 2HCO_3^- + SiO_2 \tag{71}$$

Let us consider F_{CaCO_3} and F_{CaSiO_3} the fluxes of Ca^{2+} produced by these two processes. For carbonate weathering (equation 70), one mole of Ca^{2+} produced consumes one mole of carbon (CO_2) from the atmosphere and produces two moles of DIC and alkalinity that are transported by the rivers to the ocean. For the silicate weathering (equation 71), one mole of Ca^{2+} produced consumes two moles of carbon (CO_2) from the atmosphere and produces two moles of DIC and alkalinity that are transported by the rivers to the ocean. Hence, we set

$$F_{\text{weathering}} = F_{CaCO_3} + 2F_{CaSiO_3} \tag{72}$$

$$F_{\text{river influx}} = 2F_{CaCO_3} + 2F_{CaSiO_3} \tag{73}$$

$$F^{alk}_{\text{river influx}} = 2F_{CaCO_3} + 2F_{CaSiO_3} \tag{74}$$

Similarly as with alkalinity we will use units of PgC/yr for F_{CaCO_3} and F_{CaSiO_3}, even though they are defined as fluxes of Ca^{2+}. To go from mol/yr to PgC/yr, one just has too divide by the molar mass of carbon (and multiply by the right power of 10 depending on the prefixes used).

For every two moles of DIC produced by carbonate weathering, one mole of carbon is taken from the atmosphere reservoir and one mole of carbon is coming from carbonate rocks, which do not constitute a reservoir in our model. This extra mole is thus considered as an external source of carbon, just like volcanism. The carbon entering the ocean from weathering fluxes will eventually precipitate back as $CaCO_3$ in the sediments, which releases CO_2. Thus, the net effect of carbonate weathering is to transfer $CaCO_3$ from rocks on land to sediments in the ocean, but it has no long term net effect on the atmospheric CO_2. On the other hand, since silicate weathering consumes one more mole of CO_2 from the atmopshere for the same Ca^{2+} flux, its net effect is to remove carbon from the atmopshere. In equilibrium, this net removal is compensated by volcanic outgassing.

The $F_{\mathrm{CaCO_3}}$ and $F_{\mathrm{CaSiO_3}}$ fluxes aren't constant and may depend on many factors. For example, temperature will affect the rates of reactions 70 and 71, water run-off on land will influence how much under-saturated water will come in contact with rocks for weathering, and vegetation may affect the acidity of soils and thus the rates of dissolution. Colbourn et al. (2013) provide parametrisations of all these processes for the model of terrestrial rock weathering RockGEM, which was included in the GENIE Earth system modelling framework. They showed that the temperature feedback was the dominant one and we choose to consider only this one. Following their parametrisation, we set

$$F_{\mathrm{CaCO_3}} = F_{\mathrm{CaCO_3},0}(1 + k_{Ca}\delta T_U) \tag{75}$$

$$F_{\mathrm{CaSiO_3}} = F_{\mathrm{CaSiO_3},0}e^{k_T \delta T_U} \tag{76}$$

where k_{Ca} and k_T are constants and δT_U is the temperature anomaly of the upper ocean (and atmopshere) modelled by SURFER.

2.1.8 Methane

The evolution of the methane concentration in the atmosphere is mainly controlled by 3 processes : natural and anthropogenic emissions increase the $\mathrm{CH_4}$ concentration whereas oxidation with $\mathrm{CO_2}$ decreases it.

Anthropogenic emissions can be divided in two sources, fossil emissions ($E^{CH_4}_{\text{fossil}}$) and land-use emissions ($E^{CH_4}_{\text{landuse}}$). Fossil emissions come from the industry sector and from the use and exploitation of fossil fuels. Land-use emissions result from agriculture (rice production, cattle, ...), agricultural waste burning, and burning of biomass such as forests, grasslands and peat. Natural emissions ($E^{CH_4}_{\text{natural}}$) mainly come the from anaerobic decomposition of organic matter in wetlands , but also from freshwater systems, termites, and geological sources such as volcanoes, permafrost and methane hydrates. For a detailed treatment of the different methane emissions see Saunois et al. (2020). The rate of natural emisisons may depend on temperature, and if they increase upon global warming, this could lead to positive feedbacks and eventually tipping points (Nisbet et al., 2023; Fewster et al., 2022; Archer et al., 2009). Here for simplicity we choose to have constant natural emissions. To ensure the conservation of carbon, landuse $\mathrm{CH_4}$ emissions are taken from the land reservoir, while natural $\mathrm{CH_4}$ emissions are taken directly from the $\mathrm{CO_2}$ atmospheric reservoir of carbon. The reason for this difference is explained in the next section.

Oxidation of methane ($F_{\mathrm{CH_4}ox}$, equation 77) is the main sink of methane out of the atmosphere and releases $\mathrm{CO_2}$.

$$\mathrm{CH_4} + 2\mathrm{O_2} \rightarrow \mathrm{CO_2} + 2\mathrm{H_2O} \tag{77}$$

We describe this a simple decay process :

$$F_{\mathrm{CH_4}ox} = -\frac{M_A^{\mathrm{CH_4}}}{\tau_{\mathrm{CH_4}}} \tag{78}$$

where $\tau_{\mathrm{CH_4}}$ is the atmospheric $\mathrm{CH_4}$ lifetime, which is around 10 yrs. It may vary depending on temperature and on the availability of the hydroxyl radical OH, which is necessary for the intermediate steps of reaction 77, and which itself depends on the concentrations of $\mathrm{CH_4}$, $\mathrm{N_2O}$, CO and other trace gases. Again for simplicity, we choose to keep $\tau_{\mathrm{CH_4}}$ constant and fix its value to 9.5 yrs. We add the product of oxidation to M_A.

2.1.9 Land reservoir and land-use emissions

In SURFER v3.0, we distinguish between fossil and landuse greenhouse gas emissions. While fossil CO_2 and CH_4 emissions are just added to the atmosphere, land use CO_2 and CH_4 emissions ($E^{CO_2}_{\text{landuse}}$ and $E^{CH_4}_{\text{landuse}}$) are also taken from the land reservoir. For SURFER v2.0, based on the outputs of the ZECMIP experiments (Jones et al., 2019; MacDougall et al., 2020), we parametrised the carbon flux from the land to the atmosphere in the following way

$$F_{A\to L} = k_{\mathrm{A}\to\mathrm{L}}\left(\beta_{\mathrm{L}} M_{\mathrm{A}(t_{\mathrm{PI}})}\left(1-\frac{M_{\mathrm{A}}\left(t_{\mathrm{PI}}\right)}{M_{\mathrm{A}}}\right)-\left(M_{\mathrm{L}}-M_{\mathrm{L}}(t_{\mathrm{PI}})\right)\right). \tag{79}$$

This is equivalent to saying that M_L relaxes to an equilibrium mass $M_L^{eq}(M_A)$ equal to

$$M_L^{eq}(M_A) = \beta_{\mathrm{L}} M_{\mathrm{A}}\left(t_{\mathrm{PI}}\right)\left(1-\frac{M_{\mathrm{A}}\left(t_{\mathrm{PI}}\right)}{M_{\mathrm{A}}}\right)+M_{\mathrm{L}}(t_{\mathrm{PI}}) \tag{80}$$

with a timescale $1/k_{A\to L}$.

Now suppose that we have a certain amount of land-use emissions: we take some carbon out of the land reservoir and we put it in the atmosphere reservoir, without changing anything else. Then the $F_{A\to L}$ flux, as it is, will increase and land will reabsorbate the carbon it lost until initial equilibrium is reached again. Physically, this means that the forest that was replaced by grassland or crop fields has grown back to its original size. For some of the land-use changes this is something that happens but a lot of the time, as long as the land is managed (eg for agriculture), forest regrowth will not happen. To take this into account, we subtract the cumulative CO_2 land-use emissions from the equilibrium mass to which M_L relaxes

$$M_L^{eq}(M_A,t) = \beta_{\mathrm{L}} M_{\mathrm{A}(t_{\mathrm{PI}})}\left(1-\frac{M_{\mathrm{A}}\left(t_{\mathrm{PI}}\right)}{M_{\mathrm{A}}}\right)+M_{\mathrm{L}}(t_{\mathrm{PI}})-\int_{t_0}^{t} E^{CO_2}_{\text{landuse}}(t) \tag{81}$$

This is the same procedure as in the model from Lenton (2000), except that they substract only a fraction of the cumulative landuse emissions, allowing for some forest regrowth. Here we substract all landuse emissions because, in principle, the negative emissions coming from forest regrowth should already be accounted for in the net landuse emissions (int, 2023). We can rewrite the new $F_{A\to L}$ flux as

$$F_{A\to L} = k_{\mathrm{A}\to\mathrm{L}}\left(\beta_{\mathrm{L}} M_{\mathrm{A}(t_{\mathrm{PI}})}\left(1-\frac{M_{\mathrm{A}}\left(t_{\mathrm{PI}}\right)}{M_{\mathrm{A}}}\right)-\left(M_{\mathrm{L}}-M_{\mathrm{L}^*}\right)\right) \tag{82}$$

where M_{L}^* is a new variable of the model whose time evolution is described by

$$\frac{dM_{\mathrm{L}}^*}{dt} = -E^{CO_2}_{\text{landuse}}(t) \tag{83}$$

with $M_{\mathrm{L}}^*(t_{\mathrm{PI}}) = M_{\mathrm{L}}(t_{\mathrm{PI}})$.

Note that we haven't included methane landuse emissions in equations 81-83. This means that the carbon mass in CH_4 form taken from the land reservoir will be reabsorbed by the land once methane is oxidized back to CO_2. In other words, methane landuse emissions will not lead to a net addition of CO_2 in the atmosphere through oxidation. This makes sense if you consider methane emissions coming from the anaerobic decomposition of organic matter in rice cultures or in cattle

stomachs. Indeed, the decomposed organic matter was formed not too long before by absorbing CO_2 from the atmosphere through photosynthesis, so when the methane oxidises into CO_2, it closes the loop and there is no net effect on atmospheric CO_2.

The same reasoning goes for natural emissions of methane, which mainly arise from wetlands : they should not result in a net increase of atmospheric CO_2 concentrations. To achieve that, we should in principle subtract the natural emissions of methane from the land reservoir and have a non zero positive atmosphere to land equilibrium flux that compensates the CO_2 created from oxidation. However this is impossible with the parametrisation of the atmosphere-to-land flux we chose, which is zero at preindustrial times by construction. To avoid having to introduce a new parameterisation or a more detailed representation of the carbon on land and to maintain carbon conservation, we choose to subtract the natural emissions directly from the CO_2 mass of carbon in the atmosphere. We can do this because we assume that the natural emissions are constant and so the carbon fluxes associated with them are in equilibrium. In this way, natural methane emissions will not have a net impact on CO_2 concentrations.

Natural CH_4 emissions coming from geological processes such as volcanism or natural gas leaks would have a net impact on CO_2 levels but they are negligible compared to emissions coming from wetlands (Saunois et al., 2020). Natural CH_4 emissions coming from permafrost would also have a lasting effect on CO_2 concentrations because the organic matter from which they originate was formed thousands of years before. To add the emissions from permafrost, one would need a separate parametrisation, and in the current version of SURFER, we neglect them.

2.2 Climate submodel

The equations for the climate submodel are essentially the same as in SURFER v2.0, with the addition of an oceanic box and the radiative forcing due to methane. The atmosphere is considered to be in thermal equilibrium with the surface ocean layer (U). The evolution of temperature anomalies for the three oceanic layers are given by

$$c_{\mathrm{vol}} h_{\mathrm{U}} \frac{d\delta T_{\mathrm{U}}}{\mathrm{d}t} = F\left(M_{\mathrm{A}}, M_{\mathrm{A}}^{\mathrm{CH_4}}, I\right) - \beta \delta T_{\mathrm{U}} - \gamma_{U\to I}\left(\delta T_{\mathrm{U}} - \delta T_{\mathrm{I}}\right) \tag{84}$$

$$c_{\mathrm{vol}} h_{\mathrm{I}} \frac{d\delta T_{\mathrm{I}}}{\mathrm{d}t} = \gamma_{U\to I}\left(\delta T_{\mathrm{U}} - \delta T_{\mathrm{I}}\right) - \gamma_{I\to D}\left(\delta T_{\mathrm{I}} - \delta T_{\mathrm{D}}\right) \tag{85}$$

$$c_{\mathrm{vol}} h_{\mathrm{D}} \frac{d\delta T_{\mathrm{D}}}{\mathrm{d}t} = \gamma_{I\to D}\left(\delta T_{\mathrm{I}} - \delta T_{\mathrm{D}}\right) \tag{86}$$

where $F\left(M_{\mathrm{A}}, M_{\mathrm{A}}^{\mathrm{CH_4}}, I\right)$ is the anthropogenic radiative forcing. Its expression is given by

$$F\left(M_{\mathrm{A}}, M_{\mathrm{A}}^{\mathrm{CH_4}}, I\right) = F_{2X}\log_2\left(\frac{M_{\mathrm{A}}}{M_{\mathrm{A}}\left(t_{\mathrm{PI}}\right)}\right) + \alpha_{\mathrm{CH_4}}\sqrt{M_{\mathrm{A}}^{\mathrm{CH_4}} - M_{\mathrm{A}}^{\mathrm{CH_4}}(t_{PI})} - \alpha_{\mathrm{SO_2}}\exp\left(-\left(\beta_{\mathrm{SO_2}}/I\right)^{\gamma_{\mathrm{SO_2}}}\right) \tag{87}$$

The two first terms describe the contribution of CO_2 and methane to an increased greenhouse effect. The third term corresponds to solar radiation modification in the form of SO2 injections (Martínez Montero et al., 2022).

2.3 Sea level rise submodel

Sea lever rise is estimated as the sum of four contributions : thermal expansion, and melt from the mountain glaciers, the Greenland ice sheet and the Antarctic ice sheet

$$S_{\mathrm{tot}} = S_{\mathrm{th}} + S_{\mathrm{gl}} + S_{\mathrm{GIS}} + S_{\mathrm{AIS}} \tag{88}$$

Compared to SURFER v2.0, we only change the parametrisation of thermal expansion, where we need to add a term to take into account the new intermediate layer.

$$S_{\mathrm{th}} = \alpha_U h_U \delta T_U + \alpha_I h_I \delta T_I + \alpha_D h_D \delta T_D \tag{89}$$

Here α_i is the thermal expansion coefficient corresponding to layer $i \in U, I, D$. The other contributions are the same as in Martínez Montero et al. (2022). We recall them here, and more details are provided in the original publication.

The evolution of the sea-level rise contribution from glaciers is given by the equation

$$\frac{\mathrm{d}S_{\mathrm{gl}}}{\mathrm{d}t} = \frac{1}{\tau_{\mathrm{gl}}} \left(S_{\mathrm{gleq}} \left(\delta T_{\mathrm{U}} \right) - S_{\mathrm{gl}} \right) \tag{90}$$

with

$$S_{\mathrm{gleq}} \left(\delta T_{\mathrm{U}} \right) = S_{\mathrm{gl\,pot}} \tanh \left(\frac{\delta T_{\mathrm{U}}}{\zeta} \right) \tag{91}$$

Here τ_{gl} is a relaxation timescale, $S_{\mathrm{gl\,pot}}$ is the potential sea level rise due to mountain glaciers and ζ is a sensitivity coefficient.

The contributions from Greenland and Antarctica are given by

$$S_{\mathrm{GIS}} = S_{\mathrm{GIS}p\kappa} \left(1 - V_{\mathrm{GIS}}(t) \right), \quad S_{\mathrm{AIS}} = S_{\mathrm{AIS\,por}} \left(1 - V_{\mathrm{AIS}}(t) \right), \tag{92}$$

where S_{GIS} and S_{AIS} are the sea-level rise potential of Greenland's and Antarctic ice sheet and V_{GIS}, V_{AIS} are the volume fractions of the ice sheets with respect to their preindustrial volume. The evolution of ice sheets volumes are described with the equation

$$\frac{\mathrm{d}V}{\mathrm{d}t} = \mu \left(V, \delta T_{\mathrm{U}} \right) \underbrace{\left(-V^3 + a_2 V^2 + a_1 V + c_1 \delta T_{\mathrm{U}} + c_0 \right)}_{H}, \tag{93}$$

with

$$\mu \left(V, \delta T_{\mathrm{U}} \right) = \begin{cases} 1/\tau & \text{if } H > 0 \text{ or } (H < 0 \text{ and } V > 0), \\ 0 & \text{if } H < 0 \text{ and } V = 0, \end{cases} \tag{94}$$

and

$$\tau = \tau_- + \frac{\tau_+ - \tau_-}{2} \left(1 + \tanh \left(\frac{H}{k_\tau} \right) \right). \tag{95}$$

The time scales τ_+ and τ_- are associated with the asymmetric process of freezing and melting. The first case in equation 94 was separated in two cases in SURFER v2.0, depending on the sign of H. Now we introduce a smooth transition between τ_+ and τ_- when H changes sign. This is done to avoid that small fluctuations around the equilibrium (when H is close to zero) have very different timescales. The parameter k_τ controls the smoothness of the transition; the case $k_\tau = \infty$ corresponds to SURFER v2.0. The constant parameters (a_2, a_1, c_1, c_0) are given in terms of $(T_+, V+), (T_-, V_-))$ which are the bifurcation points of the steady state structure induced by equation 93. This allows to easily calibrate SURFER on the steady state structure of more complex ice-sheet models.

$$a_2 = \frac{3\left(V_- + V_+\right)}{2}, \tag{96}$$

$$a_1 = -3V_-V_+, \tag{97}$$

$$c_1 = -\frac{\left(V_+ - V_-\right)^3}{2\left(T_+ - T_-\right)} \tag{98}$$

$$c_0 = +\frac{T_+V_-^2\left(V_- - 3V_+\right) - T_-V_+^2\left(V_+ - 3V_-\right)}{2\left(T_- - T_+\right)} \tag{99}$$

2.4 Calibration and initial conditions

We calibrate the parameters and initial conditions of the model using known physics, observations, model results, and the hypothesis that the carbon cycle was at equilibrium during preindustrial times. This is probably close to reality for processes that act on short time scales such as oceanic invasion but there is no a priori reasons why it should be true for processes involving longer time scales, such as sediments dissolution and weathering. That being said, it is standard practice and we make the following assumptions for the carbon fluxes :

$$0 = V - F_{A\to U}(t_{PI}) - F_{A\to L}(t_{PI}) - F_{\text{weathering}}(t_{PI}) \tag{100}$$

$$0 = E_{nat}^{CH_4} - F_{CH_4,ox}(t_{PI}) \tag{101}$$

$$0 = F_{A\to L}(t_{PI}) \tag{102}$$

$$0 = F_{A\to U}(t_{PI}) - F_{U\to I}(t_{PI}) + F_{\text{river}}(t_{PI}) \tag{103}$$

$$0 = F_{U\to I}(t_{PI}) - F_{I\to D}(t_{PI}) \tag{104}$$

$$0 = F_{I\to D}(t_{PI}) - F_{\text{acc}}(t_{PI}) \tag{105}$$

$$0 = -\tilde{F}_{U\to I}(t_{PI}) + \tilde{F}_{\text{river}}(t_{PI}) \tag{106}$$

$$0 = \tilde{F}_{U\to I}(t_{PI}) - \tilde{F}_{I\to D}(t_{PI}) \tag{107}$$

$$0 = \tilde{F}_{I\to D}(t_{PI}) - \tilde{F}_{\text{acc}}(t_{PI}) \tag{108}$$

$$0 = F_{\text{acc}}(t_{PI}) - F_{\text{burrial}}(t_{PI}) \tag{109}$$

From equations 106-108 we get that $\tilde{F}_{\text{acc}}(t_{PI}) = \tilde{F}_{I\to D}(t_{PI}) = \tilde{F}_{U\to I}(t_{PI}) = \tilde{F}_{\text{river influx}}(t_{PI}) = 2F_{\mathrm{CaCO_3},0} + 2F_{\mathrm{CaSiO_3},0}$. The dissolution/precipitation of $\mathrm{CaCO_3}$ produces/consumes moles of DIC and alklanity at a 1:2 ratio (see section 2.1.6), hence

we have $F_{\text{acc}}(t_{PI}) = \frac{1}{2}\tilde{F}_{\text{acc}}(t_{PI}) = F_{\text{CaCO}_3,0} + F_{\text{CaSiO}_3,0}$. We then get from equations 104,105 and 109 that $F_{U\to I}(t_{PI}) = F_{I\to D}(t_{PI}) = F_{\text{burial}}(t_{PI}) = F_{\text{acc}}(t_{PI}) = F_{\text{CaCO}_3,0}+F_{\text{CaSiO}_3,0}$. Equation 103 gives us $F_{A\to L}(t_{PI}) = -(F_{\text{CaCO}_3,0}+F_{\text{CaSiO}_3,0})$, and from equation 100 we find $V = F_{\text{CaSiO}_3,0}$. Finally, equation 101 tells us that $E_{nat}^{CH_4} = F_{CH_4,ox}(t_{PI})$ and equation 102 tells us nothing since we have $F_{A\to L}(t_{PI}) = 0$ by construction. Developing the expressions of the carbon fluxes, we get the following system of equations :

$$V = F_{\text{CaSiO}_3,0} \tag{110}$$

$$E_{nat}^{CH_4} = \frac{M_A^{CH_4}(t_{PI})}{\tau_{CH_4}} \tag{111}$$

$$0 = 0 \tag{112}$$

$$\bar{k}_{A\to U}K_0\left(M_A(t_{PI}) - \frac{m_A}{W_U K_0}M'_U(t_{PI})\right) = -\left(F_{\text{CaCO}_3,0} + F_{\text{CaSiO}_3,0}\right) \tag{113}$$

$$P^{\text{CaCO}_3} + P^{\text{org}} + k_{U\to I}M_U(t_{PI}) - k_{I\to U}M_I(t_{PI}) = F_{\text{CaCO}_3,0} + F_{\text{CaSiO}_3,0} \tag{114}$$

$$(1-\phi_U^{\text{CaCO}_3})P^{\text{CaCO}_3} + (1-\phi_U^{\text{org}})P^{\text{org}} + k_{I\to D}M_I(t_{PI}) - k_{D\to I}M_D(t_{PI}) = F_{\text{CaCO}_3,0} + F_{\text{CaSiO}_3,0} \tag{115}$$

$$2P^{\text{CaCO}_3} + \sigma_{Alk:\text{DIC}}P^{\text{org}} + \tilde{k}_{U\to I}\tilde{Q}_U(t_{PI}) - \tilde{k}_{I\to U}\tilde{Q}_I(t_{PI}) = 2\left(F_{\text{CaCO}_3,0} + F_{\text{CaSiO}_3,0}\right) \tag{116}$$

$$2(1-\phi_U^{\text{CaCO}_3})P^{\text{CaCO}_3} + \sigma_{Alk:\text{DIC}}(1-\phi_U^{\text{org}})P^{\text{org}} + \tilde{k}_{I\to D}\tilde{Q}_I(t_{PI}) - \tilde{k}_{D\to I}\tilde{Q}_D(t_{PI}) = 2\left(F_{\text{CaCO}_3,0} + F_{\text{CaSiO}_3,0}\right) \tag{117}$$

$$(1-\phi_I^{\text{CaCO}_3} - \phi_D^{\text{CaCO}_3})P^{\text{CaCO}_3} - F_{diss,0} = F_{\text{CaCO}_3,0} + F_{\text{CaSiO}_3,0} \tag{118}$$

$$\alpha_{bur}M_S(t_{PI}) = F_{\text{CaCO}_3,0} + F_{\text{CaSiO}_3,0} \tag{119}$$

The equilibrium hypothesis thus provides us with constraints relating some parameters and initial conditions. In section 2.4.1 we discuss the choice and calibration of the model parameters. A sensitivity analysis for most parameters is presented in appendix C. In section 2.4.2, we provide a set of initial conditions for the model.

2.4.1 Parameters

Carbon cycle submodel

The parameters that control the CO_2 uptake by vegetation (β_L, $k_{A\to L}$) and the CO_2 uptake by the ocean on short time scales ($\bar{k}_{A\to U}$, $k_{U\to I}$ and $\tilde{k}_{U\to I}$) are tuned so as to reproduce historical observations of CO_2 concentrations (fig 8), historical estimations of land and ocean sinks (fig 11) as well as historical and SSP runs of CMIP6 (fig 12 and 13). The parameters $k_{I\to D}$ and $\tilde{k}_{I\to D}$, which control the ocean carbon uptake on multi-centennial to multi-millennial time scales, are chosen to produce a reasonable fit with the 1Myr runs of cGENIE (see section 3.5).

The parameter $\bar{k}_{A\to U}$ is defined as $\bar{k}_{A\to U} = A_O\rho k/m_A$. With the ocean area taken as $A_O = 361\times10^{12}$ m^2, the mean sea water density taken as $\rho = 1026$ kg m^{-3}, the gas transfer velocity taken as $20\,\text{cm}\,\text{h}^{-1} = 0.2\cdot365\cdot24\,\text{m}\,\text{yr}^{-1}$ (Yang et al., 2022), the number of moles in the atmosphere taken as $m_A = 1.727\times10^{20}$ mol, we obtain $\bar{k}_{A\to U} = 4.7$ kg (mol yr)$^{-1}$. The parameter β_L, which controls the amount of CO_2 uptake by vegetation (see eq 82), is set to 1.7. This is the same value as for SURFER

v2.0, which was calibrated on the outputs of the ZECMIP experiment. The parameter $k_{A\to L}$ is set to 0.044, which is an increase by a factor 1.75 compared to SURFER v2. This is done in order to have a better match with historical CO_2 concentrations.

The parameters that dictate the DIC and alkalinity exchanges between the ocean layers are linked to the oceanic circulation and so we expect them to have similar values ($k_{i\to j} \approx \tilde{k}_{i\to j}$ for $i,j \in U,I,D$), but we don't require them to be equal because some processes such as the solubility pump may impact DIC and alkalinity independently. For simplicity, we set both $k_{U\to I}$ and $\tilde{k}_{U\to I}$ to 0.08 yr^{-1}, and both $k_{I\to D}$ and $\tilde{k}_{I\to D}$ to 0.008 yr^{-1}. Then, $k_{I\to U}$ and $\tilde{k}_{I\to U}$, $k_{D\to I}$ and $\tilde{k}_{D\to I}$ are computed from equations 114-117. We have

$$k_{I\to U} = \left(P^{\mathrm{CaCO_3}} + P^{\mathrm{org}} - (F_{\mathrm{CaCO_3},0} + F_{\mathrm{CaSiO_3},0}) + k_{U\to I} M_U(t_{PI})\right) \frac{1}{M_I(t_{PI})} \tag{120}$$

$$k_{D\to I} = \left((1-\phi_U^{\mathrm{CaCO_3}})P^{\mathrm{CaCO_3}} + (1-\phi_U^{\mathrm{org}})P^{\mathrm{org}} - (F_{\mathrm{CaCO_3},0} + F_{\mathrm{CaSiO_3},0}) + k_{I\to D} M_I(t_{PI})\right) \frac{1}{M_D(t_{PI})} \tag{121}$$

$$\tilde{k}_{I\to U} = \left(2P^{\mathrm{CaCO_3}} + \sigma_{Alk:\mathrm{DIC}} P^{\mathrm{org}} - 2(F_{\mathrm{CaCO_3},0} + F_{\mathrm{CaSiO_3},0}) + \tilde{k}_{U\to I} \tilde{Q}_U(t_{PI})\right) \frac{1}{\tilde{Q}_I(t_{PI})} \tag{122}$$

$$\tilde{k}_{D\to I} = \left(2(1-\phi_U^{\mathrm{CaCO_3}})P^{\mathrm{CaCO_3}} + \sigma_{Alk:\mathrm{DIC}}(1-\phi_U^{\mathrm{org}})P^{\mathrm{org}} - 2(F_{\mathrm{CaCO_3},0} + F_{\mathrm{CaSiO_3},0}) + \tilde{k}_{I\to D} \tilde{Q}_I(t_{PI})\right) \frac{1}{\tilde{Q}_D(t_{PI})} \tag{123}$$

With the choices for the other parameters described hereafter, we obtain $k_{I\to U} = 0.0239$ yr^{-1}, $\tilde{k}_{I\to U} = 0.0241$ yr^{-1}, $k_{D\to I} = 1.61\times10^{-3}$ yr^{-1}, and $\tilde{k}_{D\to I} = 1.60\times10^{-3}$ yr^{-1}. Overall, This correspond to a time scale range of 12.5 - 41.8 yrs ($1/k_{U\to I}$ - $1/k_{I\to U}$) for the oceanic carbon exchanges between surface and intermediate layers, and a time scale range of 125 - 621.4 yrs ($1/k_{I\to D}$ - $1/k_{D\to I}$) for the oceanic carbon exchanges between intermediate and deep layers. In terms of DIC fluxes, this gives preindustrial fluxes of 130 PgC yr^{-1} for subduction ($k_{U\to I} M_U(t_{PI})$) and 138 PgC yr^{-1} for obduction ($k_{I\to U} M_I(t_{PI})$). Although these carbon fluxes are an order of magnitude greater than the fluxes from the biological pumps, they are much less studied, and estimates in the litterature are rare . IPCC AR5 gave estimates of 90 PgC yr^{-1} and 101 PgC yr^{-1} for subduction and obduction respectivey, while IPCC AR6 gave estimates of 264 PgC yr^{-1} and 275 PgC yr^{-1} (Levy et al., 2013; int, 2023).

Most studies estimate a $CaCO_3$ export out of the ocean surface between 0.6 and 1.8 PgC/yr (see supplementary material from Sulpis et al. (2021) and reference therein). Sulpis et al. (2021) provide a tighter range of 0.77 to 1.06 PgC/yr, of which 0.34 to 0.53 PgC/yr are dissolved in the water column before reaching the sediments. We set $P_{\mathrm{CaCO_3}}$ to 1 PgC/yr, which is also the value given in Sarmiento and Gruber (2006) for the open-ocean export at a 100m depth. We calibrate $\phi_I^{\mathrm{CaCO_3}}$ and $\phi_D^{\mathrm{CaCO_3}}$ based on a parametrisation for the $CaCO_3$ flux by Archer et al. (1998)

$$\phi^{\mathrm{CaCO_3}}(z) = P^{\mathrm{CaCO_3}} \left(0.3 + 0.7 e^{\frac{z-150}{2000}}\right) \tag{124}$$

where we have slightly adapted the formula to match the geometry of our model. The fractions $\phi_I^{\mathrm{CaCO_3}}$ and $\phi_D^{\mathrm{CaCO_3}}$ are then given by

$$\phi_I^{\mathrm{CaCO_3}} = \frac{P^{\mathrm{CaCO_3}} - \phi^{\mathrm{CaCO_3}}(650)}{P_{\mathrm{CaCO_3}}} = 0.15 \tag{125}$$

$$\phi_D^{\mathrm{CaCO_3}} = \frac{\phi^{\mathrm{CaCO_3}}(650) - \phi^{\mathrm{CaCO_3}}(3150)}{P^{\mathrm{CaCO_3}}} = 0.39 \tag{126}$$

This gives us a total of 0.54 PgC/yr dissolved in the water column and 0.46 PgC/yr that rains on the sediments, which is close to both bestimates from Sulpis et al. (2021) and Sarmiento and Gruber (2006) (see figure 9.1.1).

Estimates of export of organic carbon out of the euphotic zone range from 4 PgC/yr to 12 PgC yr (DeVries and Weber (2017) and references therein). The euphotic zone is the uppermost layer of the ocean that recieves sunlight and where photosynthesis can happen. Since remineralisation of organic matter happen quite fast in the water column, estimates of carbon export can vary greatly depending on the specific definition of the euphotic zone and its depth. Based on a data-assimilated model, DeVries and Weber (2017) give an estimate of 9.1 ± 0.2 PgC/yr for the organic carbon export out of the euphotic zone and an estimate of 6.7 PgC/yr for the organic carbon export at 100m depth. In our model, we set the organic carbon export P^{org} at a 150m depth to 7 PgC/yr, which corresponds to the estimate given for the open ocean in Sarmiento and Gruber (2006). We calibrate ϕ_I^{org} and ϕ_D^{org} based on the *Martin curve* for the organic carbon flux in the water column (Martin et al., 1987)

$$\phi^{org}(z) = P^{org}\left(\frac{z}{150}\right)^{-0.858} \tag{127}$$

The fractions ϕ_I^{org} and ϕ_D^{org} are then given by

$$\phi_I^{org} = \frac{P^{org} - \phi^{org}(650)}{P_{org}} = 0.72 \tag{128}$$

$$\phi_D^{org} = \frac{\phi^{org}(650) - \phi^{org}(3150)}{P^{org}} = 0.21 \tag{129}$$

This gives us a total of 6.51 PgC/yr of organic carbon remineralised in the water column and 0.49 PgC/yr that rains on the sediments, which is close to estimates for the open ocean from Sarmiento and Gruber (2006) (see figure 6.5.2). Overall, we have a $\mathrm{CaCO_3}$ to organic carbon export ratio of 0.14 at depth 150m, and a $\mathrm{CaCO_3}$ to organic carbon rain ratio of 0.94 on the ocean floor.

For organic matter production, equation 41 suggests that for a 106 moles decrease in DIC, alkalinity will increase by 17 moles (the uptake of 18 moles of $\mathrm{H^+}$ increases alkalnity by 18 moles, while the uptake of $\mathrm{HPO_4^{2-}}$, which is one of the minor bases part of the complete definition of alkalinity (eq 12), decreases alkalinity by one mole). The ratio of alkalinity to DIC changes can be described in terms of Redfield ratios. The Redfield ratios are the ratios of carbon, nitrogen, phosphorus present in organic matter. Equation 41 suggests a Redfield ratio C:N:P of 106:16:1. The ratio of DIC decrease to alk increase is given by the ratio of C to N+P (Soetaert et al., 2007; Middelburg et al., 2020). Other equations for organic matter are proposed and there exist different estimations of the Redfield ratio. Sarmiento and Gruber (2006) neglect the phosphorus and use a C:N Redfield ratio of 117:16. We follow them and set $\sigma_{Alk:\mathrm{DIC}}$ to $-16/117$, meaning that for 1 mole uptake of DIC in organic mater production, alkalinity is increased by $16/117 = 0.14$ moles. Equivalently, for a 1 mole increase of DIC through remineralisation, alkalinity decreases by 0.14 moles.

For our parametrisation of $\mathrm{CaCO_3}$ dissolution, we need to calibrate 4 parameters. The value of $F_{diss,0}$ is computed using equilibrium conditions. From equation 118, we obtain

$$F_{diss,0} = (1 - \phi_I^{\mathrm{CaCO_3}} - \phi_D^{\mathrm{CaCO_3}})P^{\mathrm{CaCO_3}} - (F_{\mathrm{CaCO_3},0} + F_{\mathrm{CaSiO_3},0}) \tag{130}$$

With the choice of $P^{\mathrm{CaCO_3}}$, $\phi_I^{\mathrm{CaCO_3}}$, $\phi_D^{\mathrm{CaCO_3}}$ described above, and the choice for $F_{\mathrm{CaCO_3},0}$, $F_{\mathrm{CaSiO_3},0}$ described below, we get $F_{diss,0} = 0.33$ PgC yr^{-1}. The parameters α_{diss}, β_{diss} and γ_{diss} are obtained based on a parametrisation provided in Archer et al. (1998) for accumulation :

$$F_{acc}^{Archer} = \bar{\nu}_{acc} + \bar{\alpha}_{acc}[\mathrm{CO_3^{2-}}]_P + \bar{\beta}_{acc} M_{BL} + \bar{\gamma}_{acc}[\mathrm{CO_3^{2-}}]_P M_{BL} \tag{131}$$

where $[\mathrm{CO_3^{2-}}]_P$ is the carbonate concentration (in μmol/kg) in a specific place in the deep Pacific, and M_{BL} is the total $\mathrm{CaCO_3}$ mass (in PgC) in the bioturbated layer of the sediments. The different coefficients are empirically fitted to experiments done with a ocean-sediments model (Archer, 1996). We can identify $[\mathrm{CO_3^{2-}}]_P$ to the deep ocean carbonate concentration $[\mathrm{CO_3^{2-}}]_D$, and use the observation that $M_B L \approx M_S/2$ in their model runs to obtain a parametrisation in terms of SURFER variables. Furthermore, we can use the fact that they have a constant $\mathrm{CaCO_3}$ rain ($r_{\mathrm{CaCO_3}}^{Archer}$) to obtain a parametrisation for dissolution

$$\begin{aligned} F_{diss}^{Archer} &= r_{\mathrm{CaCO_3}}^{Archer} - F_{acc}^{Archer} && (132)\\ &= \bar{F}_{diss,0} + \bar{\alpha}_{diss}([\mathrm{CO_3^{2-}}]_D - [\mathrm{CO_3^{2-}}]_D(t_{PI})) + \bar{\beta}_{diss}(M_S - M_S(t_{PI})) && (133)\\ &\quad + \bar{\gamma}_{diss}([\mathrm{CO_3^{2-}}]_D - [\mathrm{CO_3^{2-}}]_D(t_{PI}))(M_S - M_S(t_{PI})) && (134) \end{aligned}$$

with

$$\bar{F}_{diss,0} = r_{\mathrm{CaCO_3}}^{Archer} - \left(\bar{\nu}_{acc} + \bar{\alpha}_{acc}[\mathrm{CO_3^{2-}}]_D(t_{PI}) + \bar{\beta}_{acc}\frac{M_S(t_{PI})}{2} + \bar{\gamma}_{acc}[\mathrm{CO_3^{2-}}]_D(t_{PI})\frac{M_S(t_{PI})}{2} \right) \tag{135}$$

$$\bar{\alpha}_{diss} = \bar{\alpha}_{acc} + \bar{\gamma}_{acc}\frac{M_S(t_{PI})}{2} \tag{136}$$

$$\bar{\beta}_{diss} = \frac{\bar{\beta}_{acc}}{2} + \bar{\gamma}_{acc}\frac{[\mathrm{CO_3^{2-}}]_D(t_{PI})}{2} \tag{137}$$

$$\bar{\gamma}_{diss} = \frac{\bar{\gamma}_{acc}}{2} \tag{138}$$

Using the values provided in the paper (see table 2), we get

$$\bar{F}_{diss,0} = 0.67 \text{ PgC yr}^{-1} \tag{139}$$

$$\bar{\alpha}_{diss} = -1.07 \times 10^{-2} \text{ PgC yr}^{-1} \ (\mu\text{mol kg}^{-1}) \tag{140}$$

$$\bar{\beta}_{diss} = 1.82 \times 10^{-5} \text{ yr}^{-1} \tag{141}$$

$$\bar{\gamma}_{diss} = -4.53 \times 10^{-6} \text{ yr}^{-1} \ (\mu\text{mol kg}^{-1})^{-1} \tag{142}$$

The values of $\bar{F}_{diss,0}$, $[\mathrm{CO_3^{2-}}]_D(t_{PI})$ and $M_S(t_{PI})$ form Archer et al. (1998) are not the same as the ones we use but this is not a problem, as we are mainly interested in the coefficients $\bar{\alpha}_{diss}$, $\bar{\beta}_{diss}$, and $\bar{\gamma}_{diss}$, which can be seen as sensitivity coefficients. For our parametrisation of dissolution, we use these coefficients with a correction factor to obtain a better match to the results of the LTMIP experiments (see section 3.4) and the 1MYr cGENIE runs (see section 3.5). We set $\alpha_{diss} = 0.6\bar{\alpha}_{diss}$, $\beta_{diss} = \bar{\beta}_{diss}$, and $\gamma_{diss} = 0.7\bar{\gamma}_{diss}$.

We split the total weathering flux evenly between silicate and carbonate weathering ($F_{CaCO_3,0} = F_{CaSiO_3,0}$) and we set them such as to obtain a preindustrial burial flux of 0.13 PgC/yr. This is the estimate given in Sarmiento and Gruber (2006).

Symbol	Comment	Value	Units
$\bar{\nu}_{acc}$		-8.63×10^{-2}	PgC yr^{-1}
$\bar{\alpha}_{acc}$		3.13×10^{-3}	PgC yr^{-1} (μmol kg^{-1})$^{-1}$
$\bar{\beta}_{acc}$		-8.25×10^{-4}	yr^{-1}
$\bar{\gamma}_{acc}$		9.07×10^{-6}	yr^{-1} (μmol kg^{-1})$^{-1}$
$r^{Archer}_{CaCO_3}$	approx 50% of $CaCO_3$ production (1.65 PgC yr^{-1})	0.825	PgC yr^{-1}
$[CO_3^{2-}]_D(t_{PI})$	identified to $[CO_3^{2-}]_P(t_{PI})$	87	μmol kg^{-1}
$M_S(t_{PI})$	approx two times $M_{BL}(t_{PI})$ (834 PgC)	1668	PgC

Table 2. Parameters from Archer et al. (1998) used for the computation of the dissolution parametrisation

For comparaison, the IPCC AR6 WG1 give an estimate of 0.2 PgC/yr. From equation 112, we have $F_{CaCO_3,0} + F_{CaSiO_3,0} = \alpha_{bur} M_S(t_{PI}) = F_{bur}(t_{PI}) = 0.13$ PgC/yr and this gives us $F_{CaCO_3,0} = F_{CaSiO_3,0} = 0.065$ PgC/yr or 5.42 Tmol/yr. This is between the value of 5 Tmol/yr set in Colbourn et al. (2013) for the globally averaged fluxes, and the value of 5.59 Tmol/yr used in Lord et al. (2016) for a similar parametrisation employed in cGENIE for 1 Myr runs (see section 3.5). From these choices, we get $\alpha_{bur} = (F_{CaCO_3,0} + F_{CaSiO_3,0}) / M_S(t_{PI}) = 0.13 / M_S(t_{PI})$. Volcanic outgassing is set to $V = F_{CaSiO_3,0} = 0.065$ PgC/yr as per equation 110. The IPCC estimate is 0.1 PgC/yr. Following Colbourn et al. (2013), we set k_{Ca} to 0.049 K^{-1} and k_T to

$$k_T = \frac{1000 E_a}{R T_0^2} \tag{143}$$

where R is the gaz constant (in J K^{-1} mol^{-1}), T_0 is the global mean preindustrial temperature (in K) and E_a is the activation energy for dissolution (in kJ mol^{-1}). West et al. (2005) provide an estimate for the activation energy : $E_a = 74 \pm 29$ kJ mol^{-1}. With $T_0 = T_U(t_{PI}) = 288.37$ K (as set in section 2.4.2), this gives a range for k_T between 0.080 K^{-1} and 0.149 K^{-1}. We choose to set $k_T = 0.095$ K^{-1}.

Natural methane emissions are set to $E^{CH_4}_{nat} = M^{CH_4}_A(t_{PI}) / \tau_{CH_4}$. With $M^{CH_4}_A(t_{PI})$ chosen as in section 2.4.2 and $\tau_{CH_4} = 9.5$ yrs , we get natural emisisons of 0.157 PgC/yr or 209 TgCH$_4$/yr. This is in the range of the top down estimate of the IPCC (176-243 TgCH$_4$/yr) and a bit below the bottom-up estimate range (245-484 TgCH$_4$/yr) (int, 2023).

Climate submodel

For the parametrisation of the heat exchange between the ocean layers, we assumed that $\gamma_{U \to I}$ and $\gamma_{I \to D}$ could be different but ended up setting $\gamma_{U \to I} = \gamma_{I \to D} = 0.8357$ W m^{-2} °C^{-1}. This is the value chosen for the unique γ in SURFER v2.0. This gives us a transient climate response (TCR) of 1.9 °C which lies in the likely range of 1.4°C - 2.2°C given by the IPCC (cite AR6). In section 4 we show that this choice gives a good fit to the estimated heat uptake by the deep ocean in the period 1971-2018, and a good fit to the multi-millennial global ocean heat uptake as simulated by the Earth System Models of Intermediate Complexity UVic and Bern3D-LPX (Clark et al. (2016), IPCC).

Symbol	Comment	Value
m_A	number of moles in the atmosphere	1.727×10^{20} mol
m_O	number of moles in the ocean	7.8×10^{22} mol
$\bar{m}_c$	carbon molar mass	12×10^{-3} kg mol^{-1}
$\bar{m}_w$	water molar mass	18×10^{-3} kg mol^{-1}
c_{vol}	sea water volumetric heat capacity	0.13 W yr m^{-3}
R	gas contant	8.314 J mol^{-1} K^{-1}
h_U	upper layer depth	150 m
h_I	intermediate layer depth	500 m
h_D	deep layer depth	2500 m
W_U	upper layer weight	$h_U \bar{m}_w m_O/(h_U + h_I + h_D)$
W_I	intermediate layer weight	$h_I \bar{m}_w m_O/(h_U + h_I + h_D)$
W_D	deep layer weight	$h_D \bar{m}_w m_O/(h_U + h_I + h_D)$
z_U	upper layer depth mid-depth point	75 m
z_I	intermediate layer mid-depth point	400 m
z_D	deep layer mid-depth point	1900 m

Table 3. Physical parameters and geometry

For the contribution of methane to the radiative forcing $F_{\mathrm{CH_4}}$ (in W m $^{-2}$), we use a common parametrisation (Myhre et al., 1998)

$$F_{\mathrm{CH_4}} = 0.036\sqrt{C_{\mathrm{CH_4}} - C_{\mathrm{CH_4}}(t_{PI})} \tag{144}$$

where $C_{\mathrm{CH_4}}$ is the methane atmospheric concentration in ppb. We have

$$C_{\mathrm{CH_4}} = \frac{M_{\mathrm{A}}^{\mathrm{CH_4}}}{\bar{m}_c m_A} 10^{21} \tag{145}$$

where $M^{\mathrm{CH_4}}$ is expressed in PgC, and thus

$$\alpha_{\mathrm{CH_4}} = 0.036\sqrt{\frac{10^{21}}{\bar{m}_c m_A}} \tag{146}$$

SLR submodel

The thermal expansion coefficient for density of a water parcel is defined as $\alpha = \frac{1}{\rho}\frac{\partial \rho}{\partial t}|_{P,S}$, where ρ, P, and S are the density, the pressure and salinity of that water parcel. To obtain the averaged thermal exapansion coefficients for each ocean layer α_U, α_I and α_D, we proceed in 3 steps, similarly as in Williams et al. (2012). First we use the GLODAPv2.2016b mapped climatology (Lauvset et al., 2016) to compute the thermal expansion coefficient at each ocean point. To do this, we use the International Thermodynamic Equation Of Seawater - 2010 (TEOS-10) and the python implementation of the GSW

Symbol	Comment	Value
$F_{CaCO_3,0}$	PI weathering of carbonate rocks	0.065 PgC yr $^{-1}$
$F_{CaSiO_3,0}$	PI weathering of silicate rocks	0.065 PgC yr $^{-1}$
K_{Ca}	parametrisation of carbonate weathering flux	0.049 K $^{-1}$
K_T	parametrisation of silicate weathering flux	0.095 K $^{-1}$
$k_{A\to L}$	controls rate of carbon uptake by vegetation	0.050 yr $^{-1}$
β_L	controls amount of carbon uptake by vegetation	1.7
$\bar{k}_{A\to U}$	controls rate of air-sea CO_2 exchanges	4.7 kg (mol yr)$^{-1}$
$k_{U\to I}$	controls rate of DIC transfer via ocean mixing from layer U to I	0.08 yr $^{-1}$
$k_{I\to D}$	controls rate of DIC transfer via ocean mixing from layer I to D	0.008 yr $^{-1}$
$\tilde{k}_{U\to I}$	controls rate of alkalinity transfer via ocean mixing from layer U to I	0.08 yr $^{-1}$
$\tilde{k}_{I\to D}$	controls rate of alkalinity transfer via ocean mixing from layer I to D	0.008 yr $^{-1}$
P_{org}	organic matter export at 150m	7 PgC yr $^{-1}$
P_{CaCO_3}	$CaCO_3$ export at 150m	1 PgC yr $^{-1}$
$\phi_{org,I}$	fraction of organic matter rain that remineralises in layer I	0.72
$\phi_{org,D}$	fraction of organic matter rain that remineralises in layer D	0.21
$\phi_{CaCO_3,I}$	fraction of $CaCO_3$ rain that dissolves in layer I	0.15
$\phi_{CaCO_3,D}$	fraction of $CaCO_3$ rain that dissolves in layer D	0.39
$\sigma_{Alk:\mathrm{DIC}}$	alkalinity to DIC changes in organic matter production and remineralisation	$-16/117$
α_{diss}	parametrisation of $CaCO_3$ sediments dissolution	-6.41×10^{-3} PgC yr^{-1} (μmol kg^{-1})
β_{diss}	parametrisation of $CaCO_3$ sediments dissolution	1.82×10^{-5} yr^{-1}
γ_{diss}	parametrisation of $CaCO_3$ sediments dissolution	-3.17×10^{-6} yr^{-1} (μmol kg^{-1})$^{-1}$
τ_{CH_4}	atmospheric lifetime of methane	9.5 years
V	volcanic outgassing	$F_{CaSiO3,0}$
$k_{I\to U}$	controls rate of DIC transfer via ocean mixing from layer I to U	eq 120
$k_{D\to I}$	controls rate of DIC transfer via ocean mixing from layer D to I	eq 121
$\tilde{k}_{I\to U}$	controls rate of alkalinity transfer via ocean mixing from layer I to U	eq 122
$\tilde{k}_{D\to I}$	controls rate of alkalinity transfer via ocean mixing from layer D to I	eq 123
$F_{diss,0}$	parametrisation of $CaCO_3$ sediments dissolution	eq 130
α_{bur}	parametrisation of $CaCO_3$ sediments burial	$(F_{CaCO_3,0}+F_{CaSiO_3,0})/M_S(t_{PI})$
$E^{CH_4}_{nat}$	natural methane emissions	$M_{CH_4}(t_{PI})/\tau_{CH_4}$

Table 4. Parameters for the carbon cycle submodel. Second part of the table contains parameters that are computed from equilibrium conditions (equations 110-119).

Symbol	Comment	Value
$F_{2\times}$	extra radiative forcing due to a doubling of atmospheric CO_2	3.9 W m $^{-2}$
β	climate feedback parameter	1.1143 W m $^{-2}$ °C $^{-1}$
$\gamma_{U\to I}$	parametrisation of heat exchange between ocean layers	0.8357 W m $^{-2}$ °C $^{-1}$
$\gamma_{I\to D}$	parametrisation of heat exchange between ocean layers	0.8357 W m $^{-2}$ °C $^{-1}$
α_{CH_4}	parametrisation of radiative forcing of methane	0.791 W m $^{-2}$ (PgC)$^{-1/2}$
α_{SO_2}	parametrisation of radiative forcing of	65 W m $^{-2}$
β_{SO_2}	parametrisation of radiative forcing of	2246 TgS yr $^{-1}$
γ_{SO_2}	parametrisation of radiative forcing of	0.23

Table 5. Parameters for the climate submodel.

Parameter	Comment	Value
$S_{gl\,pot}$	sea level rise potential from mountain glaciers	0.5 m
ξ	sensitivity coefficient for glacier parametrisation	2°C
τ_{gl}	timescale for glacier melt	200 yr
α_U	thermal expansion coefficient for layer U	2.20×10^{-4} K^{-1}
α_I	thermal expansion coefficient for layer I	1.61×10^{-4} K^{-1}
α_D	thermal expansion coefficient for layer D	1.35×10^{-4} K^{-1}

Table 6. Parameter values for the sea level rise submodel.

Oceanographic toolbox of TEOS-10 (McDougall and Barker, 2011). Second, we average over each horizontal level of the GLODAPv2.2016b climatology to obtain a vertical profile of the thermal expansion coefficient (see fig 4) Third, we average over each of our defined ocean layers, using the the areas of each horizontal level as weights for the horizontally averaged values of the thermal expansion coefficient. We obtain

$$\alpha_U = 2.20 \times 10^{-4} \text{ K}^{-1} \tag{147}$$

$$\alpha_I = 1.61 \times 10^{-4} \text{ K}^{-1} \tag{148}$$

$$\alpha_D = 1.35 \times 10^{-}4 \text{ K}^{-1} \tag{149}$$

This is close to the values used in SURFER v2.0 ($\alpha_U = 2.3 \times 10^{-4}$ K^{-1} and $\alpha_D = 1.3 \times 10^{-4}$ K^{-1}) . In section 4, we show that this choice of expansion coefficients give a reasonable fit to the the thermosteric sea level rise on multi-millennial time scales as simulated by the Earth System Models of Intermediate Complexity UVic and Bern3D-LPX (Clark et al., 2016).

All the other parameters of the sea level rise submodel are the same as in SURFER v2.0 and are recapped in tables 6 and 7.

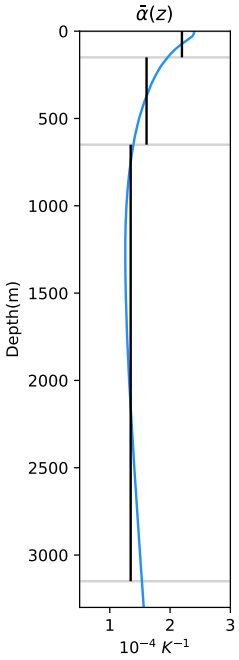

Figure 4. Blue : Horizontally averaged thermal expansion coefficient $\bar{\alpha}(z)$ for the global ocean, computed from the GLODAPv2.2016b mapped climatology (Lauvset et al., 2016). Black : averages over SURFER's ocean layers.

Parameter	Greenland's value	Antarctica's value
T_+	$1.52°\mathrm{C}$	$6.8°\mathrm{C}$
T_-	$0.3°\mathrm{C}$	$4.0°\mathrm{C}$
V_+	0.77	0.44
V_-	0.3527	-0.3200
τ_+	5500 years	5500 years
τ_-	470 years	3000 years
k_τ	0.05	0.05
S_{pot}	$7.4\ \mathrm{m}$	$55\ \mathrm{m}$

Table 7. Parameter values used for Greenland and Antarctic ice sheets

2.4.2 Initial conditions

As in SURFER v2.0, the initial mass of carbon in atmospheric CO_2, $M_A(t_{PI})$, is set such as to have a preindustrial atmospheric CO_2 concentration of 280 ppm. We have

$$M_A(t_{PI}) = 280 \times 10^{-18} m_A \bar{m}_C = 580.27 \text{ PgC} \tag{150}$$

The initial mass of carbon in atmospheric CH_4, $M_A^{CH_4}(t_{PI})$, is set such as to have a preindustrial atmospheric CH_4 concentration of 720 ppb. We have

$$M_A^{CH_4}(t_{PI}) = 720 \times 10^{-21} m_A \bar{m}_C = 1.49 \text{ PgC} \tag{151}$$

The initial mass of carbon in land soils and vegetation $M_L(t_{PI})$ is set to 2200 PgC, as in SURFERv2.0. Hence, we have $M_L^*(t_{PI}) = M_L(t_{PI}) = 2200$ PgC. The initial mass of carbon in erodible $CaCO_3$ sediments, $M_S(t_{PI})$, is set to 1750 PgC, which is the estimate provided by the IPCC.

For each ocean layer, we have 17 quantities (T, S, K_0, K_1, K_2, K_w, K_b, $[H^+]$, $[H_2CO_3^*]$, $[HCO_3^-]$, $[CO_3^{2-}]$, $[OH^-]$, $[H_3BO_3]$, $[H(BO)_4^-]$, DIC, Alk, pCO_2) that are linked by a nonlinear system of 13 equations (equations 11, 13, 20-25, 26, 27-30 (+31)). This means that you can only set 4 of these quantities independently otherwise the system will be overdetermined (i.e. there are more equations than unknowns and in general there is no solution). Equation 31 for the pressure dependance of the dissociation constants isn't counted because it can be combined with equations 27-30. For each ocean layer, we will set temperature, salinity, alkalinity and DIC, except for the surface layer where we set $[H_2CO_3^*]$ instead of DIC. This is because equilibrium conditions give a constraint on the $H_2CO_3^*$ mass (and thus $[H_2CO_3^*]$) in the upper layer. Equation 113 give us

$$M'_U(t_{PI}) = \frac{W_U K_0}{m_A} M_A(t_{PI}) + \frac{W_U}{\bar{k}_{A\to U} m_A} (F_{CaSiO_3,0} + F_{CaCO_3 0}) \tag{152}$$

We obtain $M'_U(t_{PI}) = 8.37$ PgC and $[H_2CO_3^*]_U(t_{PI}) = M'_U(t_{PI})/(W_U \bar{m}_C) \times 10^{18} = 10.44$ μmol kg^{-1}. To fix the other quantities, we use the GLODAPv2.2016b mapped climatologies (Lauvset et al., 2016), which include climatologies for temperature, salinity, alkalnity, dissolved inorganic carbon, preindustrial dissolved inorganic carbon and pH among other biogechemical variables. The climatologies are computed based on data gathered between 1972 and 2013. The dissolved inorganic carbon data is normalized to 2002, and the pH is computed based on temperature, alkalinity and the normalised DIC. Following the same averaging method as for the computation of the thermal expansion coefficients (see section 2.4.1) , we compute global averages of these data fields over our defined ocean layers. Obtained values can be found in table 8. We set the initial (and constant) salinites S_U, S_I, S_D of our ocean layers to the computed averages from the GLODAP data. The temperatures of the ocean layers are defined as

$$T_i(t) = T_{i,0} + \delta T_i(t) \qquad \text{for } i \in \{U, I, D\} \tag{153}$$

By definition, the initial conditions for the temperature anomalies δT_i are zero. We set $T_{i,0}$ such that $T_i(2002)$, obtained from experimental runs, is approximately equal to the temperature average computed from the GLODAP data. We set $\tilde{Q}_U(t_{PI})$,

	Upper layer (0-150m)	Intermediate layer (150-650m)	Deep layer (650-3150m)
Preindustrial DIC (μmol kg^{-1})	2017.65	2152.62	2264.92
Total alkalinity (μmol kg^{-1})	2310.61	2310.60	2363.49
Temperature (°C / °K)	16.34 / 289.49	8.95 / 282.10	2.88 / 275.93
Salinity (psu)	34.93	34.77	34.69

Table 8. GLODAPv2.2016b quantities averaged over ocean layers equivalent to those of SURFER.

$\tilde{Q}_I(t_{PI})$, $\tilde{Q}_D(t_{PI})$, $M_I(t_{PI})$, and $M_D(t_{PI})$ based on the computed averages for DIC and Alk, converted to carbon masses with equations 14 and 15. $M_U(t_{PI})$ is computed the from the fixed $[\mathrm{H_2CO_3}]_U(t_{PI})$, S_U, $T_{U,0}$, $Alk_U(t_{PI})$. Details for the computation are provided in appendix B. We obtain $M_U(t_{PI}) = 1622.35$ PgC, which corresponds to $\mathrm{DIC}_U(t_{PI}) = 2022.16$ μmol kg^{-1}. This is only 0.22% off compared to the averaged value for the upper layer obtained from GLODAP. Total dissolved inorganic carbon in the ocean is 37664 PgC, which is close to the 38000 PgC estimate from the IPCC.

For the sea level rise components, as in SURFER v2.0, we set $S_{gl}(t_{PI}) = 0$, $V_{GIS}(t_{PI}) = 1$, and $V_{AIS}(t_{PI}) = 1$. All initial conditions a recapped in table 9.

In Figure 5, we compare the horizontally averaged vertical depth profiles of GLODAP to the vertical profiles of SURFER for different model quantities. The vertical profiles of SURFER are computed by running the model from 1750 to 2002, forced with historical $\mathrm{CH_4}$ and $\mathrm{CO_2}$ emissions, and starting from the initial conditions described above. We observe that the chosen initial conditions produce a model state in 2002 that matches the GLODAP data.

Variable	Comment	Initial (PI) Value
M_A	mass of carbon in atmospheric CO_2	580.27 PgC
$M_A^{CH_4}$	mass of carbon in atmospheric CH_4	1.49 PgC
M_L	mass of carbon on land (soils+vegetation)	2200 PgC
M_L^*	additionnal land variable that integrates land use emission	2200 PgC
M_U	dissolved inorganic carbon mass in ocean layer U	1622.20 PgC
M_I	dissolved inorganic carbon mass in ocean layer I	5756.73 PgC
M_D	dissolved inorganic carbon mass in ocean layer D	30285.24 PgC
Q_U	alkalnity mass in ocean layer U	1853.77 PgC
Q_I	alkalnity mass in ocean layer I	6176.21 PgC
Q_D	alkalnity mass in ocean layer D	30285.24 PgC
M_S	erodible $CaCO_3$ sediments mass	1750 PgC
δT_U	temperature anomaly in ocean layer U	0 K
δT_I	temperature anomaly in ocean layer I	0 K
δT_D	temperature anomaly in ocean layer D	0 K
S_{gl}	sea level rise contribution from mountain glaciers	0 msle
V_{GIS}	volume fraction of Greenland ice sheet with respect to preindustrial value	1
V_{AIS}	volume fraction of Antarctic ice sheet with respect to preindustrial value	1
S_U	salinity of ocean layer U (constant)	34.93 psu
S_I	salinity of ocean layer I (constant)	34.77 psu
S_D	salinity of ocean layer D (constant)	34.69 psu
$T_{U,0}$	preindustrial temperature of ocean layer U (constant)	288.37 K
$T_{I,0}$	preindustrial temperature of ocean layer I (constant)	281.74 K
$T_{D,0}$	preindustrial temperature of ocean layer D (constant)	275.98 K

Table 9. Initial conditions for SURFER v3.0. The upper part of the table correspond to the model 17 variables. The lower part of the table fixes salinity and preindustrial temperature, this is necessary to compute the dissociation constants and the solubility constant of CO_2.

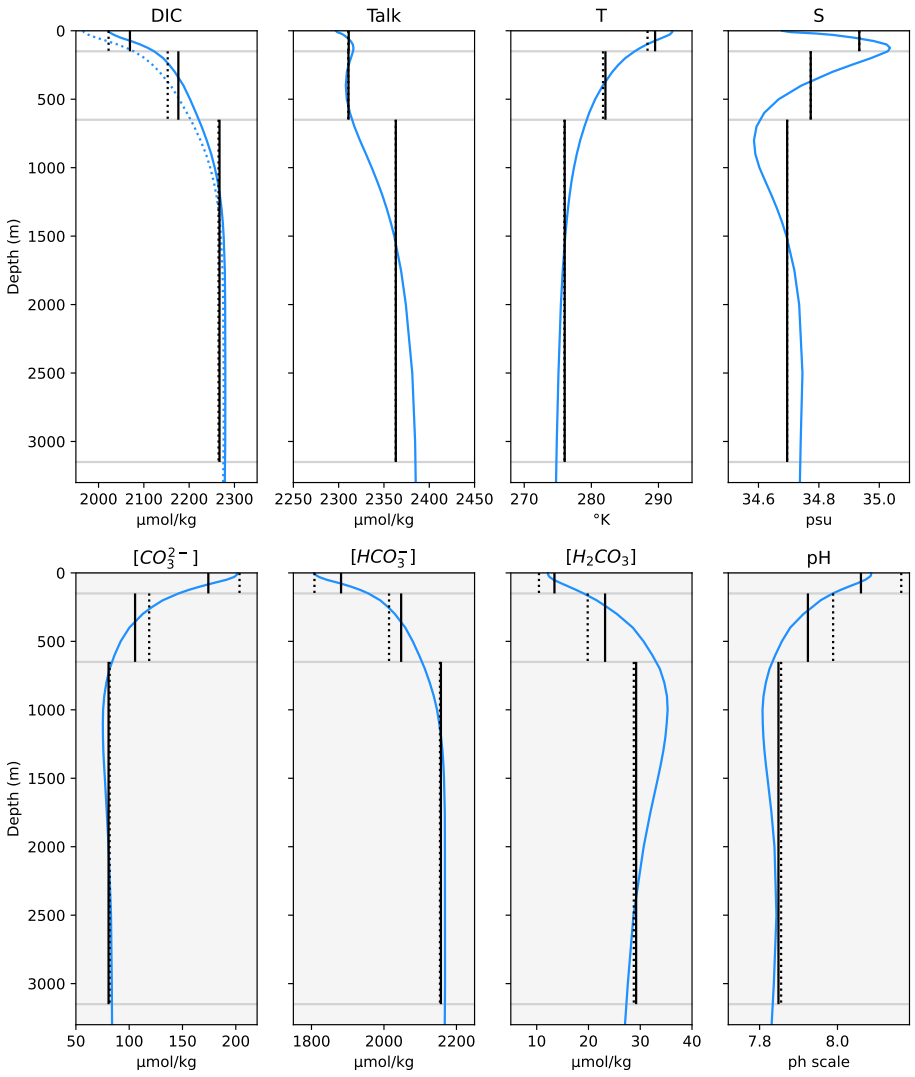

Figure 5. Blue : Horizontally averaged quantities from the GLODAPv2.2016b mapped climatologies (Lauvset et al., 2016). Black (dotted) : initial conditions of SURFER. Black (plain) : quantities in 2002 as simulated by SURFER when forced with historical CO_2 and CH_4 emissions and initialized in 1750 with initial conditions given in table 9. The carbonate species are not provided in the GLODAP climatologies. We computed their values at each ocean point based on the climatalogies of DIC, Alk, temperature and salinity, and then averaged them hoizontally. Details for the computation of the carbonates species can be found in appendix B.

2.5 Numerics

The model has been implemented in python 3.0. using the library solve_ivp with the integration method LSODA (link to python doc?). The LSODA method is a method that has an automatic stiffness detection and that switches accordingly between an Adams and BDF method (Petzold, 1983). The local error estimates are kept below $atol + rtol \times abs(y)$ where $atol$ and $rtol$ are parameters that control the relative and absolute accuracy and where y is a model variable. By default, we set atol to 10^{-3} for the variables $M_A^{\mathrm{CH_4}}$ M_S, δT_U, δT_I, δT_D, S_{gl}, V_{GIS}, V_{AIS} , and we set $atol$ to 10^{-6} for the other variables. The reason for this difference is that the variables in the first group are susceptible to have small or near zero values, meaning that $atol$ will dominate the local error estimate. If it is too small, the solver will take too many steps and be slow. We set $rtol$ to 10^{-6} for all variables. The model runs fast. When forced with $\mathrm{CO_2}$ and $\mathrm{CH_4}$ emissions of a given SSP scenario, runs of 10^3 to 10^6 yrs take typically around 1 second on a labtop with processor Intel® Core™ i5-10210U CPU @ 1.60GHz × 8. The run time is not a linear function of simulated time because the LSODA method uses an adaptative time step. Appendix D provides more details on the model speed in different setups.

The solve_ivp library is a well established library and we consequently assume that the model equations are solved accurately. Still, we perform an additional test and check that the carbon is correctly conserved in the numerical integration of the model. It is the indeed the case (see appendix D), giving us full confidence in the numerical implementation.

3 Numerical results and comparisons

In this following section, we test our model and show that it is an adequate representation of the real climate system. We show that it reproduces well know dynamics of the carbon cycle and we compare outputs of the model with outputs of other models for larger and larger time scales.

3.1 Carbon cycle dynamics and lifetime of atmospheric $\mathrm{CO_2}$

In section 2.1, we explained the global carbon cycle. Here, we focus on the fate of atmospheric $\mathrm{CO_2}$: what becomes of the large amounts of $\mathrm{CO_2}$ we are injecting in the atmosphere? This question is not new and has been explored by many (Archer et al., 1997, 1998, 2009; Ridgwell and Hargreaves, 2007; Lord et al., 2016). Multiple processes act together to remove $\mathrm{CO_2}$ from the atmosphere. Over decadal to millennial timescales, equilibration of the atmosphere with the dissolved inorganic carbon pool in the ocean removes approximately X%. Furthermore, equilibration with CaCO3 sediments removes an additional Y% over multimillennial timescales. A prevalent hypothesis posits that the remaining Z% will eventually be sequestered through enhanced weathering of silicate rocks over a span of a few hundred thousand years. The objective of this section is twofold : to provide an explanation of these processes, and, more importantly, to demonstrate their reliable simulation by SURFER. We conduct several experiments, the results of which are illustrated in figure **??**. Subsequent paragraphs provide detailed insights, while figure **??** offers a succinct overview. We conclude this section by discussing the role of vegetation.

Oceanic invasion

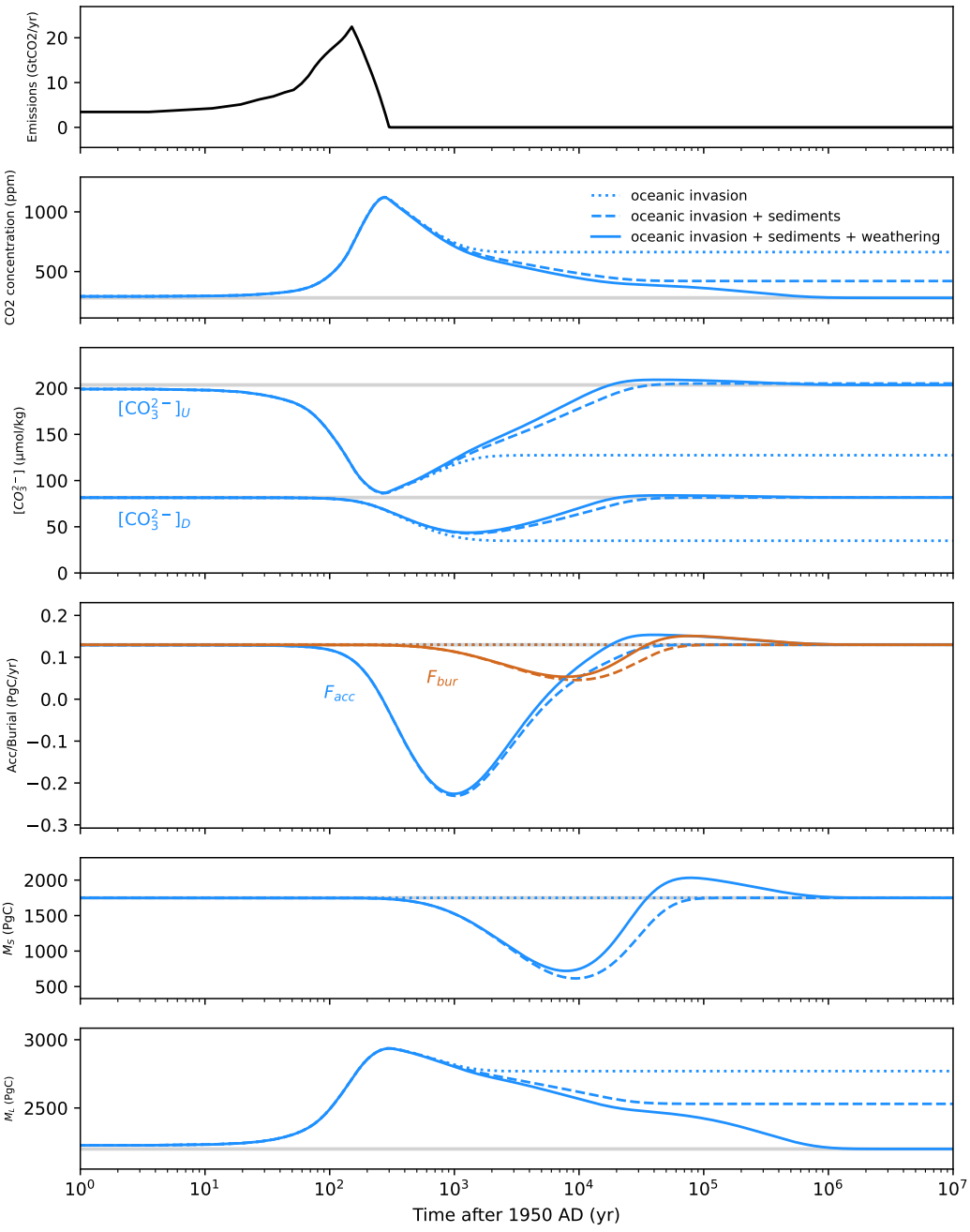

Figure 6. Schematic diagram of the model and its components.

In the first experiment (dotted line in figure 6), we focus solely on oceanic invasion and neglect the roles of sedimentary and weathering feedbacks (we keep F_{acc}, $F_{\mathrm{CaCO_3}}$, and $F_{\mathrm{CaSiO_3}}$ constant and equal to their preindustrial value). Over a timescale ranging from a few months to several years, air-sea CO_2 exchanges between the atmosphere and the surface ocean reach equilibrium. The equations governing oceanic invasion can be combined into the following expression, illustrating how CO_2 uptake by the ocean depletes carbonate ions.

$$2\mathrm{HCO_3^-} \rightleftharpoons \mathrm{CO_3^{2-}} + \mathrm{CO_2} \tag{154}$$

Mixing with the intermediate layer on decadal timescales, and with the deep layer on centennial timescales, distributes the surface CO_3^{2-} decrease in the ocean interior and brings back to the surface rich CO_3^{2-} and low pCO_2 waters, allowing further carbon uptake by the ocean. Consequently, it's the rate of mixing in the ocean interior ($k_{U\to I}$ and $k_{I\to D}$) rather than the rate of air-sea CO_2 exchanges ($\bar{k}_{A\to U}$) that is the limiting factor for the rate of CO_2 uptake by the ocean (Sarmiento and Gruber, 2006). This is corroborated by the sensitivity analysis performed in Appendix C. Altering the value of $\bar{k}_{A\to U}$ has almost no effect on the atmospheric CO_2 levels. Conversely, increasing $k_{U\to I}$ and $k_{I\to D}$ accelerates CO_2 uptake by the ocean. In SURFER simulations, atmospheric CO_2 concentrations equilibrate with the entire ocean DIC pool in approximately X years.

Sea-floor and terrestrial neutralization

I the second experiment (dashed lines in figure 6), we allow interactions between the ocean and deep sea $CaCO_3$ sediments, while still neglecting weathering feedbacks (we allow F_{acc} to change, and keep $F_{\mathrm{CaCO_3}}$ and $F_{\mathrm{CaSiO_3}}$ constant). As the deep ocean CO_3^{2-} concentration decreases due to the oceanic invasion of CO_2, waters become less saturated with respect to CO_3^{2-}, causing an increase in dissolution (or increase in accumuation) of deep sea $CaCO_3$ sediments and a release of carbonate ions. Some of these carbonate ions can then react with CO_2 to from bicarbonate ions, resulting in overall (reverse) reaction 40 for dissolution, and leading to further oceanic CO_2 uptake. This process is called sea-floor neutralisation, as it is the dissolution of previously deposited deep sea sediments that allow the neutralisation of CO_2 (Archer et al., 1997, 1998). Moreover, the increased dissolution compared to the preindustrial state creates an imbalance between the CO_2 uptake by weathering and the CO_2 release by accumulation and volcanism, resulting in additionnal CO_2 drawdown from the atmosphere. This second process is called terrestrial neutralisation, as it is the dissolution of carbonate and silicate rocks on land that neutralise the CO_2. It's worth noting that it is sometimes referred to as terrestrial $CaCO_3$ neutralisation, when only the weathering of carbonate rocks is considered (Archer et al., 1997, 1998; Ridgwell and Hargreaves, 2007).

We observe both terrestrial and sea-floor neutralisation processes in SURFER simulations. Terrestrial neutralisation happens whenever the alkalinity input to the ocean from weathering fluxes is higher than the alkalinity output by accumulation of $CaCO_3$ on sea floor sediments ($\tilde{F}_{\text{river}} > \tilde{F}_{\text{acc}}$). This is equivalent to saying that the input of bicarbonate ions to the ocean from weathering fluxes is higher than the output of these bicarbonate ions by precipitation and accumulation in $CaCO_3$ sediments. Sea-floor neutralisation happens whenever accumulation is negative (net dissolution of sediments). Comparison with "oceanic invasion only" experiment (dotted lines) shows that once the CO_3^{2-} concentration decreases in the deep ocean, increased dissolution of sediments (decreased accumulation) act to balance that. The erodible sediments mass decrease, because accumulation is smaller than burial. Accumulation increases with CO_3^{2-} concentrations, and when it becomes positive again,

sea floor-neutralisation ends. The sediments eventually reach a new equilibrium (accumulation = burial), but at this point, accumulation is still weaker than its preindustrial value and doesn't balance the alkalinity input from weathering fluxes. This means that terrestrial neutralisation continues to occur, leading to additional CO_2 uptake and a further increase in CO_3^{2-} concentrations, until a balance is reached between weathering and accumulation fluxes. Understanding theses consequences is not trivial and believe that the following line of reasoning helps :

1. We short-circuit the atmosphere : dealing with the balance between $F_{\text{weathering}}$, $F_{A \to U}$ and V can be tedious, so we consider the atmosphere and ocean as a whole (equivalent to consider them in quasi-equilibrium with respect to carbon exchange ?). The DIC input to the atmosphere-ocean system is $F_{CaCO_3,0} + F_{CaCO_3,0}$, which is the sum of volcanism $V = F_{CaSiO_3}$ and the carbon coming from carbonate rocks on land $F_{CaCO_3} = F_{CaCO_3,0}$. The alkalinity input remains the same and is equal to $2\left(F_{CaCO_3,0} + F_{CaCO_3,0}\right)$.

2. We think in terms of CO_3^{2-} fluxes : the DIC and alkalinity input at a 1:2 ratio is equivalent to a CO_3^{2-} input flux equal to $F_{CaCO_3,0} + F_{CaCO_3,0}$, and imbalance between weathering and accumulation fluxes lead to an increase of DIC and alkalinity in a 1:2 ratio, which is equivalent to a build up of CO_3^{2-}.

3. We apply Le Chateliers's principle to the carbonate system : build up of CO_3^{2-} ions will push the equilibrium of reaction 154 towards the production of HCO_3^- , consuming CO_2. This decreases oceanic pCO_2 and thus also atmospheric CO_2 concentrations.

4. We consider the equilibrium condition : the increase in CO_3^{2-} concentrations will lead to an increase in accumulation (reduced dissolution) until it balances the equivalent CO_3^{2-} input flux. This brings back accumulation and the erodible $CaCO_3$ stock to their original value.

Both sea-floor and terrestrial neutralisation are examples of carbonate compensation, where changes in the deep CO_3^{2-} concentration will be compensated by changes in dissolution (and accumulation) (Broecker and Peng, 1987). In the case of sea-floor neutralisation, the change in CO_3^{2-} concentration is due to oceanic invasion of CO_2; in the case of terrestrial neutralisation, it is due to an imbalance between weathering and accumulation fluxes.

Weathering feedbacks and final removal by enhanced silicate weathering

In the third experiment (plain lines in figure 6), we run the "full" version of SURFER v3.0, that is we include sedimentary and weathering feedbacks (we allow F_{acc}, F_{CaCO_3}, and F_{CaSiO_3} to change). In the first 10000 years after the emissions, we observe a similar behaviour as the run without the weathering feedbacks (dashed lines): oceanic invasion removes CO_2 from the atmosphere and depletes the oceanic CO_3^{2-} concentration. Then sea-floor and terrestrial neutralisation will act to restore the CO_3^{2-} concentration while leading to further CO_2 drawdown from the atmosphere. Now with increased weathering fluxes, terrestrial neutralisation is enhenced. As a consequence, the CO_3^{2-} concentration and the erodible sediments mass regrow faster than for the constant weathering experiment (dashed lines), and overshoot their preindustrial values. The sediments mass increase until accumulation is equal to burial. At this point, the sediments are in equilibrium but the whole system isn't. Indeed

we now have slightly higher output of alkalinity (HCO_3^-- ions) from the ocean by accumulation than input by weathering fluxes. To understand what is happening, we can follow the same line of reasoning as above :

1. The DIC input flux to the atmosphere-ocean system is equal to $F_{CaCO_3} + V = F_{CaCO_3} + F_{CaSiO_3,0}$. The alkalinity flux is equal to $2\left(F_{CaCO_3} + F_{CaSiO_3}\right)$.

2. Under the pH range of our experiments, CO3– and HCO_3^-- are the dominant species contributing to DIC and alkalinity, and we can make the approximation $CO_3^{2-} \approx \mathrm{Alk} - \mathrm{DIC}$, giving us a CO_3^{2-} input flux to the ocean approximately equal to $F_{CaCO_3} + 2F_{CaSiO_3} - F_{CaSiO_3,0}$. Through the process of carbonate compensation, accumulation on sediments will adjust to balance this flux and will hence tend to $F_{\text{acc}} \approx F_{CaCO_3} + 2F_{CaSiO_3} - F_{CaSiO_3,0}$. As we can see from figure **??**, this happens after around X years. Note that this leads to a higher accumulation flux than for preindustrail times (overshoot) but also to higher outputs of alkalinity and DIC out of the ocean-atmospehre system than inputs from weahtering and volcanism.

3. This imbalance leads to a 1:1 decrease in alkalinity and DIC concetrations, which is equivalent to a decrease in HCO_3^-. Le Chatelier's principle tells us that this decrease is then partly compensated by the reaction of CO_3^{2-} ions with dissolved CO_2, and hence leads to a decrease in oceanic CO_3^{2-} and atmospheric CO_2 concentrations.

4. This continues until equilibrium is reached, when we have $F_{CaSiO_3} = F_{CaSiO_3,0}$, which happens when $\delta T_U = 0$, and in our case, when CO_2 has returned to preindustrial levels.

As we can see, it is the imbalance between increased silicate weathering and volcanism that allows a return to preindustrial conditions. If we had kept silicate weathering constant and only considered a variable carbonate weathering, we would still observe a slightly enhenced CO_2 uptake by terrestrial neutralisation, but the atmospheric CO_2 would not have returned to its preindustrial value . See (Colbourn et al., 2013, 2015) for such experiments in a higher complexity model. As explained earlier, this difference in behaviour arises from the additional mole of CO_2 consumed by silicate weathering compared to carbonate weathering (see equations 70 and 71).

Vegetation

Finally, we discuss the role of vegetation. On decadal to centennial vegetation absorbs a significant fraction of the atmospheric CO_2. For example, it is estimated that the land reservoir has absorbed around 1/3 of our cumulative carbon emissions up to this day (Friedlingstein et al., 2022), see figure 10. On centennial to millenial time scales, the land carbon sink is expected to decrease and and may become negative for high emission scenarios, meaning that the land and vegetation reservoirs would release some of the carbon they had previously absorbed (¢ite IPCC, ch5 , fig 5.30) + (Zickfeld et al., 2013; Tokarska et al., 2016), see also figure 13. On longer time scales, it is not very clear what will happen to the land sink. Vegetation is often neglected altogether when studying the lifetime of atmospheric CO_2 on multi-millennial time scales. In SURFER v3.0, the vegetation relaxes to an equilibrium value that depends on climatic conditions, specifically the amount of CO_2 in the atmosphere M_A , and on land-use change (see eq 81). In the experiments conducted for this section, we haven't included land-use

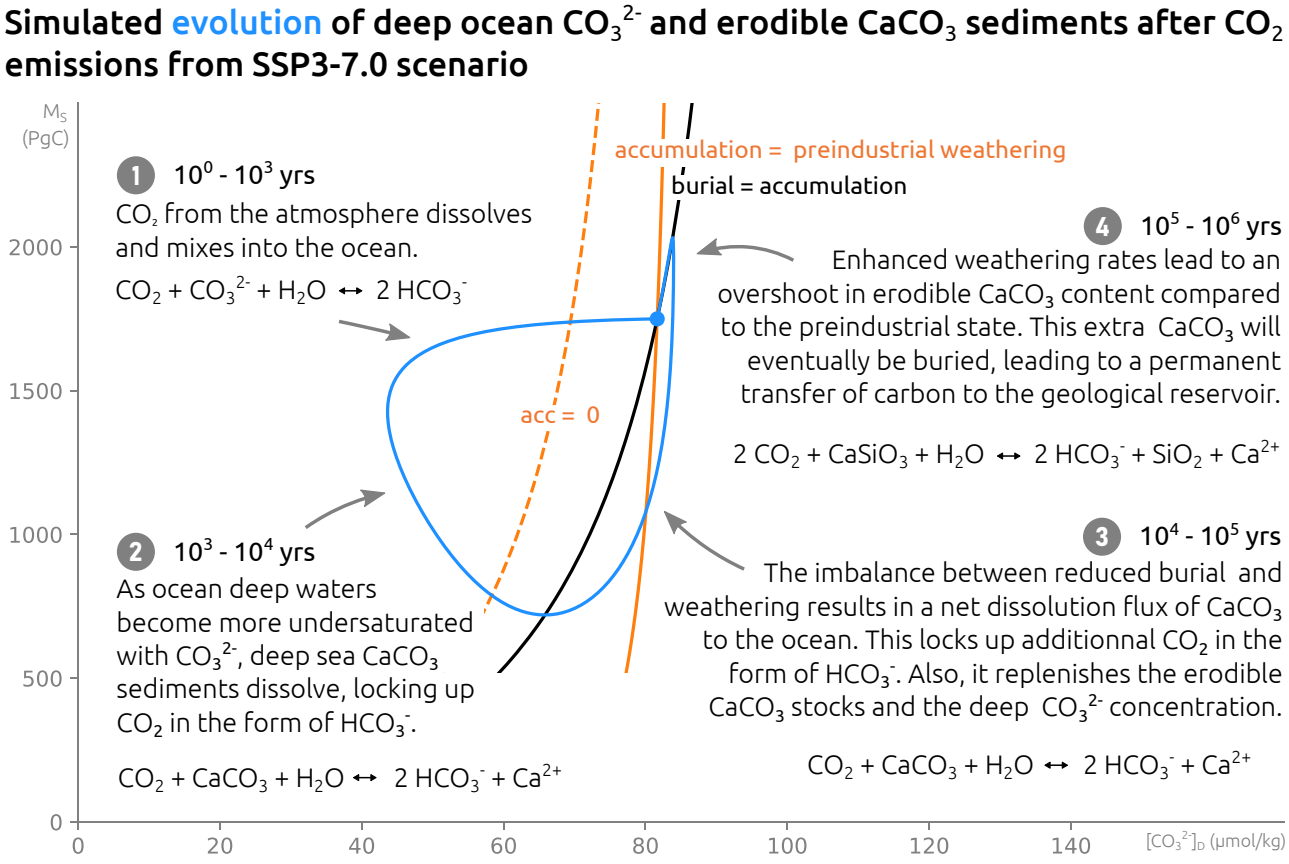

Figure 7. This figure presents a summary of the processes that act to remove CO_2 from the atmosphere and that are discussed in section 3.1. The blue curve correspond to the simulated evolution of deep ocean CO_3^{2-} and erodible $CaCO_3$ sediments after CO_2 emissions from SSP3-7.0 scenario. The blue dot corresponds to the initial and final equilibrium conditions. The SURFER setup is the same as for the third experiment presented in figure 6 (plain blue lines). Only the fossil CO_2 emissions are used to force the model. Land-use CO_2 and methane emissions are omitted. Sediments and weathering are included, as well as vegetation, although it is not mentioned in the figure. The figure is inspired from figure in Lord et al. (2015) and figure in Archer et al. (1998).

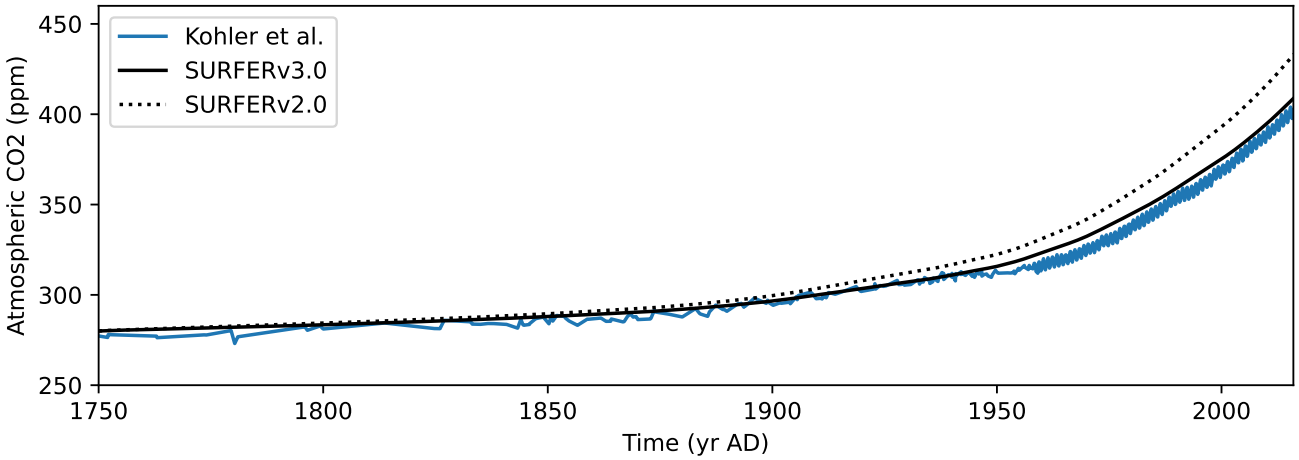

Figure 8. Historical atmopsheric CO_2 concentrations. Comparaison between observations (Köhler et al., 2017) and outputs from SURFER v2.0 and SURFER v3.0 when forced with historical emissions.

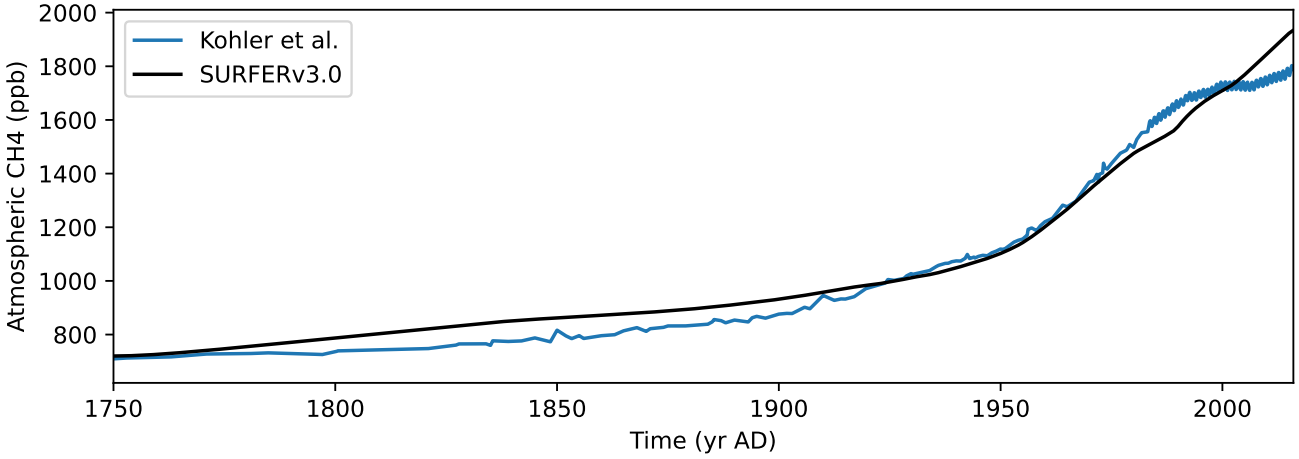

Figure 9. Historical atmopsheric CH_4 concentrations. Comparaison between observations (Köhler et al., 2017) and outputs from SURFER v2.0 and SURFER v3.0 when forced with historical emissions.

changes, and so as the different processes discussed above bring back the atmospheric CO_2 to its preindustrial value, the land reservoir will release all the carbon it had absorbed in the first few centuries after the bulk of the emissions.

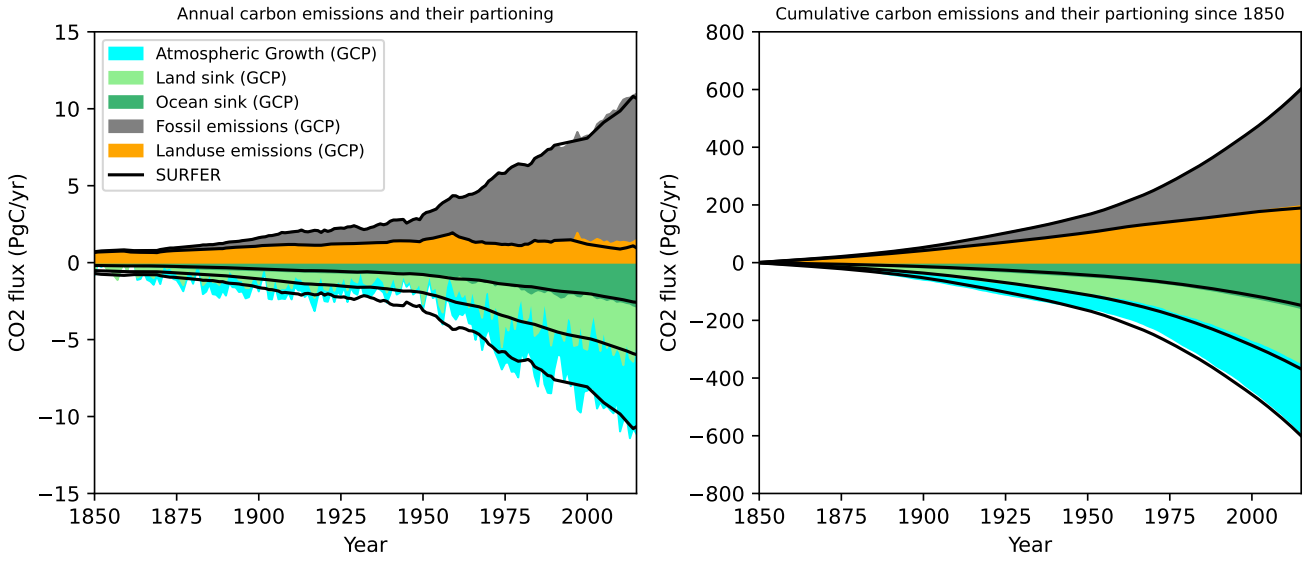

Figure 10. Carbon budget (Friedlingstein et al., 2022)

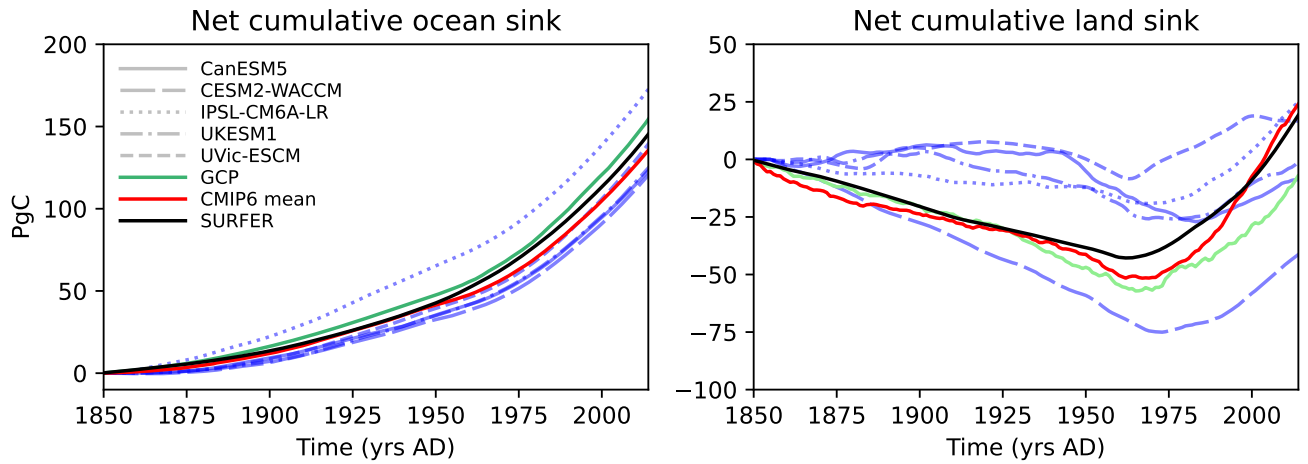

Figure 11. Net cumulative ocean and land sinks. Comparaison between estimations from the global carbon project (Friedlingstein et al., 2022), outputs from isolated GCMs (and an EMIC) runs, the CMIP6 mean and output SURFER v3.0 when forced with historical emissions.

3.2 Historical period

3.3 CMIP6 projections

3.4 LTMIP

We compare SURFER with outputs from the LTMIP (Long Tail Model Intercomparaison Project) informal project Archer et al. (2009). In this project the response of different models was compared for emissions pulses of 1000 PgC and 5000 PgC. In particular, it was compared how the CO_2 is drawndown of the atmosphere during the 10000 years following the pulse. The models consisted of EMICS (UVIC2.8, Climber, GENIE, LTCM(?), MESMO(?)) , a GCM (MPI_UW?), or conceptual models (GEOCYC, CC-sed). We have also included the results from the LOSCAR model Zeebe (2012). Five experiments where performed, each time adding a new process. The baseline experiments considers only the oceanic invasion of CO_2 (1000 and 5000), then are added in the following order : climate feedbacks (essentially a temperature dependence of solubility and dissociation constants, as well as circulation changes) (1000_c and 5000_c) , sediments feedbacks (1000_cs and 5000_cs), weathering feedbacks (1000_csw and 5000_csw) and vegetation feedbacks (1000_cswv and 5000_cswv). More detailed information about the models and the experiments can be found in Archer et al. (2009).

Now, we will quickly describe how we performed each experiment with SURER. The _cswv experiment is just the standard version of SURFER. For the weathering experiment, we have set K_{AL} to zero, so that vegetation is kept constant (is this true in the new version of the model?) and phase no influence ($F_{AL} = 0$). Additionnaly, for the sediment experiment, we have kept $FCaCO_3$ and FCASIO3 to their preindustrial values, thus eliminating temperature dependence and consequently any weathering feedback. To eliminate the role of sediments in the climate experiment, we have kept the burial and accumulation fluxes constant and equal to their preindustrail values (more explanation needed). Finally for the baseline experiment, we have kept the solubility and dissociation cosntants constant (hehe). The baseline case, is essentially equivalent to the old version of SURFER (except for the pressure dependence of the dissociation constants). These different settings of the model are recapped in table (need to make table and reference it) that can be found in the appendix.

Results for the 1000 PgC and 5000 PgC experiments can be found in figure 14 and 16. Overall, SURFER is in the range of the other other models. Only for the 5000 PgC baseline experiments the CO_2 concentrations in SURFER stabilize just above the range of the other models (number of ppms ?). We observe that the old version of SURFER, although it reahces an equilibrium CO_2 concentration similar as to the other models, doesn't absorb CO_2 from the atmosphere quick enough in the first thousand years after the pulse. THis is improved in the new version SURFER thanks to the addition of a third oceanic layer at intermediate depth.

The five experiments performed for both emissions pulses allow us to define and quantify some feedbacks in the carbon cycle. By substracting the results of two consecutive experiments where the second one has just one more process added, we can compute the isolated effect of this process. For example and for the 1000 PgC pulse, the climate feedback is obtained by substracting the 1000 experiment to the 1000_c experiment, the sediment feedback is obtained by substratcing for each model the 1000_c experiment to the 1000_cs experiment, and so on... Not all experiments where performed for each models so feed-

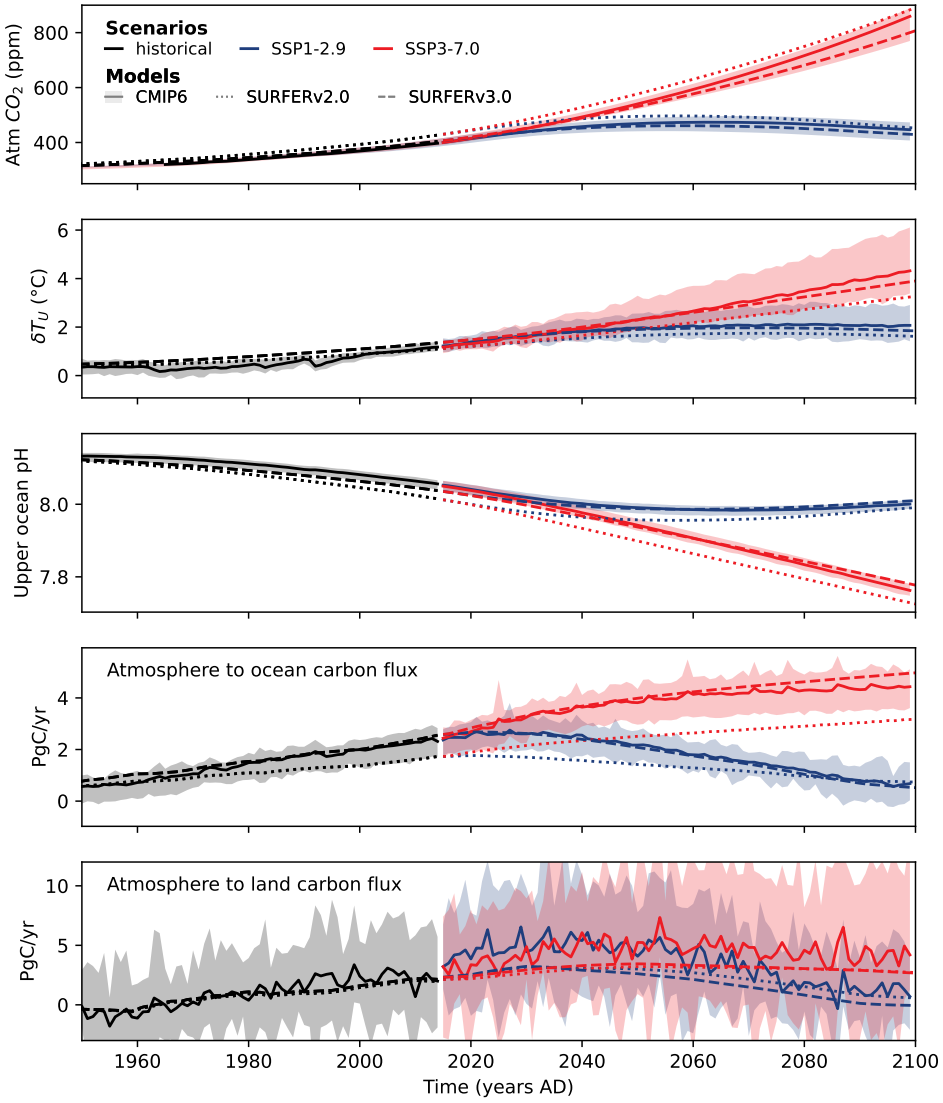

Figure 12. Schematic diagram of the model and its components.

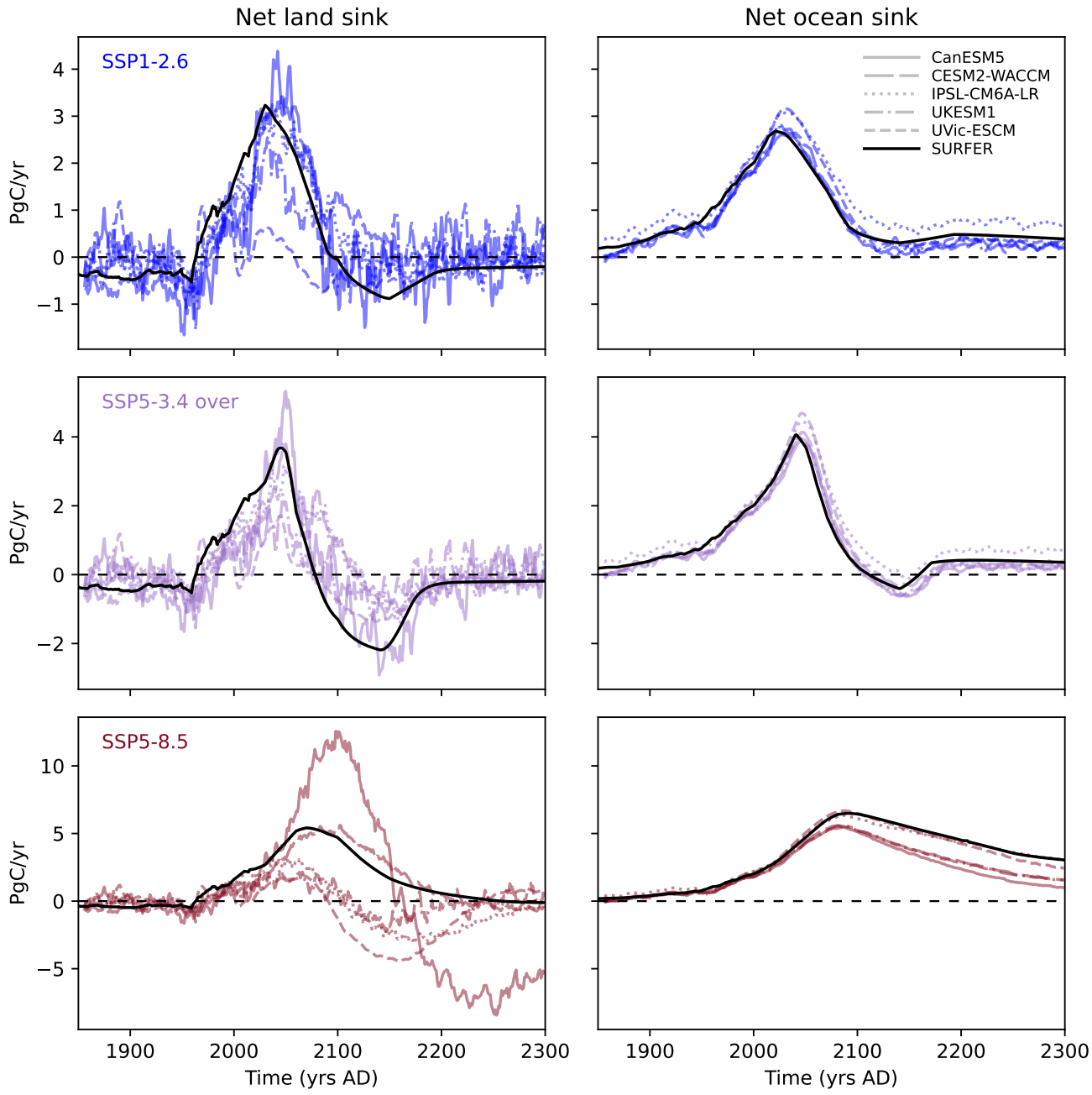

Figure 13. Comparaison of projections from CMIP6 models and SURVER v2.0 and SURFER v3.0 for SSP1-2.9 and SSP3-7.0 emission scenarios.

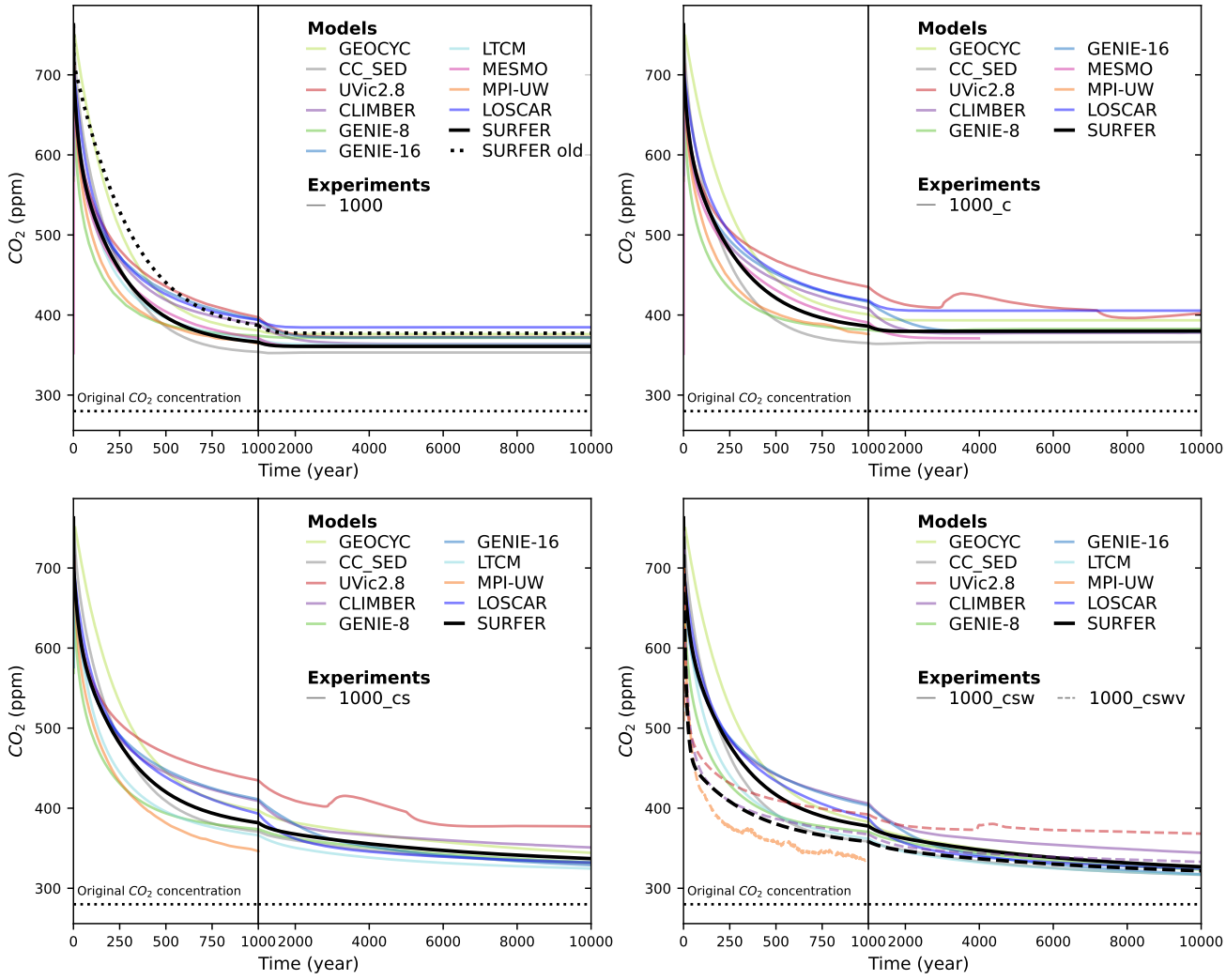

Figure 14. Schematic diagram of the model and its components.

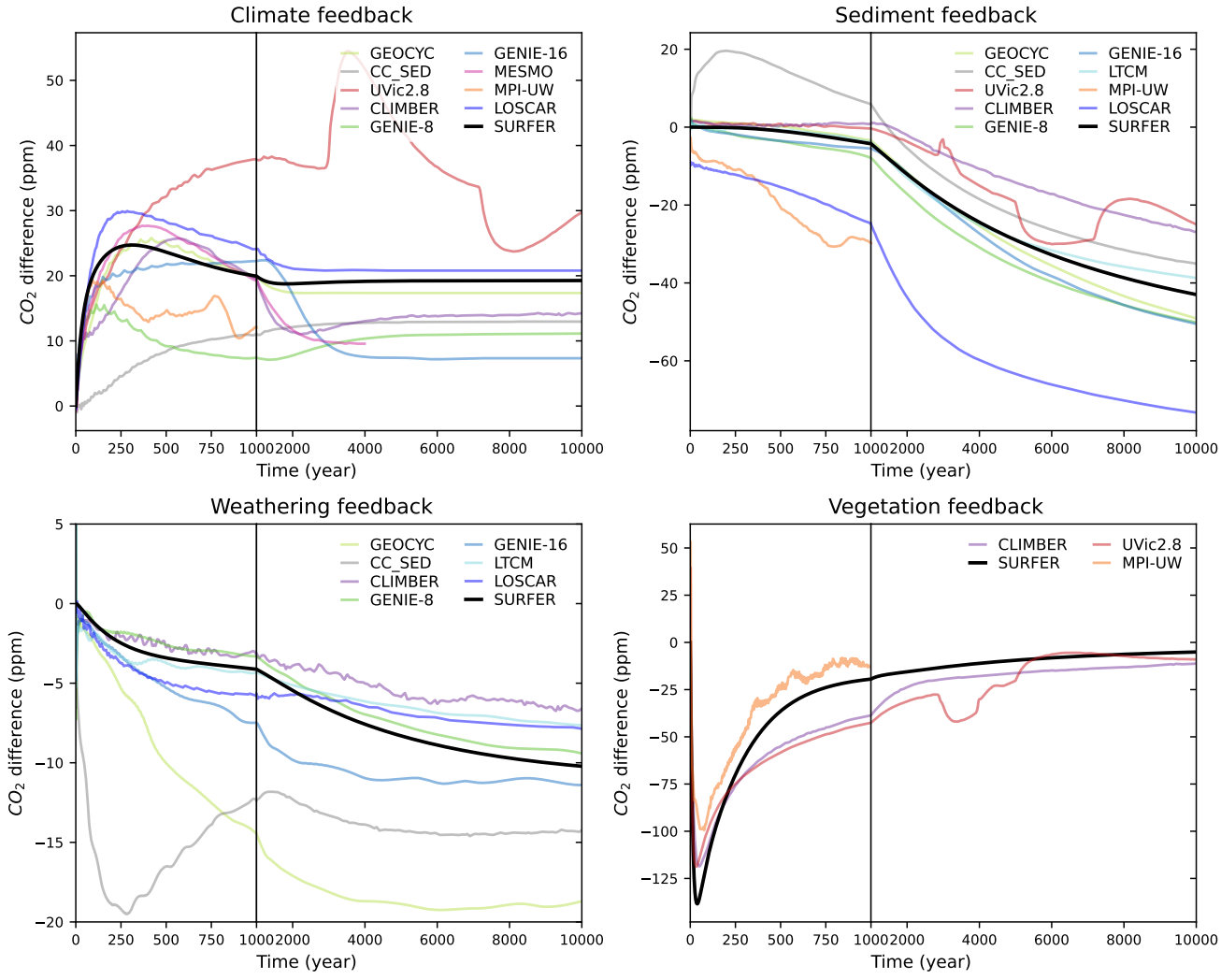

Figure 15. Schematic diagram of the model and its components.

backs can't be computed for each models. All experiments are only available for Climber and SURFER. For the LTCM model, no experiments where performed with climate feedbacks included, so the sediment feedback was taken as _cs - _baseline. For the UVIC2.8 and MPI-UW models, no weathering experiments where performed , so the vegetation feedback is computed as _cswv - _cs.

For the 1000 PgC experiments, SURFER has very similar feedbacks to the LOSCAR model. This is also true for the 5000 PGC , although a bit less convincingly for the weathrin feedback. THis is nice because LOSCAR is another box model but is is more complicated than SURFER. In has more boxes and a more complicated sediments representation with 10 different sediment layers. So to see that SURFER can obtain similar dynamics while being more simple is quite pleasing. FOr both pulse experiments, the climate feedbacks increases and then stabilizes at a higher value compared to the other models (except UVIC2.8). This is a similar behavior to the GEOCYC and LOSCAR models. For the other models (except UVIC2.8) the climate feedback decreases to lower values after around a 1000 years. This is probably due to circulation changes. The GEOCYC, LOSCAR and SURFER models don't have dynamics oceanic circulation and thus can't model that (need to chack if this makes sense). For the sediment feedback we are rather on the high range of the models. This is consistent with figure 18 where the sea-floor $CaCO_3$ accumulation fluxes are plotted for experiments 1000_csw and 5000_csw. We observe that SURFER is in the high range of dissolution (negative accumulation,more or less) and so it makes sense that it has a high sediment feedback.

Every plot together.

5x2 plots (5 lines for the 5 models (normal,C,CS,CSW, CSWV) and two colimns for the emission pulses

4x2 for the feedbacks

1x2 for the accuùmulation

3.5 cGENIE

Comparaison of plots. Overshoot is interesting

Isolate one scenario + different quantities. Comparaison with CS.

Again, ploting the trajectory in MS CO32 lane is insightful for understand the different phases in the dynamics.

4 Sea level rise and importance of long time scale processes

4 models, two versions of UVIC : UVIC2.8 and UVIC2.9. Both have sediments but UVIC2.9 has a slow CO_2 uptake. Two versions of BERN, the comprehensive one has sediments while the reduced one has no sediments. This might explain why temeperatures come down slowly (I could plot CO_2 and SAT for all models , data easily accessible!). Might explain why UVIC2.9 has a way bigger thermosteric SLR (drives the mean up).

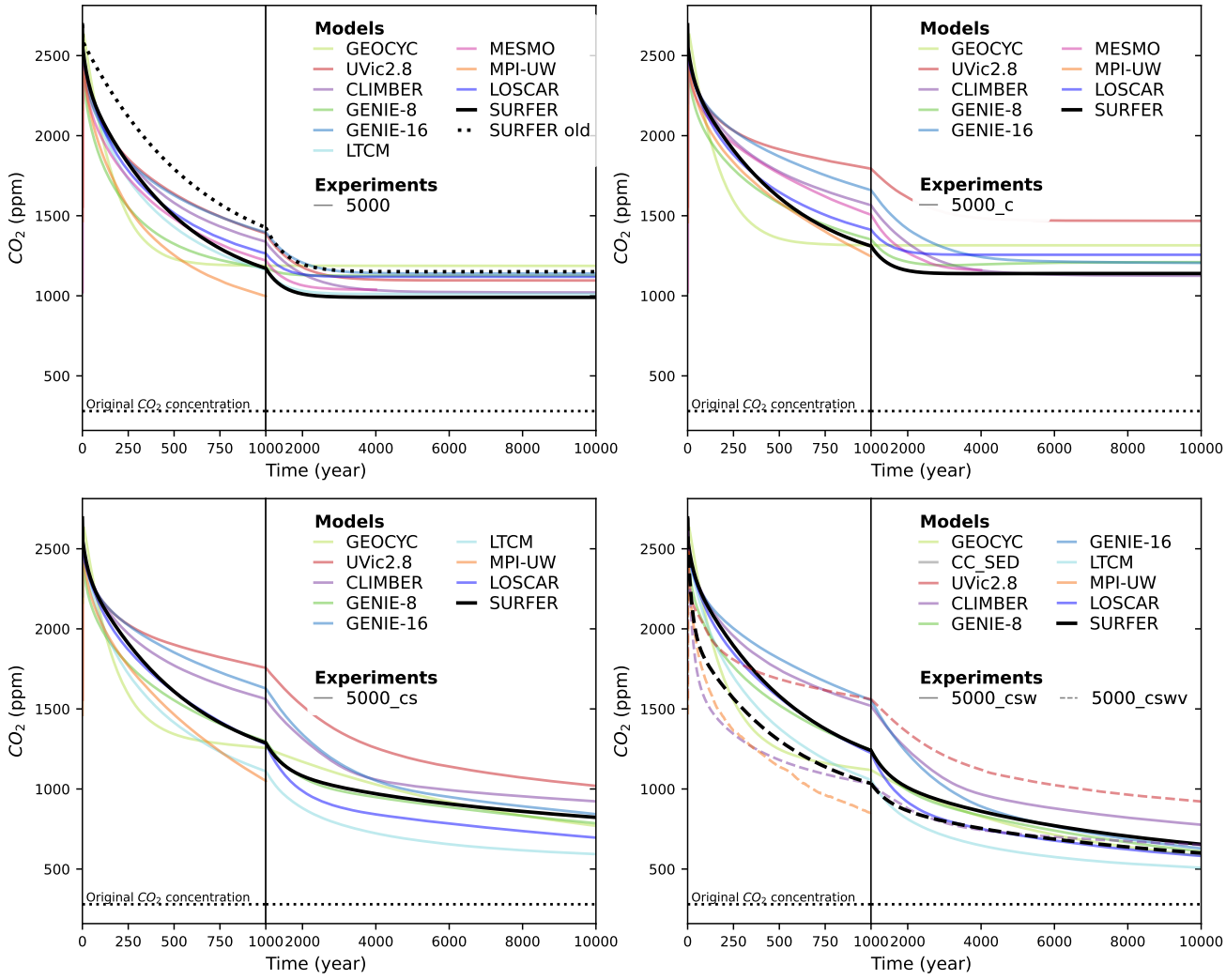

Figure 16. Schematic diagram of the model and its components.

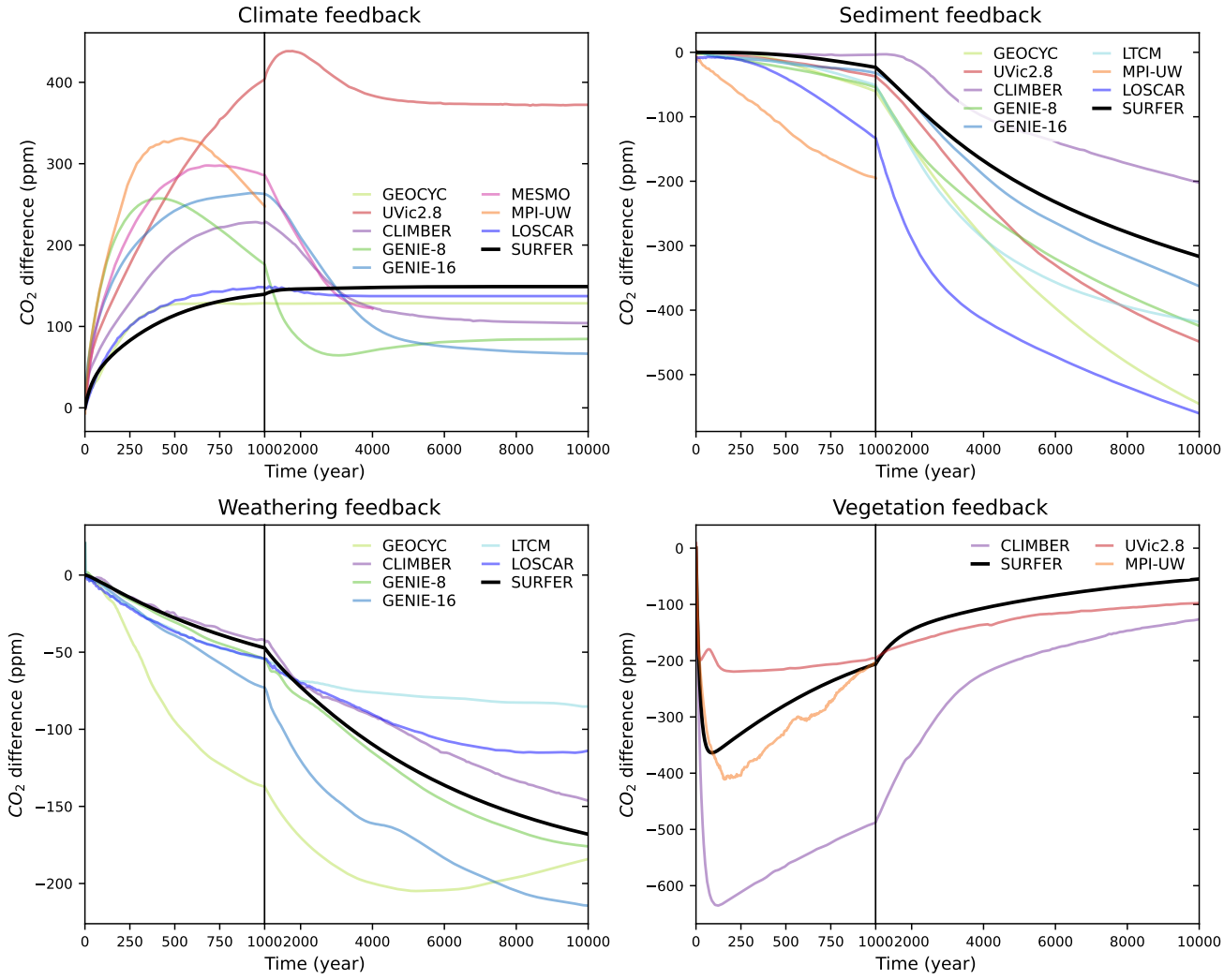

Figure 17. Schematic diagram of the model and its components.

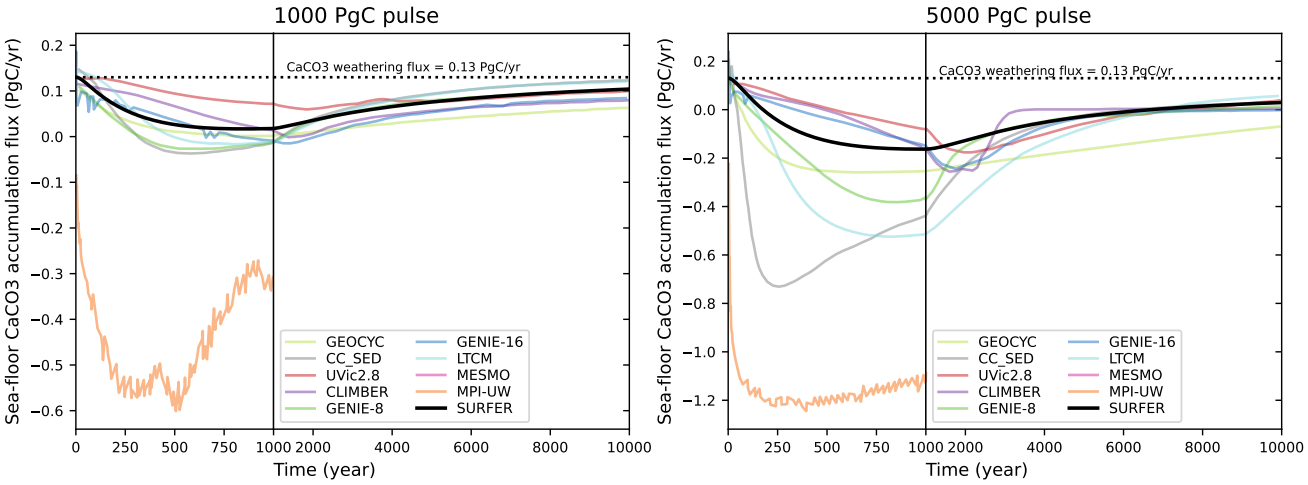

Figure 18. Schematic diagram of the model and its components.

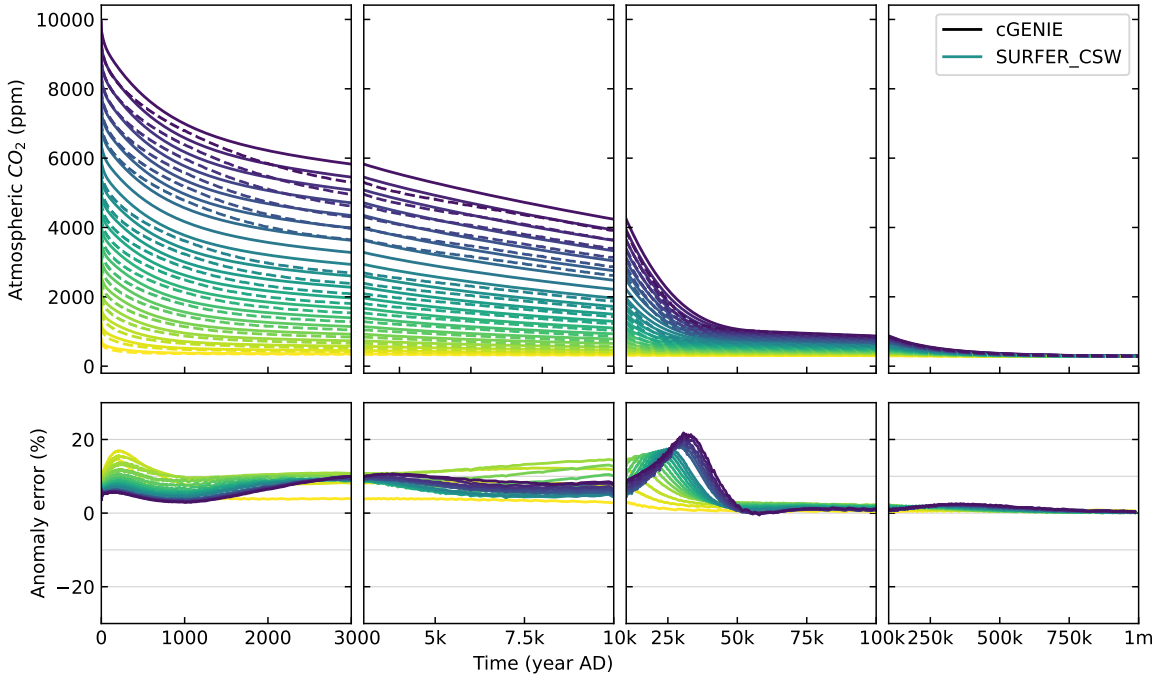

Figure 19. Schematic diagram of the model and its components.

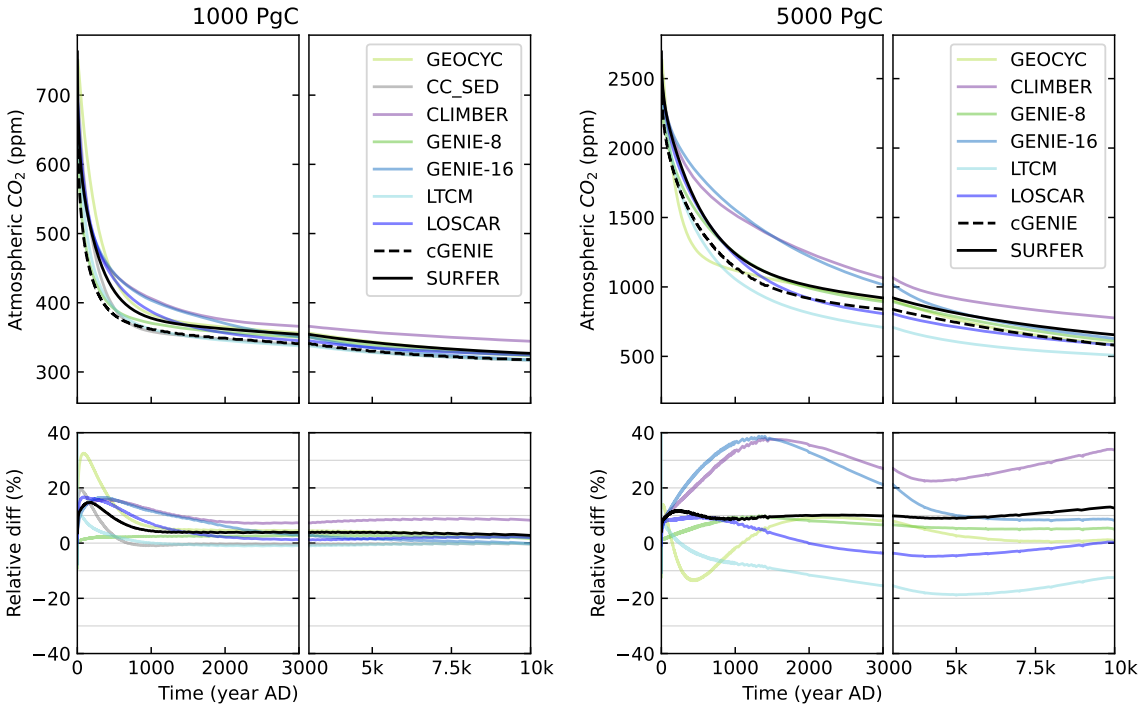

Figure 20. Schematic diagram of the model and its components.

5 Discussion

Surfer is good Explain advantages of surfer over gcms and emics that we compared to. Also advantages over emulators and response functions because process based and dynamic carbon cycle. Advantages and differences over other simialr carbon cycle models (Lenton, LOSCAR and references therein), Mention simple earth system models. Captures the dynamics in more transparent, although less physical manner. In brief , surfer is easy to modify , fast and transparent .

However it does have limitations. First it is not independent of bigger models because it is tuned with their results in mind. Spatial extent doesn't exist. No oceanic circulation. Missing some feedbacks there, see figure with climate feedbacks. Feebacks for hothouse Earth . Paper in preparation.Also,the are other processes than silicate weathering that are susceptible of affecting the CO_2 drawdown on very long time scales. For examples, changes in organic carbon burial and (voir thèse Gaëlle leloup). Doesn't include astronomical forcing. This is currently under addition.

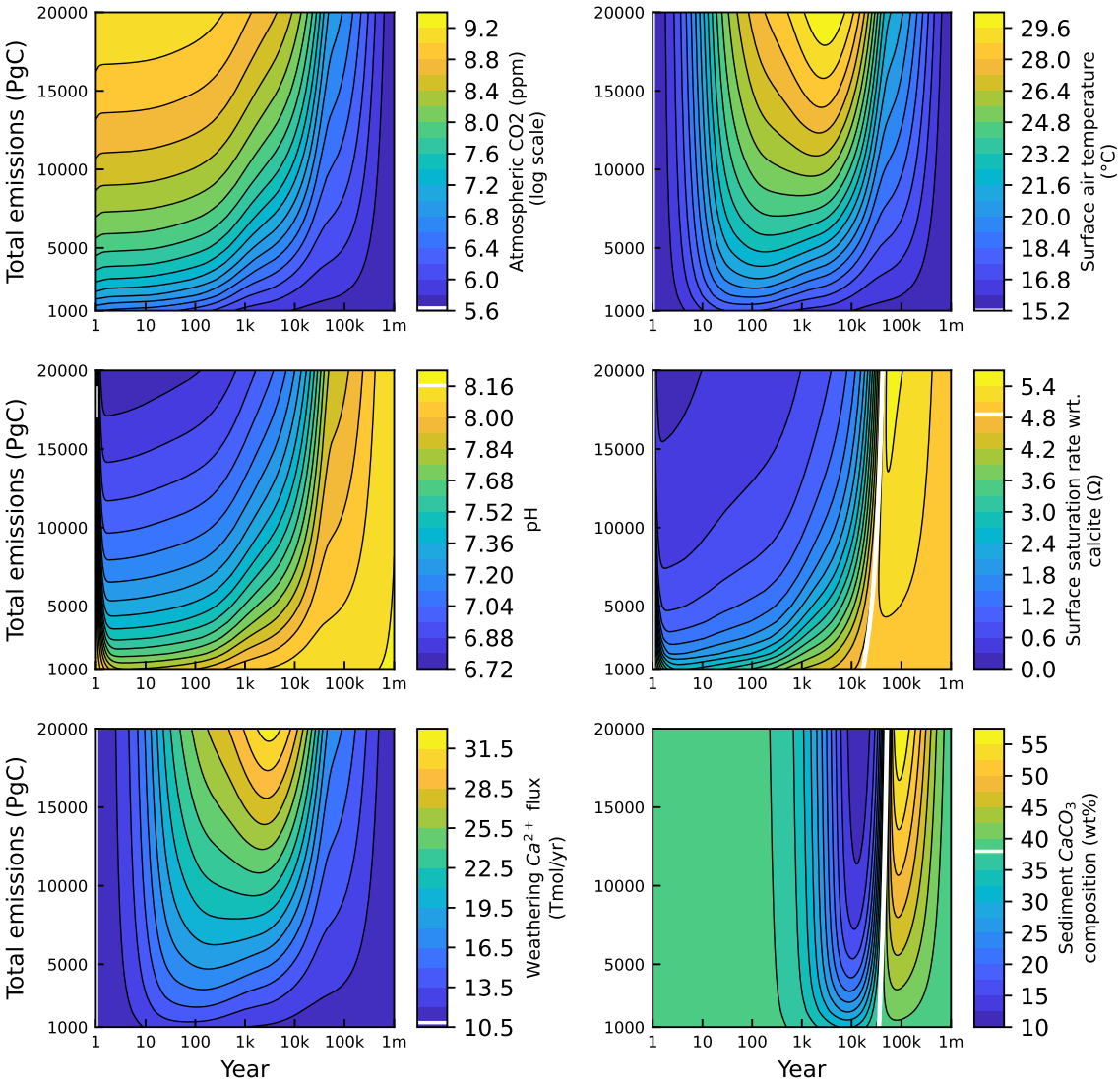

Figure 21. Schematic diagram of the model and its components.

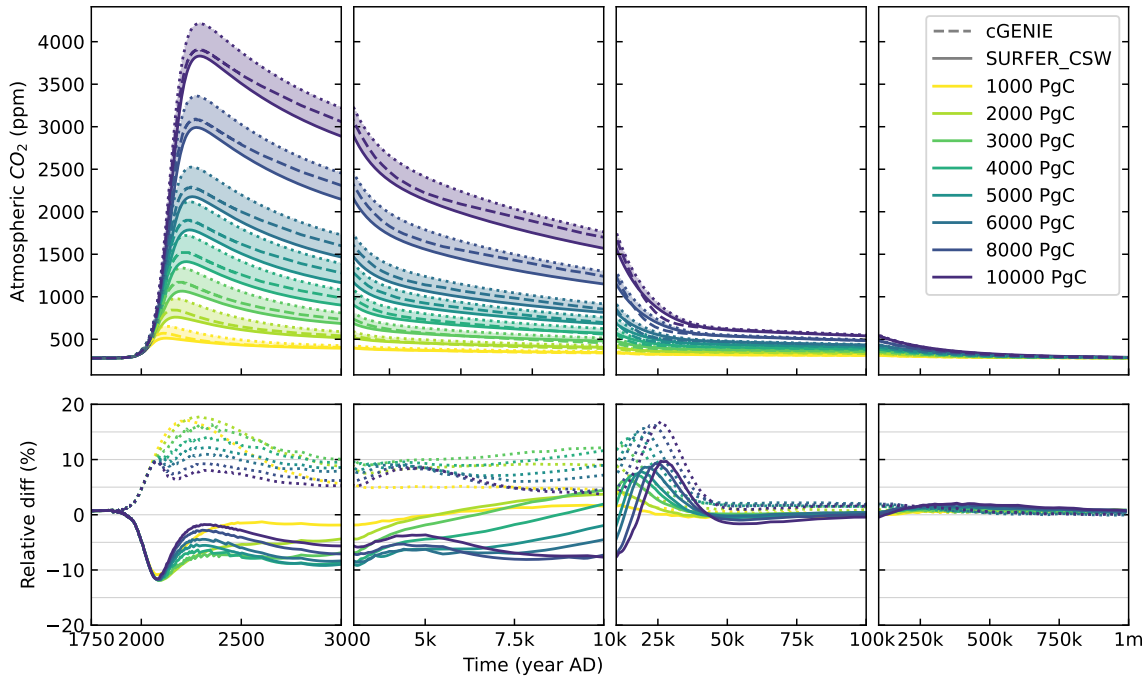

Figure 22. Schematic diagram of the model and its components.

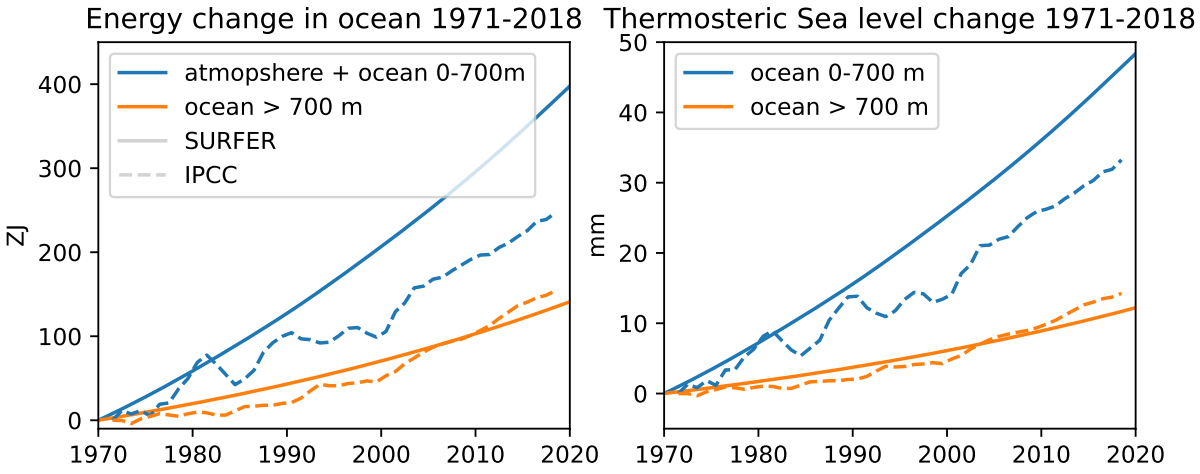

Figure 23. Schematic diagram of the model and its components.

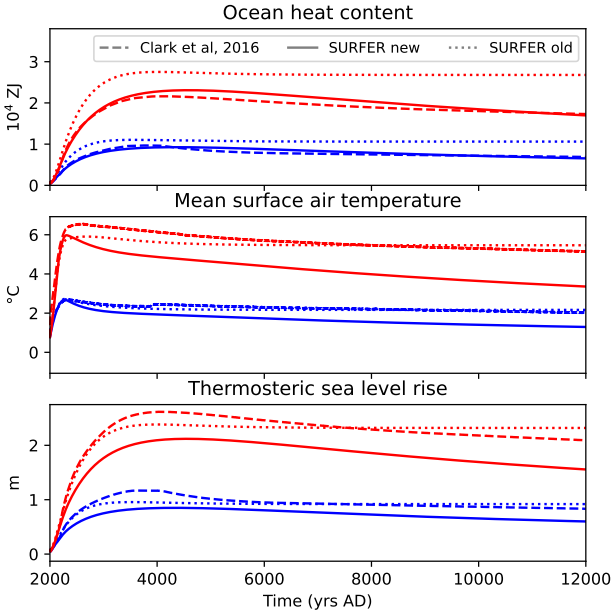

Figure 24. Schematic diagram of the model and its components.

6 Conclusions

We wanted SURFER to be an transparent and easy to understand, flexible and fast model. However we initially excluded some process in the carbon cycle. Now we have shown that we can include these while keeping the model transparent, flexible and fast.

Code availability. TEXT

Data availability. TEXT

Code and data availability. TEXT

Sample availability. TEXT

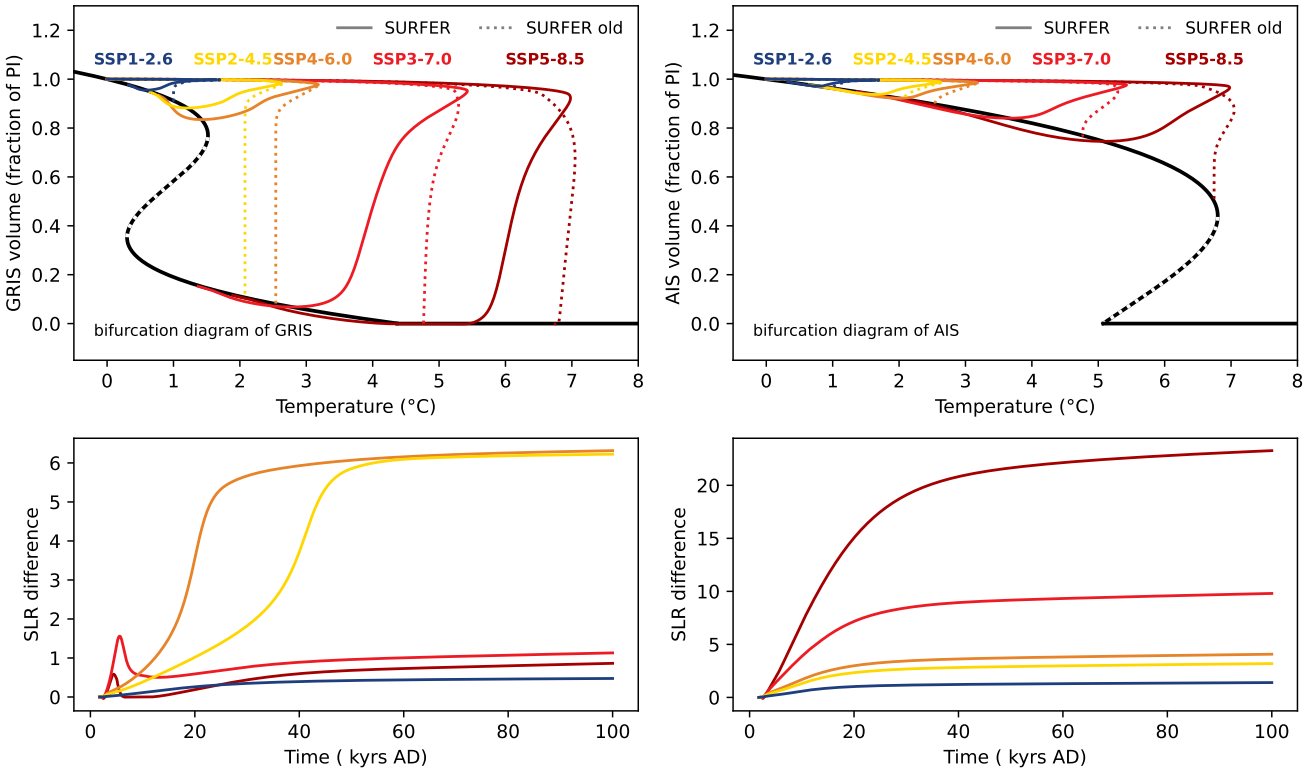

Figure 25. Schematic diagram of the model and its components.

Video supplement. TEXT

Appendix A: Scenarios

Appendix B: Alkalinity and solving the carbonate system

In SURFER v2.0, we approximated alkalinity by carbonate alkalinity

$$\mathrm{Alk} \approx \mathrm{Alk}_C = \left[\mathrm{HCO}_3^-\right] + 2\left[\mathrm{CO}_3^{2-}\right] \tag{B1}$$

To compute $[\mathrm{H}^+]$ and the other carbonate species, we had to rewrite eq B1 as a function of the 4 know quantities DIC, Alk, T, and S and the unknown qantity $[\mathrm{H}^+]$. Using the definition of DIC (eq 11) and of the dissocisation constants K_1 and K_2 (eq 20 and eq 21) we can express DIC as a function of $[\mathrm{HCO}_3^-]$ and $[\mathrm{H}^+]$

$$\mathrm{DIC} = \left(1 + \frac{K_2}{[\mathrm{H}^+]} + \frac{[\mathrm{H}^+]}{K_1}\right)[\mathrm{HCO}_3^-] \tag{B2}$$

or equivalently, we can express $[HCO_3^-]$ as a function of DIC and $[H^+]$

$$[HCO_3^-] = \frac{DIC \cdot K_1[H^+]}{K_1K_2 + K_1[H^+] + [H^+]^2} \tag{B3}$$

Using equation 21, we can then express $[CO_3^{2-}]$ as a function of DIC and $[H^+]$

$$\begin{aligned}[CO_3^{2-}] &= \frac{[HCO_3^-]K_2}{[H^+]} \\ &= \frac{DIC \cdot K_1K_2}{K_1K_2 + K_1[H^+] + [H^+]^2}\end{aligned} \tag{B4}$$

Inserting eqs B3 and B4 in B1, we get

$$Alk \approx Alk_C = DIC \cdot \frac{K_1[H^+] + K_1K_2}{K_1K_2 + K_1[H^+] + [H^+]^2} \tag{B5}$$

which we can solve for $[H^+]$, given Alk, DIC and the dissociations constants K_1 and K_2 (which depend on T and S). To do so, we write eq B5 as a degree 2 polynomial equation

$$P_C([H^+]) \equiv [H^+]^2 + a_1[H^+] + a_0 \tag{B6}$$

with

$$a_1 = K_1\left(1 - \frac{DIC}{Alk}\right) \tag{B7}$$

$$a_0 = K_1K_2\left(1 - \frac{2 \cdot DIC}{Alk}\right) \tag{B8}$$

The positive root is given by

$$[H^+] = \frac{K_1}{2 \cdot Alk}\left(\sqrt{(DIC - Alk)^2 - 4\frac{K_2}{K_1}Alk \cdot (Alk - 2 \cdot DIC)} + (DIC - Alk)\right) \tag{B9}$$

Then, $[HCO_3^-]$ can be computed from equation B3, $[CO_3^{2-}]$ can be computed from equation B4, and finally, $[H_2CO_3]$ can be computed from equation 20.

In SURFERv3.0, we approximate alkalinity by the carbonate, borate and water self-ionisation alkalinity

$$Alk \approx Alk_{CBW} = \left[HCO_3^-\right] + 2\left[CO_3^{2-}\right] + \left[OH^-\right] - \left[H^+\right] + \left[B(OH)_4^-\right] \tag{B10}$$

As before, to compute $[H^+]$ and the other carbonate species, we have to rewrite eq B10 as a function of the 4 know quantities DIC, Alk, T, and S and the unknown qantity $[H^+]$. We already know how express $[HCO_3^-]$ and $[CO_3^{2-}]$ as a function of DIC and $[H^+]$ (eqs B3 and B4). Equation 22 further gives us

$$\left[OH^-\right] = \frac{K_w}{[H^+]} \tag{B11}$$

and we can use equations 23 and 24 to obtain

$$\left[\mathrm{B(OH)_4^-}\right] = \frac{c_b \cdot S \cdot K_b}{[\mathrm{H^+}] + K_b} \tag{B12}$$

Inserting these results in equation B10, we get

$$\mathrm{Alk} \approx \mathrm{Alk}_{CBW} = \mathrm{DIC} \cdot \frac{K_1[\mathrm{H^+}] + K_1K_2}{K_1K_2 + K_1[\mathrm{H^+}] + [\mathrm{H^+}]^2} + \frac{K_w}{[\mathrm{H^+}]} - \left[\mathrm{H^+}\right] + \frac{c_b \cdot S \cdot K_b}{[\mathrm{H^+}] + K_b} \tag{B13}$$

which we can solve for $[\mathrm{H^+}]$, given Alk, DIC and the dissociations constants K_1, K_2, K_w and K_b (which depend on T and S). To do this, we write eq B13 as a polynomial equation that is now of degree 5

$$P_{CBW}([\mathrm{H^+}]) \equiv [\mathrm{H^+}]^5 + q_4[\mathrm{H^+}]^4 + q_3[\mathrm{H^+}]^3 + q_2[\mathrm{H^+}]^2 + q_1[\mathrm{H^+}] + q_0 \tag{B14}$$

with

$$q_4 = \mathrm{Alk} + K_1 + K_b \tag{B15}$$

$$q_3 = (\mathrm{Alk} - \mathrm{DIC} + K_b)K_1 + (\mathrm{Alk} - c_b \cdot S)K_b + K_1K_2 - K_w \tag{B16}$$

$$q_2 = (\mathrm{Alk} - 2 \cdot \mathrm{DIC} + K_b)K_1K_2 + (\mathrm{Alk} - \mathrm{DIC} - c_b \cdot S)K_1K_b - K_1K_w - K_bK_w \tag{B17}$$

$$q_1 = (\mathrm{Alk} - 2 \cdot \mathrm{DIC} - c_b \cdot S)K_1K_2K_b - K_1K_2K_w - K_1K_bK_w \tag{B18}$$

$$q_0 = -K_1K_2K_bK_w \tag{B19}$$

We solve this equation using the Newton-Raphson method. In order to ensure a quick convergence, we need a good initial guess that is not too far from the real solution. We adopt the following procedure from Munhoven (2013) and Humphreys et al. (2022). We define the following coefficients

$$c_2 = K_b\left(1 - \frac{c_b \cdot S}{\mathrm{Alk}}\right) + K_1\left(1 - \frac{\mathrm{DIC}}{\mathrm{Alk}}\right) \tag{B20}$$

$$c_1 = K_1K_b\left(1 - \frac{c_b \cdot S}{\mathrm{Alk}} - \frac{\mathrm{DIC}}{\mathrm{Alk}}\right) + K_1K_2\left(1 - 2\frac{\mathrm{DIC}}{\mathrm{Alk}}\right) \tag{B21}$$

$$c_0 = K_1K_2K_b\left(1 - \frac{2 \cdot \mathrm{DIC} + c_b \cdot S}{\mathrm{Alk}}\right) \tag{B22}$$

from which we construct the quantities

$$H_{min} = \frac{-c_2 + \sqrt{c_2^2 - 3c_1}}{3} \tag{B23}$$

and

$$H_0 = H_{min} + \sqrt{-\frac{H_{min}^3 + c_2H_{min}^2 + c_1H_{min} + c_0}{\sqrt{c_2^2 - 3c_1}}} \tag{B24}$$

The initial guess for the Newton-Raphson method is taken as

$$[\mathrm{H}^+]_0 = \begin{cases} 10^{-3} & \text{if } \mathrm{Alk} \leq 0, \\ H_0 & \text{if } 0 < \mathrm{Alk} < 2 \cdot \mathrm{DIC} + c_b \cdot S \text{ and } c_2^2 - 3c_1 > 0, \\ 10^{-7} & \text{if } 0 < \mathrm{Alk} < 2 \cdot \mathrm{DIC} + c_b \cdot S \text{ and } c_2^2 - 3c_1 < 0, \\ 10^{-10} & \text{if } \mathrm{Alk} \geq 2 \cdot \mathrm{DIC} + c_b \cdot S, \end{cases} \tag{B25}$$

The rationale behind this choice is given in Munhoven (2013) and Humphreys et al. (2022). With it, we only need 5 Newton-Raphson iterations to obtain a precise value for $[\mathrm{H}^+]$ and pH, which is defined as

$$pH = -\log_{10}([\mathrm{H}^+]) \tag{B26}$$

Once $[\mathrm{H}^+]$ is computed, $[\mathrm{HCO}_3^-]$ and $[\mathrm{CO}_3^{2-}]$ can be computed from equations B3 and B4, $[\mathrm{H_2CO_3}]$ can be computed from equation 20, $\left[\mathrm{OH}^-\right]$ can be computed from equation B11, and $\left[\mathrm{B(OH)}_4^-\right]$ can be computed from equation B12. Equation B10 is solved following this procedure at every time step of the numerical integration of the model. This is because we need $[\mathrm{H}^+]_U$ for the computation of B_U in the atmosphere to upper ocean carbon flux $F_{A\to U}$ (see equations 38 and 39), and we need $[\mathrm{CO}_3^{2-}]_D$ for the computation of the dissolution flux F_{diss} (see eq 65). This is also the procedure used to obtain climatologies (and vertical profiles) of the carbonate species from the GLODAP climatologies of DIC, Alk, temperature and salinity (see figure 5). In this case we computed the carbonate species at each ocean point where DIC, Alk, temperature and salinity were all given.

To determine the initial condition for the dissolved inorganic carbon mass in the upper layer $M_U(t_{PI})$, we need to compute DIC_U as a function of $\mathrm{Alk}_U(t_{PI})$, $T_U(t_{PI})$, S_U, and $\mathrm{H_2CO}^*_{3U}(t_{PI})$, which is fixed by equilibrium conditions (eq 152). Now DIC is an unknown and we can't use the procedure described above. Instead, we write Alk as a function of $[\mathrm{H_2CO}_3^*]$ and $[\mathrm{H}^+]$ (and the dissociation). Using equations 20 and 21 we get

$$[\mathrm{HCO}_3^-] = \frac{K_1[\mathrm{H_2CO}_3^*]}{[\mathrm{H}^+]} \tag{B27}$$

$$[\mathrm{CO}_3^{2-}] = \frac{K_1 K_2[\mathrm{H_2CO}_3^*]}{[\mathrm{H}^+]^2} \tag{B28}$$

and thus

$$Alk \approx Alk_{CBW} = \frac{K_1[\mathrm{H_2CO_3}]}{[\mathrm{H}^+]} + 2\frac{K_1 K_2[\mathrm{H_2CO_3}]}{[\mathrm{H}^+]^2} + \frac{K_w}{[\mathrm{H}^+]} - \left[\mathrm{H}^+\right] + \frac{c_b \cdot S \cdot K_b}{[\mathrm{H}^+] + K_b} \tag{B29}$$

This equation can be solved numerically for $[\mathrm{H}^+]$ using any algorithm. The speed of the algorithm is not of great importance here since we only perform the computation for the setting of the initial conditions, and not at each time step of the numerical integration. Once $[\mathrm{H}^+]$ is obtained, $[\mathrm{HCO}_3^-]$ and $[\mathrm{CO}_3^{2-}]$ are recovered with equations 20 and 21 and DIC can then be computed as the sum of $[\mathrm{HCO}_3^-]$, $[\mathrm{CO}_3^{2-}]$ and $[\mathrm{H_2CO}_3^*]$.

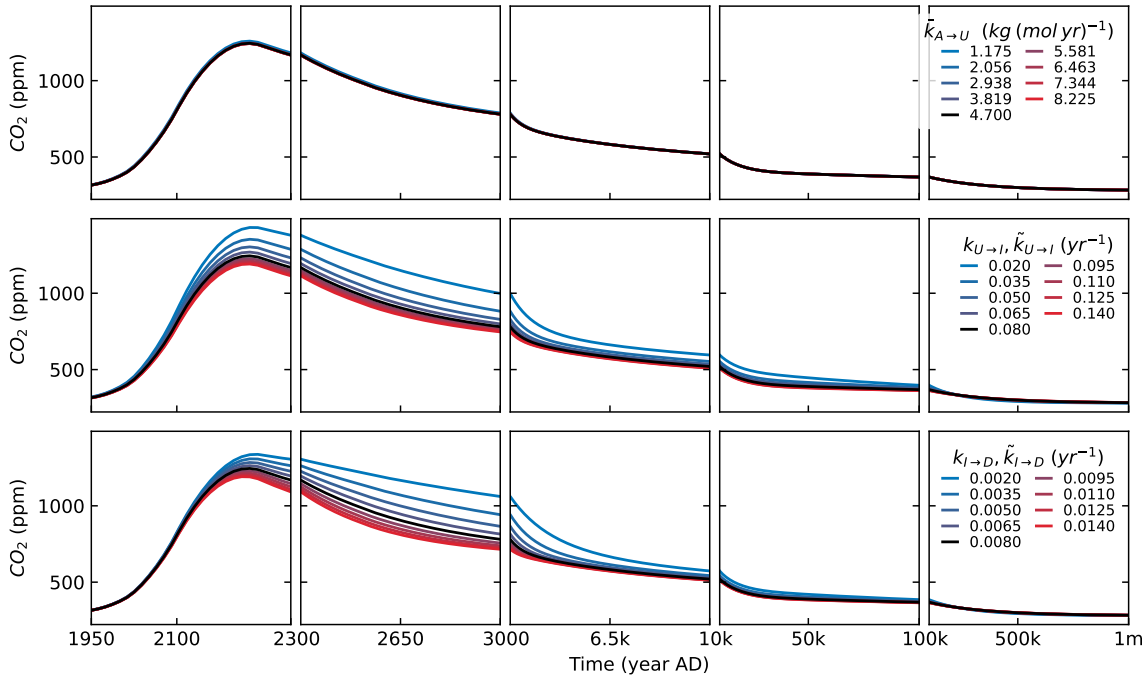

Figure C1. Schematic diagram of the model and its components.

Appendix C: Sensitivity analysis

Appendix D: Numerics and model verification

We performed speed tests of the model for two different setups : in one case the model was forced with $mathrmCO_2$ and CH_4 emissions from SSPxxx scenario (figure D1), and in the other case the model was started with a xxx PgC perturbation in the atmosphere (figure D2) , similar as for the pulse experiments in section 3.5. In both cases, we timed the model for simulated times ranging from 10 to 10^6 years and for $rtol$ ranging from 10^{-6} to 10^{-3}. We also compared with SURFER v2.0, ran on the same machine. For a fair comparison, we have re-coded SURFER v2.0 in python (original version is in Julia) and used the LSODA numerical method to integrate the model, as for SURFER v3.0. And only used CO2 forcing, not methane.

In the SSP setup, runing time increases with simulated time but no linearly. There is a sharp increase in running time when the simulated time reaches around 200 years. This is the time where the bulk of the emissions happen (simulation starts in 1750, and most emissions happen in the interval 1950-2200). Once emissions have stopped, there is only a small increase of running time with simulated time, even for simulated times up to a million years. This is because the LSODA integration method uses an adaptative time step : when the model gets closer to equilibrium (after long simulated times), the time steps

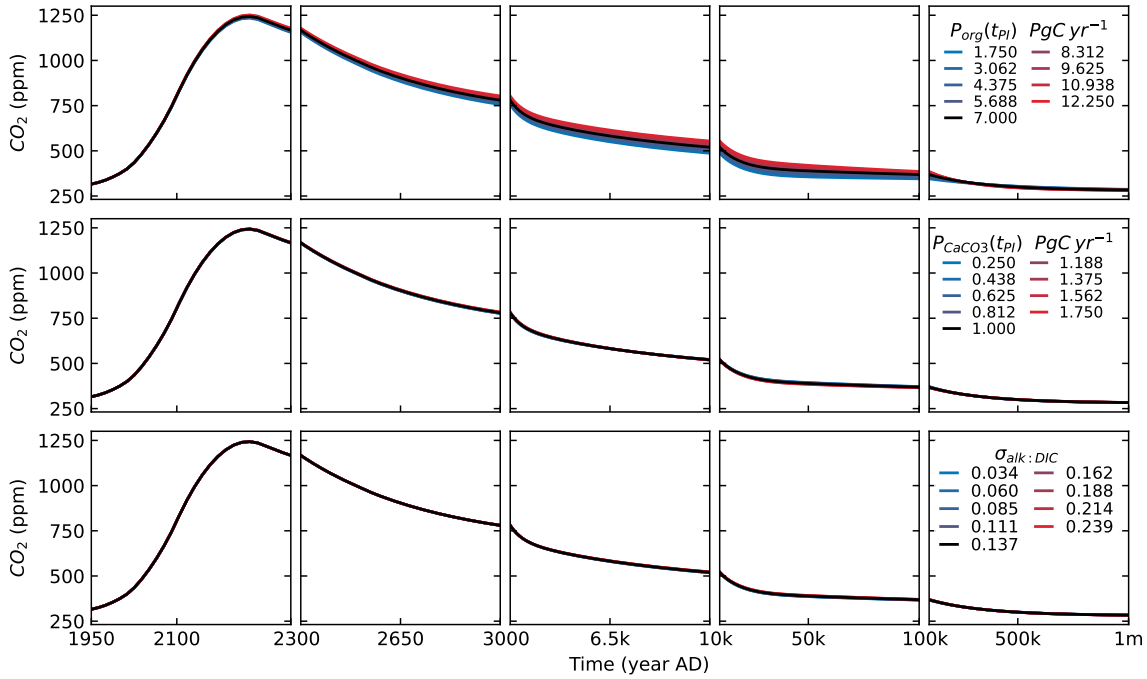

Figure C2. Schematic diagram of the model and its components.

get bigger, meaning that a million year simulation is not much more computationally demanding than an hundred thousand year simulation. As expected, with everything else equal, the running time is lower for higher $rtol$. Choosing $rtol = 10^{-3}$ instead of $rtol = 10^{-6}$ decreases the running time by a factor 10. This doesn't impact much the projections of atmospheric CO_2 or any other variables but can reduce significantly the accuracy for computed quantities such as the air-sea or atmosphere to land carbon fluxes $F_{A\to U}$ and $F_{A\to L}$ (see figure D3). This is due to catastrophic cancellation errors. Indeed, these fluxes are computed as differences of almost equal quantities, and so even a small relative error on each quantity can lead to large relative error on the difference. We recommend changing the $rtol$ depending on the uses cases of the model. In most cases, setting $rtol = 10^{-3}$ is sufficient, but if the user wishes to study the atmosphere-to-land or atmosphere-ocean fluxes (as we do for example in figure 12), setting $rtol = 10^{-6}$ is probably safer.

SURFERv3.0 takes abut the same amount of steps as SURFERv2.0. A bit more for longer simulated times becauses it reaches equilibrium later. But it tke more time per steps. THis is because we have twice as many eqautions and also because solving the carbonate system is more complex. Overall SURFERv3.0 is about six times slower for $rtol$ betwen 10^{-3} and 10^{-5} and About ten times slower than SURFER v2.0 for $rtol = 10^{-5}$. We believe that the added complexity is worth this speep loss.

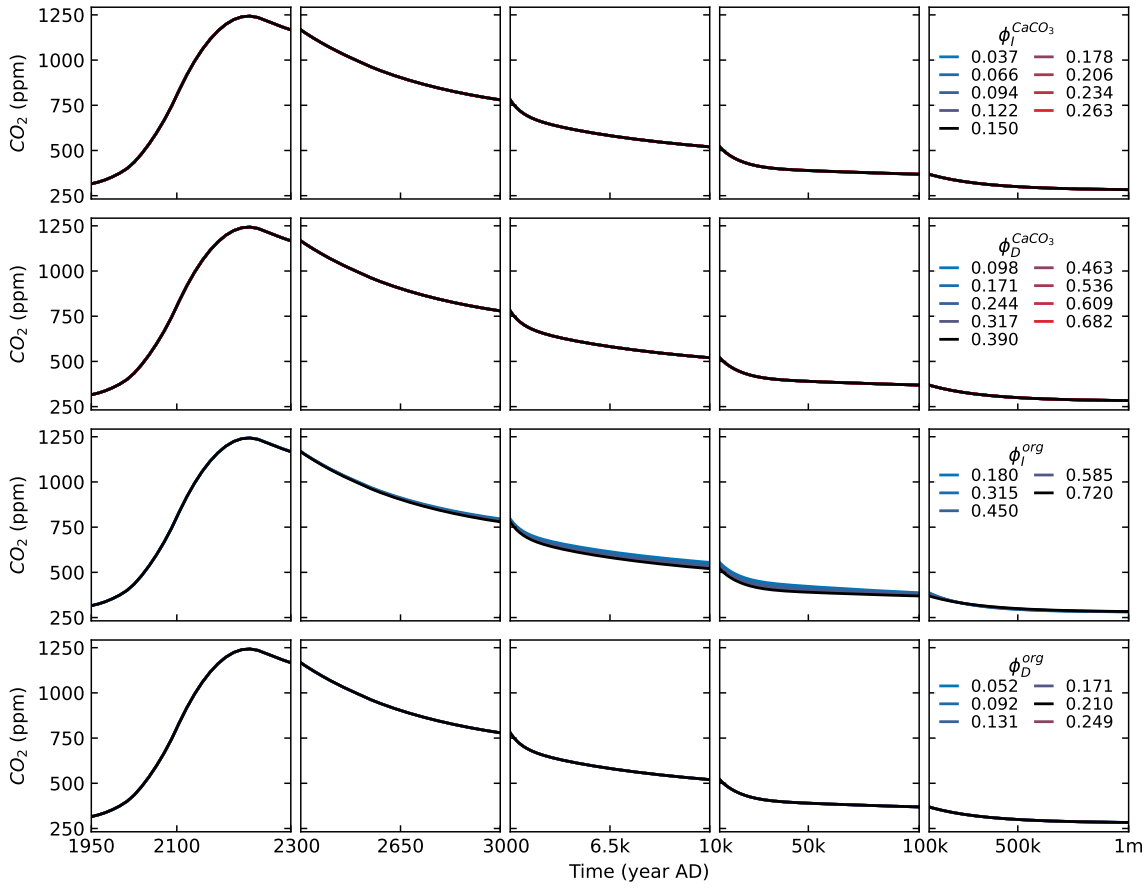

Figure C3. Schematic diagram of the model and its components.

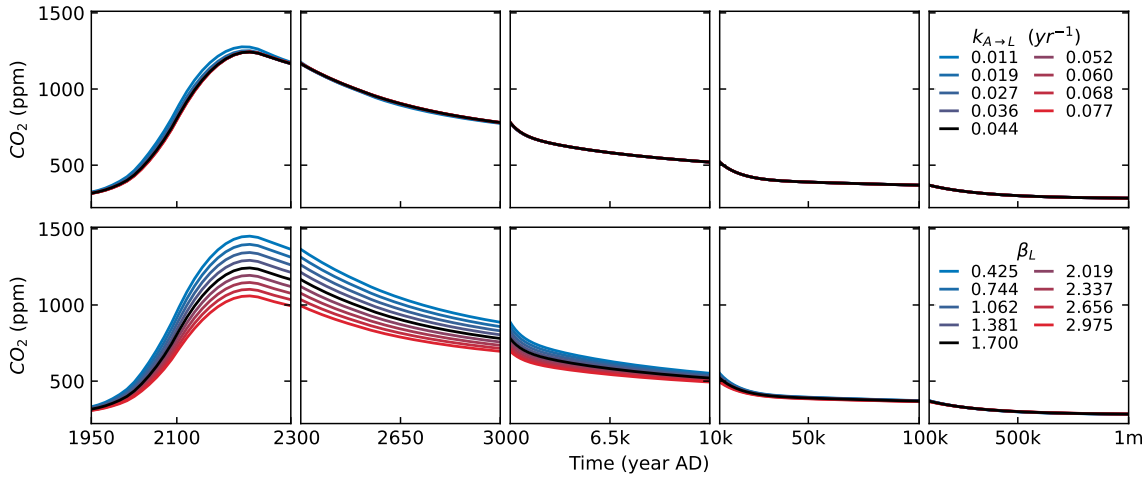

Figure C4. Schematic diagram of the model and its components.

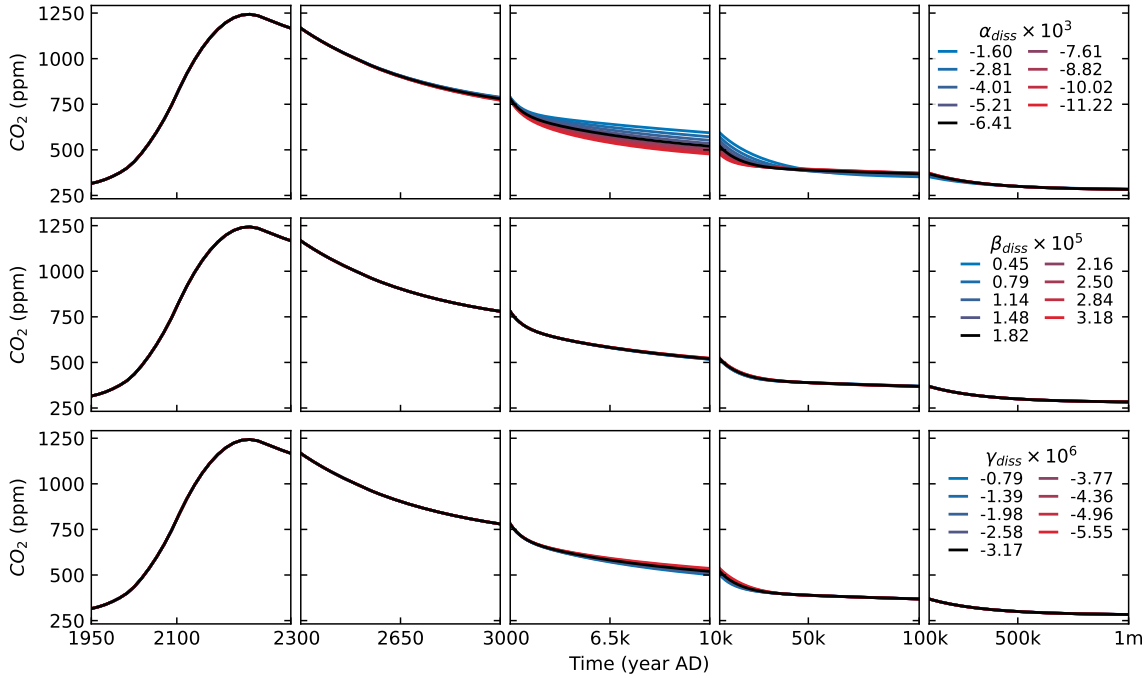

Figure C5. Schematic diagram of the model and its components.

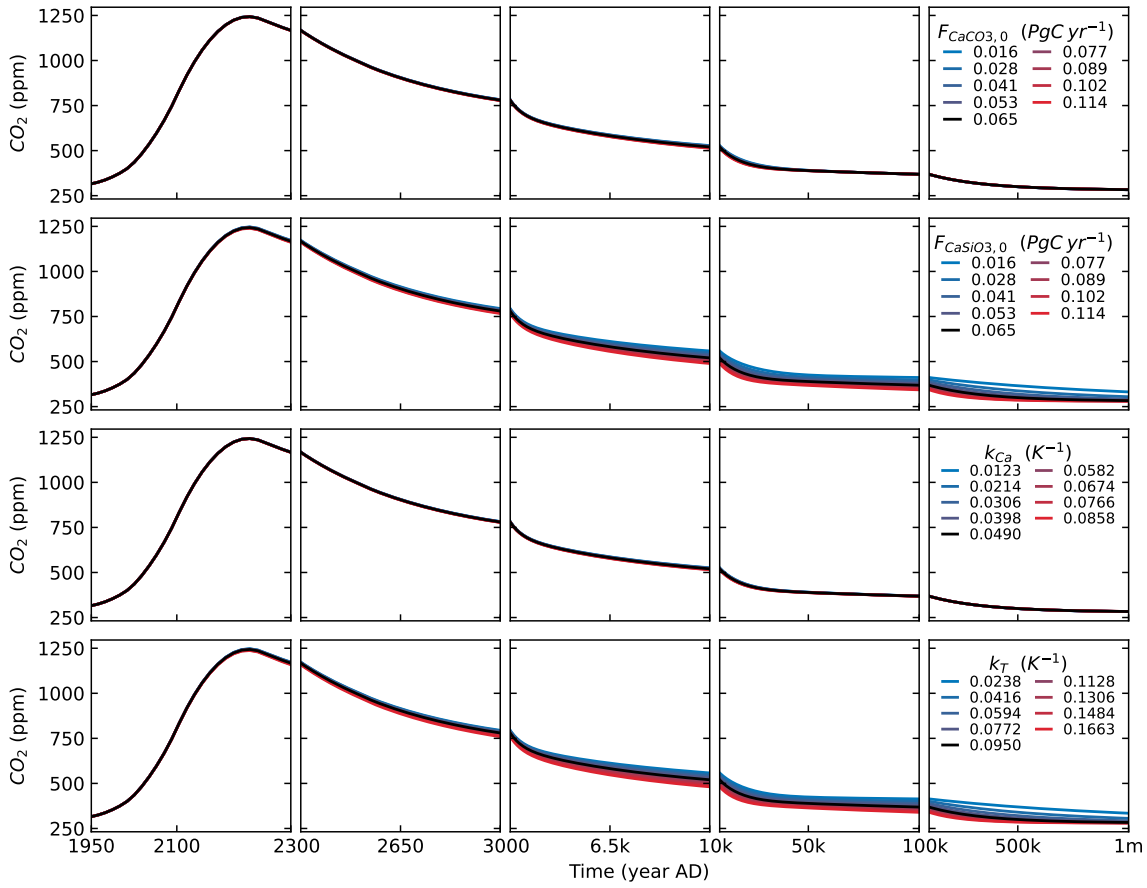

Figure C6. Schematic diagram of the model and its components.

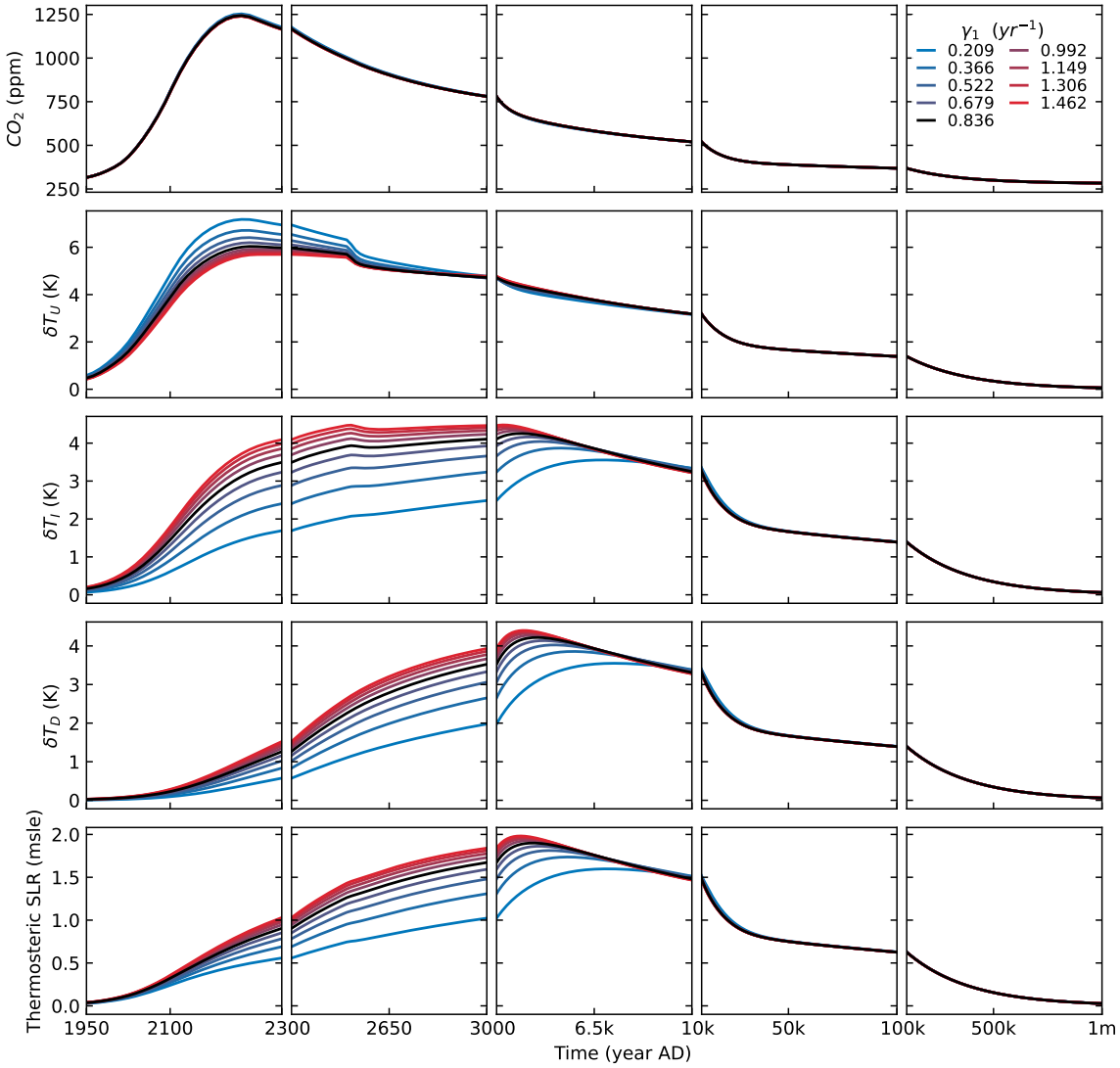

Figure C7. Schematic diagram of the model and its components.

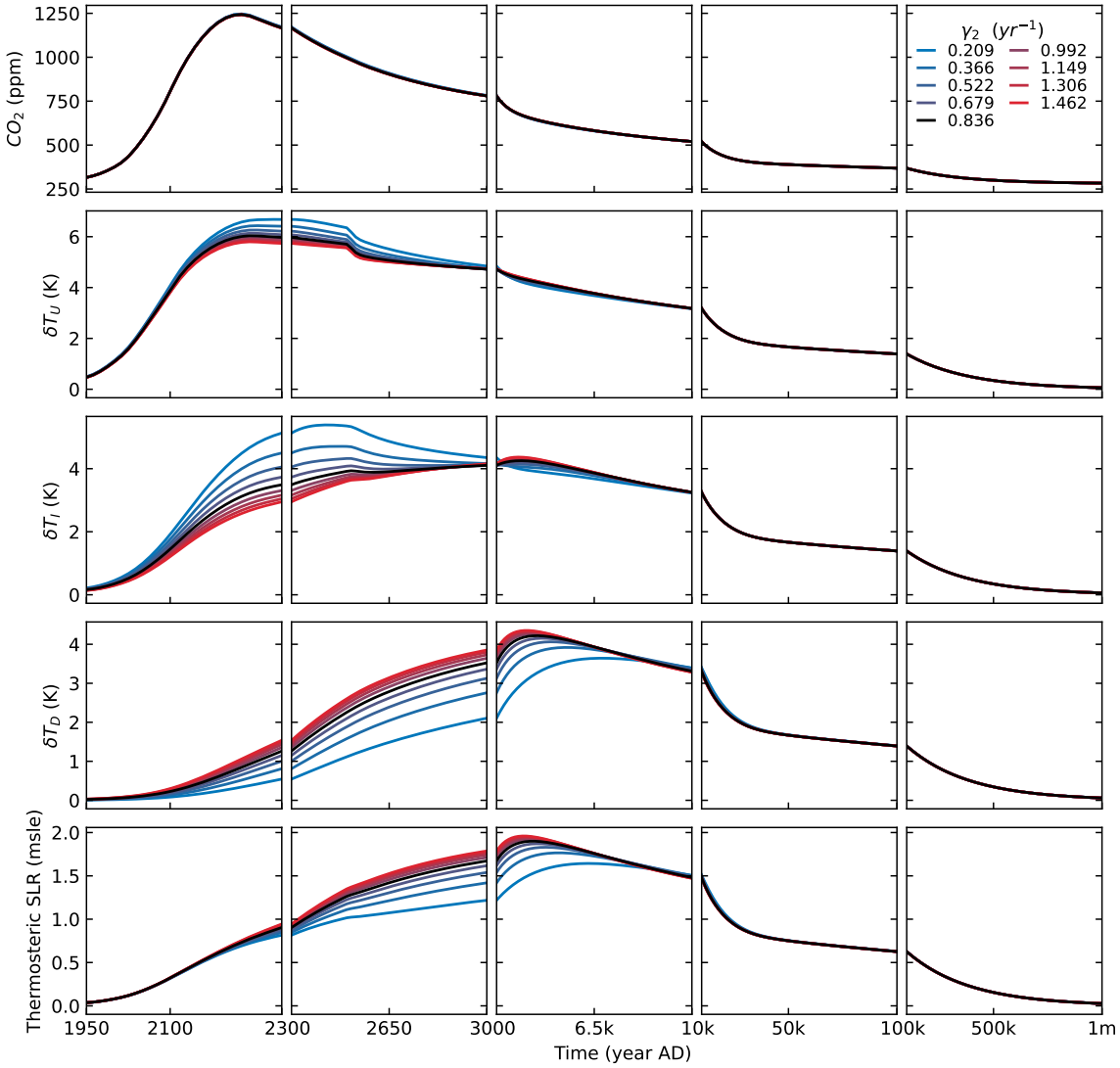

Figure C8. Schematic diagram of the model and its components.

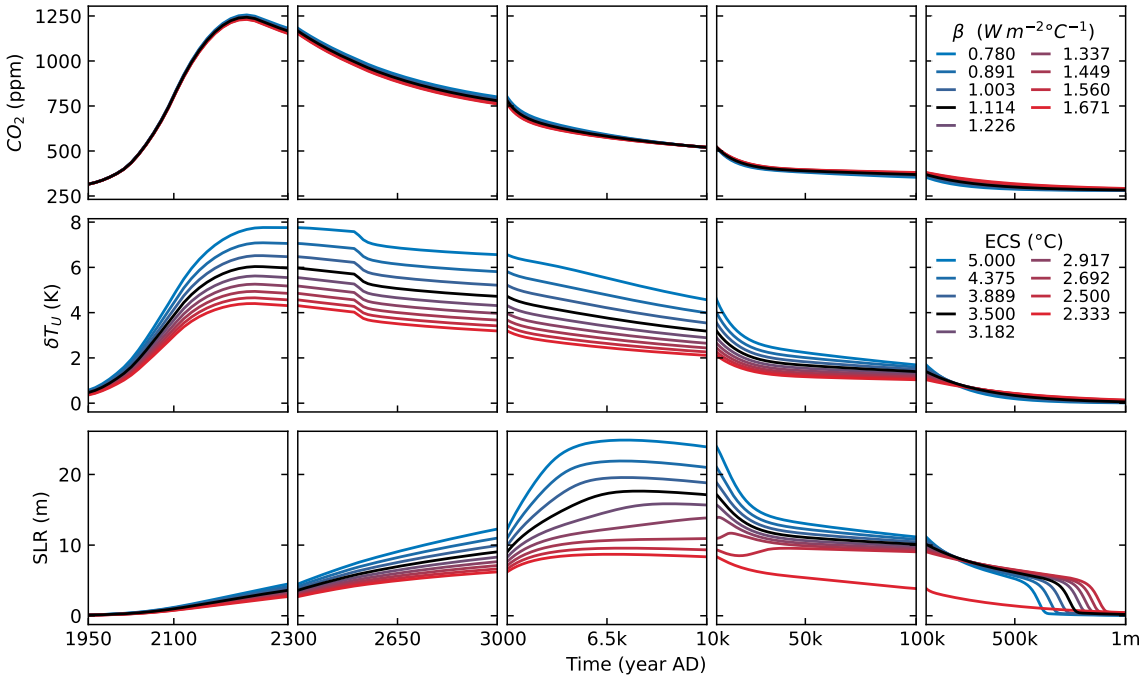

Figure C9. Schematic diagram of the model and its components.

We observe similar results for the pulse experiment, with fewer differences between the choices of $rtol$. Overall pulse experiments are faster than experiment with a forcing, both for SURFERv3.0 and SURFER v2.0. This is due to a combination of less steps in the integration, and less time needed per step.

A small note for the potential user : the adaptive time step means that if you start the model close to equilibrium and your different emisions forcing don't happen soon enough, the solver will start to take big steps very quickly and might miss the emissions altogether if they happen on a reduced time span. To avoid this, one can start the forcing sooner. Another solution is to play with the atol, rtol parameters or to impose a maximal time step, but this is at the expense of increasing runtime, especially for simulation of longer time scales.

Our model equations, based on conservation laws tell us that the derivative of the total sum of carbon present in all reservoirs must be equal to sources (volcanism+weathering of carbonate rocks + fossil CO_2 and CH_4 emissions) minus sinks (burial). In figure D4, we show that for a standard run forced by SSPX scenario, our numercial solution obeys this conservation law.

Author contributions. TEXT

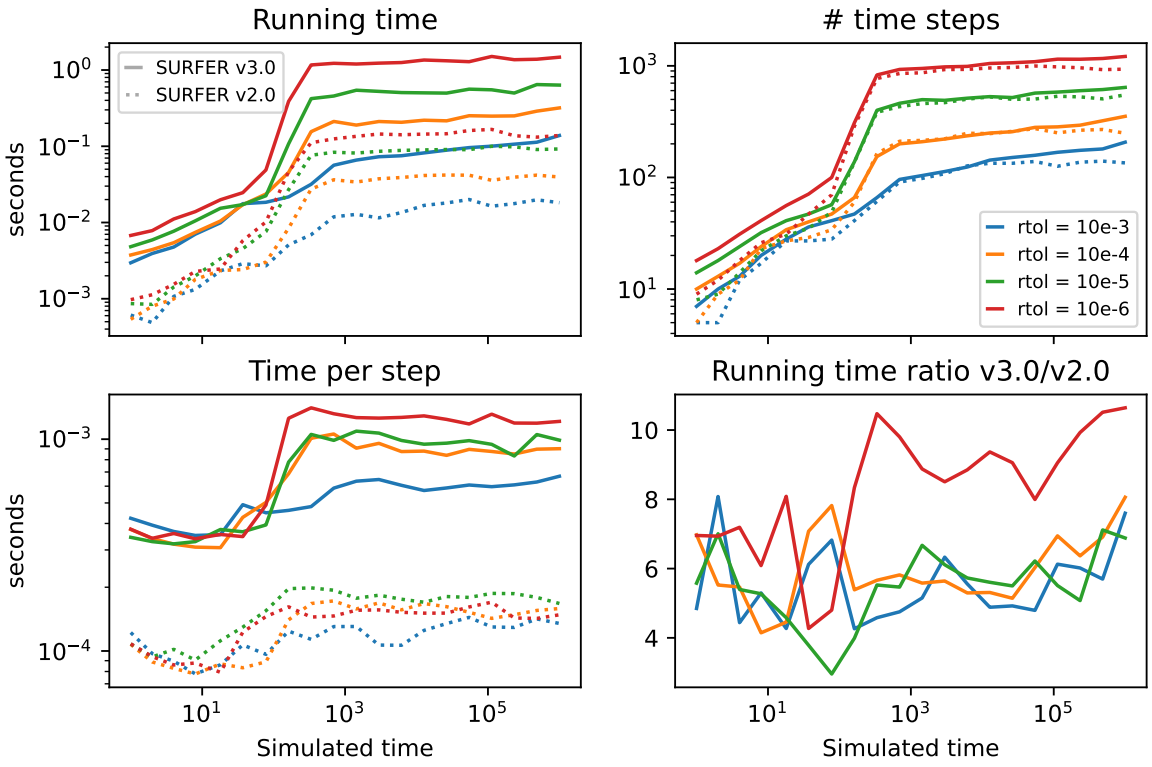

Figure D1. Schematic diagram of the model and its components.

Competing interests. TEXT

Disclaimer. TEXT

Acknowledgements. TEXT

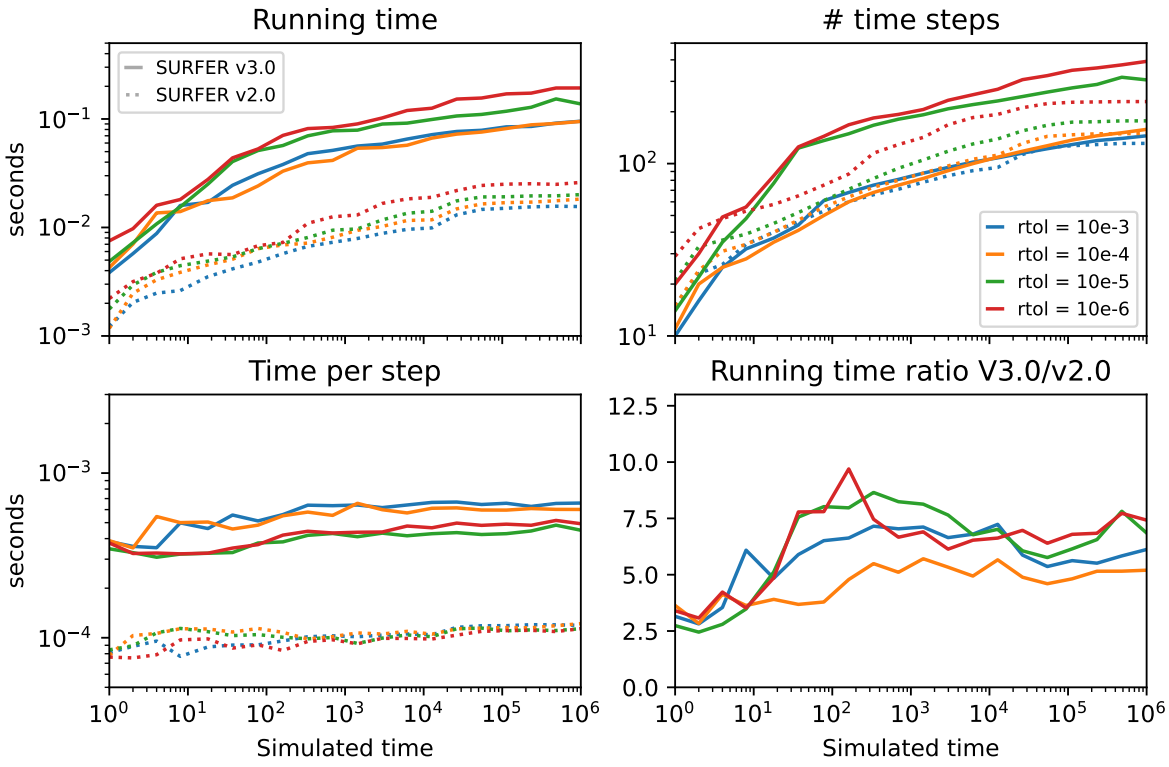

Figure D2. Schematic diagram of the model and its components.

References

Global Carbon and Other Biogeochemical Cycles and Feedbacks, in: Climate Change 2021 – The Physical Science Basis: Working Group I Contribution to the Sixth Assessment Report of the Intergovernmental Panel on Climate Change, edited by Intergovernmental Panel on Climate Change (IPCC), pp. 673–816, Cambridge University Press, Cambridge, https://doi.org/10.1017/9781009157896.007, 2023.

Archer, D.: Modeling the calcite lysocline, Journal of Geophysical Research, 96, 17 037, https://doi.org/10.1029/91JC01812, 1991.

Archer, D.: A data-driven model of the global calcite lysocline, Global Biogeochemical Cycles, 10, 511–526, https://doi.org/10.1029/96GB01521, 1996.

Archer, D., Kheshgi, H., and Maier-Reimer, E.: Multiple timescales for neutralization of fossil fuel CO_2, Geophysical Research Letters, 24, 405–408, https://doi.org/10.1029/97GL00168, 1997.

Archer, D., Kheshgi, H., and Maier-Reimer, E.: Dynamics of fossil fuel CO_2 neutralization by marine $CaCO_3$, Global Biogeochemical Cycles, 12, 259–276, https://doi.org/10.1029/98GB00744, 1998.

Archer, D., Eby, M., Brovkin, V., Ridgwell, A., Cao, L., Mikolajewicz, U., Caldeira, K., Matsumoto, K., Munhoven, G., Montenegro, A., and Tokos, K.: Atmospheric Lifetime of Fossil Fuel Carbon Dioxide, Annual Review of Earth and Planetary Sciences, 37, 117–134, https://doi.org/10.1146/annurev.earth.031208.100206, 2009.

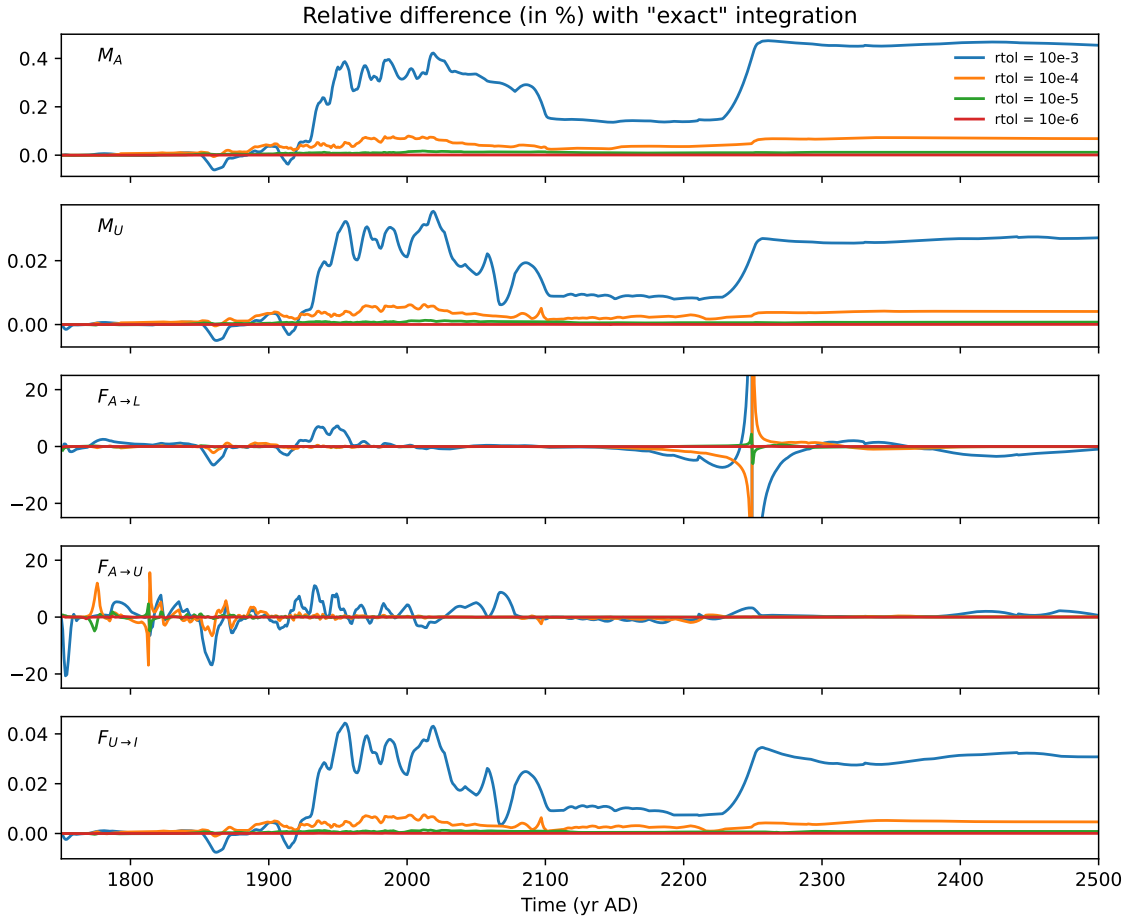

Figure D3. Exact integration : for all variables, we set $atol = 10^{12}$ and $rtol = 10^{12}$.

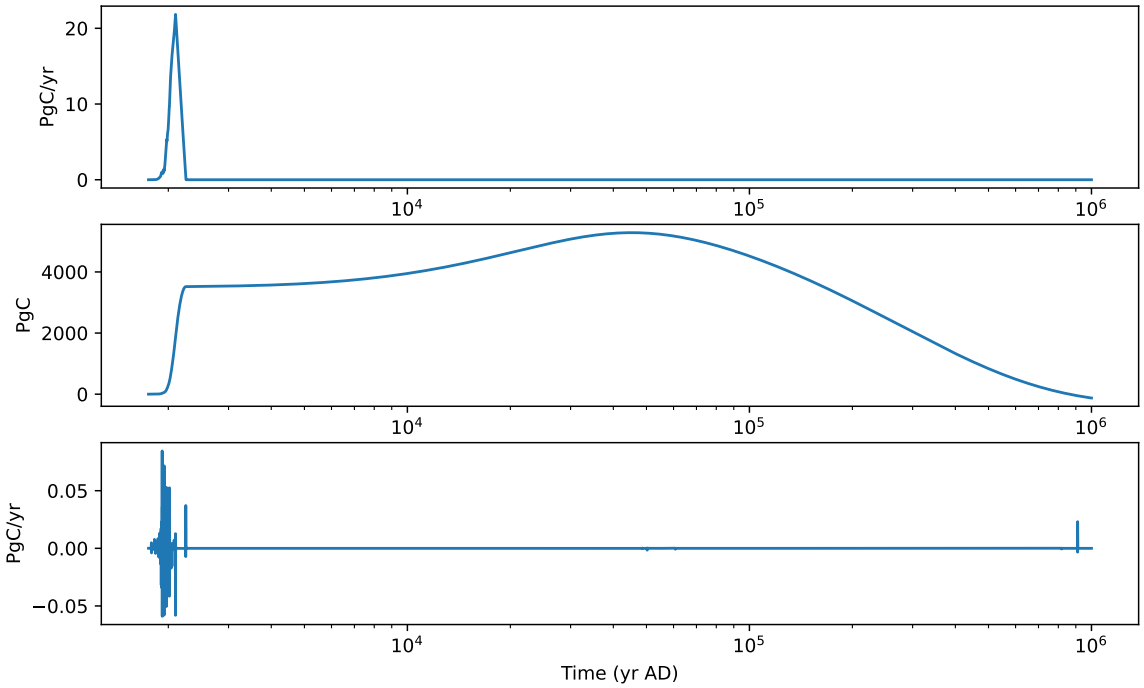

Figure D4. Schematic diagram of the model and its components.

Armstrong McKay, D. I., Staal, A., Abrams, J. F., Winkelmann, R., Sakschewski, B., Loriani, S., Fetzer, I., Cornell, S. E., Rockström, J., and Lenton, T. M.: Exceeding 1.5°C global warming could trigger multiple climate tipping points, Science, 377, eabn7950, https://doi.org/10.1126/science.abn7950, 2022.

Berger, W. H.: Planktonic Foraminifera: Selective solution and the lysocline, Marine Geology, 8, 111–138, https://doi.org/10.1016/0025-3227(70)90001-0, 1970.

Breedam, J. V., Goelzer, H., and Huybrechts, P.: Semi-equilibrated global sea-level change projections for the next 10 000 years, 2020.

Broecker, W. S. and Peng, T.-H.: The role of CaCO3 compensation in the glacial to interglacial atmospheric CO2 change, Global Biogeochemical Cycles, 1, 15–29, https://doi.org/10.1029/GB001i001p00015, _eprint: https://onlinelibrary.wiley.com/doi/pdf/10.1029/GB001i001p00015, 1987.

Clark, P. U., Shakun, J. D., Marcott, S. A., Mix, A. C., Eby, M., Kulp, S., Levermann, A., Milne, G. A., Pfister, P. L., Santer, B. D., Schrag, D. P., Solomon, S., Stocker, T. F., Strauss, B. H., Weaver, A. J., Winkelmann, R., Archer, D., Bard, E., Goldner, A., Lambeck, K., Pierrehumbert, R. T., and Plattner, G.-K.: Consequences of twenty-first-century policy for multi-millennial climate and sea-level change, Nature Climate Change, 6, 360–369, https://doi.org/10.1038/nclimate2923, 2016.

Colbourn, G., Ridgwell, A., and Lenton, T. M.: The Rock Geochemical Model (RokGeM) v0.9, Geoscientific Model Development, 6, 1543–1573, https://doi.org/10.5194/gmd-6-1543-2013, 2013.

Colbourn, G., Ridgwell, A., and Lenton, T. M.: The time scale of the silicate weathering negative feedback on atmospheric CO2, Global Biogeochemical Cycles, 29, 583–596, https://doi.org/10.1002/2014GB005054, _eprint: https://onlinelibrary.wiley.com/doi/pdf/10.1002/2014GB005054, 2015.

DeVries, T. and Weber, T.: The export and fate of organic matter in the ocean: New constraints from combining satellite and oceanographic tracer observations, Global Biogeochemical Cycles, 31, 535–555, https://doi.org/10.1002/2016GB005551, _eprint: https://onlinelibrary.wiley.com/doi/pdf/10.1002/2016GB005551, 2017.

Dickson, A. G.: Thermodynamics of the dissociation of boric acid in synthetic seawater from 273.15 to 318.15 K, Deep Sea Research Part A. Oceanographic Research Papers, 37, 755–766, https://doi.org/10.1016/0198-0149(90)90004-F, 1990.

Dickson, A. G. and Millero, F. J.: A comparison of the equilibrium constants for the dissociation of carbonic acid in seawater media, p. 11, 1987.

Fewster, R. E., Morris, P. J., Ivanovic, R. F., Swindles, G. T., Peregon, A. M., and Smith, C. J.: Imminent loss of climate space for permafrost peatlands in Europe and Western Siberia, Nature Climate Change, 12, 373–379, https://doi.org/10.1038/s41558-022-01296-7, 2022.

Friedlingstein, P., O'Sullivan, M., Jones, M. W., Andrew, R. M., Gregor, L., Hauck, J., Le Quéré, C., Luijkx, I. T., Olsen, A., Peters, G. P., Peters, W., Pongratz, J., Schwingshackl, C., Sitch, S., Canadell, J. G., Ciais, P., Jackson, R. B., Alin, S. R., Alkama, R., Arneth, A., Arora, V. K., Bates, N. R., Becker, M., Bellouin, N., Bittig, H. C., Bopp, L., Chevallier, F., Chini, L. P., Cronin, M., Evans, W., Falk, S., Feely, R. A., Gasser, T., Gehlen, M., Gkritzalis, T., Gloege, L., Grassi, G., Gruber, N., Gürses, , Harris, I., Hefner, M., Houghton, R. A., Hurtt, G. C., Iida, Y., Ilyina, T., Jain, A. K., Jersild, A., Kadono, K., Kato, E., Kennedy, D., Klein Goldewijk, K., Knauer, J., Korsbakken, J. I., Landschützer, P., Lefèvre, N., Lindsay, K., Liu, J., Liu, Z., Marland, G., Mayot, N., McGrath, M. J., Metzl, N., Monacci, N. M., Munro, D. R., Nakaoka, S.-I., Niwa, Y., O'Brien, K., Ono, T., Palmer, P. I., Pan, N., Pierrot, D., Pocock, K., Poulter, B., Resplandy, L., Robertson, E., Rödenbeck, C., Rodriguez, C., Rosan, T. M., Schwinger, J., Séférian, R., Shutler, J. D., Skjelvan, I., Steinhoff, T., Sun, Q., Sutton, A. J., Sweeney, C., Takao, S., Tanhua, T., Tans, P. P., Tian, X., Tian, H., Tilbrook, B., Tsujino, H., Tubiello, F., van der Werf, G. R., Walker, A. P., Wanninkhof, R., Whitehead, C., Willstrand Wranne, A., Wright, R., Yuan, W., Yue, C., Yue, X., Zaehle, S., Zeng, J., and Zheng, B.: Global Carbon Budget 2022, Earth System Science Data, 14, 4811–4900, https://doi.org/10.5194/essd-14-4811-2022, 2022.

Henson, S. A., Laufkötter, C., Leung, S., Giering, S. L. C., Palevsky, H. I., and Cavan, E. L.: Uncertain response of ocean biological carbon export in a changing world, Nature Geoscience, 15, 248–254, https://doi.org/10.1038/s41561-022-00927-0, number: 4 Publisher: Nature Publishing Group, 2022.

Humphreys, M. P., Lewis, E. R., Sharp, J. D., and Pierrot, D.: PyCO2SYS v1.8: marine carbonate system calculations in Python, Geoscientific Model Development, 15, 15–43, https://doi.org/10.5194/gmd-15-15-2022, publisher: Copernicus GmbH, 2022.

Jones, C. D., Frölicher, T. L., Koven, C., MacDougall, A. H., Matthews, H. D., Zickfeld, K., Rogelj, J., Tokarska, K. B., Gillett, N. P., Ilyina, T., Meinshausen, M., Mengis, N., Séférian, R., Eby, M., and Burger, F. A.: The Zero Emissions Commitment Model Intercomparison Project (ZECMIP) contribution to C4MIP: quantifying committed climate changes following zero carbon emissions, Geoscientific Model Development, 12, 4375–4385, https://doi.org/10.5194/gmd-12-4375-2019, publisher: Copernicus GmbH, 2019.

Kohfeld, K. E. and Ridgwell, A.: Glacial-interglacial variability in atmospheric CO2, in: Geophysical Monograph Series, edited by Le Quéré, C. and Saltzman, E. S., vol. 187, pp. 251–286, American Geophysical Union, Washington, D. C., https://doi.org/10.1029/2008GM000845, 2009.

Köhler, P., Nehrbass-Ahles, C., Schmitt, J., Stocker, T. F., and Fischer, H.: A 156 kyr smoothed history of the atmospheric greenhouse gases CO_2, CH_4, and N_2O and their radiative forcing, Earth System Science Data, 9, 363–387, https://doi.org/10.5194/essd-9-363-2017, publisher: Copernicus GmbH, 2017.

Lauvset, S. K., Key, R. M., Olsen, A., van Heuven, S., Velo, A., Lin, X., Schirnick, C., Kozyr, A., Tanhua, T., Hoppema, M., Jutterström, S., Steinfeldt, R., Jeansson, E., Ishii, M., Perez, F. F., Suzuki, T., and Watelet, S.: A new global interior ocean mapped climatology: the 1○ × 1○ GLODAP version 2, 2016.

Lenton, T. M.: Land and ocean carbon cycle feedback effects on global warming in a simple Earth system model, Tellus B, 52, 1159–1188, https://doi.org/10.1034/j.1600-0889.2000.01104.x, 2000.

Lenton, T. M., Held, H., Kriegler, E., Hall, J. W., Lucht, W., Rahmstorf, S., and Schellnhuber, H. J.: Tipping elements in the Earth's climate system, Proceedings of the National Academy of Sciences, 105, 1786–1793, https://doi.org/10.1073/pnas.0705414105, 2008.

Lenton, T. M., Rockström, J., Gaffney, O., Rahmstorf, S., Richardson, K., Steffen, W., and Schellnhuber, H. J.: Climate tipping points — too risky to bet against, Nature, 575, 592–595, https://doi.org/10.1038/d41586-019-03595-0, 2019.

Levy, M., Bopp, L., Karleskind, P., Resplandy, L., Ethe, C., and Pinsard, F.: Physical pathways for carbon transfers between the surface mixed layer and the ocean interior, Global Biogeochemical Cycles, 27, 1001–1012, https://doi.org/10.1002/gbc.20092, _eprint: https://onlinelibrary.wiley.com/doi/pdf/10.1002/gbc.20092, 2013.

Lord, N. S., Ridgwell, A., Thorne, M. C., and Lunt, D. J.: The 'long tail' of anthropogenic CO2 decline in the atmosphere and its consequences for post-closure performance assessments for disposal of radioactive wastes, Mineralogical Magazine, 79, 1613–1623, https://doi.org/10.1180/minmag.2015.079.6.37, publisher: Cambridge University Press, 2015.

Lord, N. S., Ridgwell, A., Thorne, M. C., and Lunt, D. J.: An impulse response function for the "long tail" of excess atmospheric CO_2 in an Earth system model, Global Biogeochemical Cycles, 30, 2–17, https://doi.org/10.1002/2014GB005074, 2016.

MacDougall, A. H., Frölicher, T. L., Jones, C. D., Rogelj, J., Matthews, H. D., Zickfeld, K., Arora, V. K., Barrett, N. J., Brovkin, V., Burger, F. A., Eby, M., Eliseev, A. V., Hajima, T., Holden, P. B., Jeltsch-Thömmes, A., Koven, C., Mengis, N., Menviel, L., Michou, M., Mokhov, I. I., Oka, A., Schwinger, J., Séférian, R., Shaffer, G., Sokolov, A., Tachiiri, K., Tjiputra, J., Wiltshire, A., and Ziehn, T.: Is there warming in the pipeline? A multi-model analysis of the Zero Emissions Commitment from CO2, 2020.

Martin, J. H., Knauer, G. A., Karl, D. M., and Broenkow, W. W.: VERTEX: carbon cycling in the northeast Pacific, Deep Sea Research Part A. Oceanographic Research Papers, 34, 267–285, https://doi.org/10.1016/0198-0149(87)90086-0, 1987.

Martínez Montero, M., Crucifix, M., Couplet, V., Brede, N., and Botta, N.: SURFER v2.0: a flexible and simple model linking anthropogenic CO_2 emissions and solar radiation modification to ocean acidification and sea level rise, Geoscientific Model Development, 15, 8059–8084, https://doi.org/10.5194/gmd-15-8059-2022, 2022.

McDougall, T. J. and Barker, P. M.: Getting started with TEOS-10 and the Gibbs Seawater (GSW) Oceanographic Toolbox, SCOR/IAPSO WG127, 2011.

Mehrbach, C., Culberson, C. H., Hawley, J. E., and Pytkowicx, R. M.: MEASUREMENT OF THE APPARENT DISSOCIATION CONSTANTS OF CARBONIC ACID IN SEAWATER AT ATMOSPHERIC PRESSURE1, Limnology and Oceanography, 18, 897–907, https://doi.org/10.4319/lo.1973.18.6.0897, 1973.

Middelburg, J. J., Soetaert, K., and Hagens, M.: Ocean Alkalinity, Buffering and Biogeochemical Processes, Reviews of Geophysics, 58, e2019RG000 681, https://doi.org/10.1029/2019RG000681, _eprint: https://onlinelibrary.wiley.com/doi/pdf/10.1029/2019RG000681, 2020.

Millero, F. J.: The thermodynamics of the carbonate system in seawater, Geochimica et Cosmochimica Acta, 43, 1651–1661, https://doi.org/10.1016/0016-7037(79)90184-4, 1979.

Millero, F. J.: Thermodynamics of the carbon dioxide system in the oceans, Geochimica et Cosmochimica Acta, 59, 661–677, https://doi.org/10.1016/0016-7037(94)00354-O, 1995.

Montero, M. M., Brede, N., Couplet, V., Crucifix, M., Botta, N., and Wieners, C.: Lost options commitment: how short-term policies affect long-term scope of action, Tech. Rep. arXiv:2309.07743, arXiv, http://arxiv.org/abs/2309.07743, arXiv:2309.07743 [physics] type: article, 2023.

Munhoven, G.: Mathematics of the total alkalinity–pH equation – pathway to robust and universal solution algorithms: the SolveSAPHE package v1.0.1, Geoscientific Model Development, 6, 1367–1388, https://doi.org/10.5194/gmd-6-1367-2013, publisher: Copernicus GmbH, 2013.

Myhre, G., Highwood, E. J., Shine, K. P., and Stordal, F.: New estimates of radiative forcing due to well mixed greenhouse gases, Geophysical Research Letters, 25, 2715–2718, https://doi.org/10.1029/98GL01908, 1998.

Nisbet, E. G., Manning, M. R., Dlugokencky, E. J., Michel, S. E., Lan, X., Röckmann, T., Denier van der Gon, H. A. C., Schmitt, J., Palmer, P. I., Dyonisius, M. N., Oh, Y., Fisher, R. E., Lowry, D., France, J. L., White, J. W. C., Brailsford, G., and Bromley, T.: Atmospheric Methane: Comparison Between Methane's Record in 2006–2022 and During Glacial Terminations, Global Biogeochemical Cycles, 37, e2023GB007 875, https://doi.org/10.1029/2023GB007875, _eprint: https://onlinelibrary.wiley.com/doi/pdf/10.1029/2023GB007875, 2023.

Petzold, L.: Automatic Selection of Methods for Solving Stiff and Nonstiff Systems of Ordinary Differential Equations, SIAM Journal on Scientific and Statistical Computing, 4, 136–148, https://doi.org/10.1137/0904010, publisher: Society for Industrial and Applied Mathematics, 1983.

Planchat, A., Bopp, L., Kwiatkowski, L., and Torres, O.: Carbonate pump feedbacks on alkalinity and the carbon cycle in the 21st century and beyond, 2023.

Ridgwell, A. and Hargreaves, J. C.: Regulation of atmospheric CO $_2$ by deep-sea sediments in an Earth system model: REGULATION OF CO $_2$ BY DEEP-SEA SEDIMENTS, Global Biogeochemical Cycles, 21, n/a–n/a, https://doi.org/10.1029/2006GB002764, 2007.

Sarmiento, J. L. and Gruber, N.: Ocean biogeochemical dynamics, Princeton University Press, Princeton, oCLC: ocm60651167, 2006.

Saunois, M., Stavert, A. R., Poulter, B., Bousquet, P., Canadell, J. G., Jackson, R. B., Raymond, P. A., Dlugokencky, E. J., Houweling, S., Patra, P. K., Ciais, P., Arora, V. K., Bastviken, D., Bergamaschi, P., Blake, D. R., Brailsford, G., Bruhwiler, L., Carlson, K. M., Carrol, M., Castaldi, S., Chandra, N., Crevoisier, C., Crill, P. M., Covey, K., Curry, C. L., Etiope, G., Frankenberg, C., Gedney, N., Hegglin, M. I., Höglund-Isaksson, L., Hugelius, G., Ishizawa, M., Ito, A., Janssens-Maenhout, G., Jensen, K. M., Joos, F., Kleinen, T., Krummel, P. B., Langenfelds, R. L., Laruelle, G. G., Liu, L., Machida, T., Maksyutov, S., McDonald, K. C., McNorton, J., Miller, P. A., Melton, J. R., Morino, I., Müller, J., Murguia-Flores, F., Naik, V., Niwa, Y., Noce, S., O'Doherty, S., Parker, R. J., Peng, C., Peng, S., Peters, G. P., Prigent, C., Prinn, R., Ramonet, M., Regnier, P., Riley, W. J., Rosentreter, J. A., Segers, A., Simpson, I. J., Shi, H., Smith, S. J., Steele, L. P., Thornton, B. F., Tian, H., Tohjima, Y., Tubiello, F. N., Tsuruta, A., Viovy, N., Voulgarakis, A., Weber, T. S., van Weele, M., van der Werf, G. R., Weiss, R. F., Worthy, D., Wunch, D., Yin, Y., Yoshida, Y., Zhang, W., Zhang, Z., Zhao, Y., Zheng, B., Zhu, Q., Zhu, Q., and Zhuang, Q.: The Global Methane Budget 2000–2017, Earth System Science Data, 12, 1561–1623, https://doi.org/10.5194/essd-12-1561-2020, publisher: Copernicus GmbH, 2020.

Soetaert, K., Hofmann, A. F., Middelburg, J. J., Meysman, F. J. R., and Greenwood, J.: The effect of biogeochemical processes on pH, Marine Chemistry, 2007.

Steffen, W., Rockström, J., Richardson, K., Lenton, T. M., Folke, C., Liverman, D., Summerhayes, C. P., Barnosky, A. D., Cornell, S. E., Crucifix, M., Donges, J. F., Fetzer, I., Lade, S. J., Scheffer, M., Winkelmann, R., and Schellnhuber, H. J.: Trajectories of the Earth System in the Anthropocene, Proceedings of the National Academy of Sciences, 115, 8252–8259, https://doi.org/10.1073/pnas.1810141115, 2018.

Sulpis, O., Jeansson, E., Dinauer, A., Lauvset, S. K., and Middelburg, J. J.: Calcium carbonate dissolution patterns in the ocean, Nature Geoscience, 14, 423–428, https://doi.org/10.1038/s41561-021-00743-y, number: 6 Publisher: Nature Publishing Group, 2021.

Tokarska, K. B., Gillett, N. P., Weaver, A. J., Arora, V. K., and Eby, M.: The climate response to five trillion tonnes of carbon, Nature Climate Change, 6, 851–855, https://doi.org/10.1038/nclimate3036, number: 9 Publisher: Nature Publishing Group, 2016.

Uppström, L. R.: The boron/chlorinity ratio of deep-sea water from the Pacific Ocean, Deep Sea Research and Oceanographic Abstracts, 21, 161–162, https://doi.org/10.1016/0011-7471(74)90074-6, 1974.

Volk, T. and Hoffert, M. I.: Ocean Carbon Pumps: Analysis of Relative Strengths and Efficiencies in Ocean-Driven Atmospheric CO2 Changes, in: The Carbon Cycle and Atmospheric CO2: Natural Variations Archean to Present, pp. 99–110, American Geophysical Union (AGU), https://doi.org/10.1029/GM032p0099, _eprint: https://onlinelibrary.wiley.com/doi/pdf/10.1029/GM032p0099, 1985.

Weiss, R.: Carbon dioxide in water and seawater: the solubility of a non-ideal gas, Marine Chemistry, 2, 203–215, https://doi.org/10.1016/0304-4203(74)90015-2, 1974.

West, A. J., Galy, A., and Bickle, M.: Tectonic and climatic controls on silicate weathering, Earth and Planetary Science Letters, 235, 211–228, https://doi.org/10.1016/j.epsl.2005.03.020, 2005.

Williams, R. G., Goodwin, P., Ridgwell, A., and Woodworth, P. L.: How warming and steric sea level rise relate to cumulative carbon emissions, Geophysical Research Letters, 39, https://doi.org/10.1029/2012GL052771, _eprint: https://onlinelibrary.wiley.com/doi/pdf/10.1029/2012GL052771, 2012.

Yang, M., Bell, T. G., Bidlot, J.-R., Blomquist, B. W., Butterworth, B. J., Dong, Y., Fairall, C. W., Landwehr, S., Marandino, C. A., Miller, S. D., Saltzman, E. S., and Zavarsky, A.: Global Synthesis of Air-Sea CO2 Transfer Velocity Estimates From Ship-Based Eddy Covariance Measurements, Frontiers in Marine Science, 9, https://www.frontiersin.org/articles/10.3389/fmars.2022.826421, 2022.

Zeebe, R. E.: LOSCAR: Long-term Ocean-atmosphere-Sediment CArbon cycle Reservoir Model v2.0.4, Geosci. Model Dev., 2012.

Zickfeld, K., Eby, M., Weaver, A. J., Alexander, K., Crespin, E., Edwards, N. R., Eliseev, A. V., Feulner, G., Fichefet, T., Forest, C. E., Friedlingstein, P., Goosse, H., Holden, P. B., Joos, F., Kawamiya, M., Kicklighter, D., Kienert, H., Matsumoto, K., Mokhov, I. I., Monier, E., Olsen, S. M., Pedersen, J. O. P., Perrette, M., Philippon-Berthier, G., Ridgwell, A., Schlosser, A., Deimling, T. S. V., Shaffer, G., Sokolov, A., Spahni, R., Steinacher, M., Tachiiri, K., Tokos, K. S., Yoshimori, M., Zeng, N., and Zhao, F.: Long-Term Climate Change Commitment and Reversibility: An EMIC Intercomparison, Journal of Climate, 26, 5782–5809, https://doi.org/10.1175/JCLI-D-12-00584.1, publisher: American Meteorological Society Section: Journal of Climate, 2013.